Master's thesis

NTNU
Norwegian University of Science and Technology
Faculty of Medicine and Health Sciences
Kavli Institute for Systems Neuroscience

Vidar Langseth Saasen

DNA Repair Enzyme NEIL3 Impacts Hippocampal Spatial Representations

Master's thesis in Neuroscience
Supervisor: Jing Ye
Co-supervisor: Magnar Bjørås
May 2022

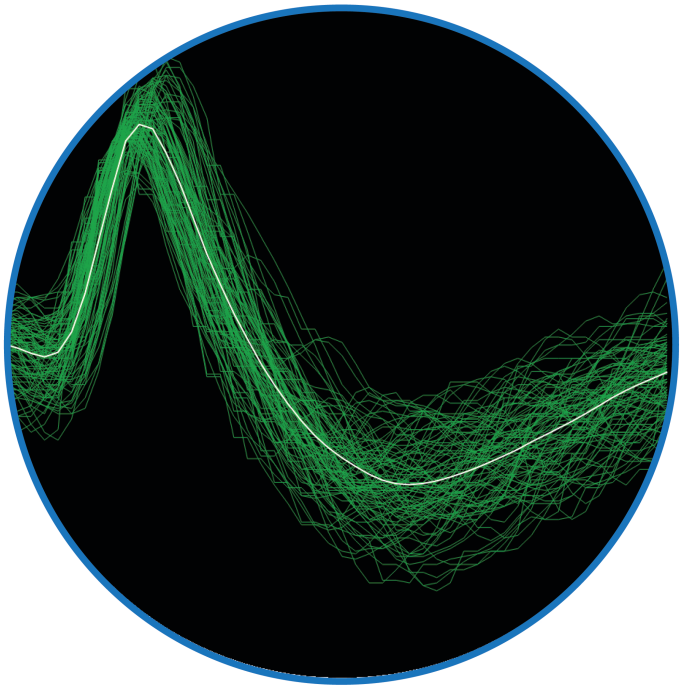

NTNU
Norwegian University of
Science and Technology

Vidar Langseth Saasen

DNA Repair Enzyme NEIL3 Impacts Hippocampal Spatial Representations

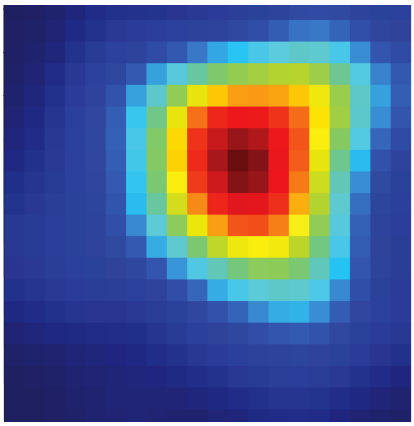

Master's thesis in Neuroscience
Supervisor: Jing Ye
Co-supervisor: Magnar Bjørås
May 2022

Norwegian University of Science and Technology
Faculty of Medicine and Health Sciences
Kavli Institute for Systems Neuroscience

NTNU
Norwegian University of
Science and Technology

Abstract

The endonuclease VIII-like 3 (NEIL3) DNA glycosylase is an enzyme that has a role in initiating DNA base excision repair pathways. Recently, there has been emerging evidence highlighting the non-canonical roles of NEIL3 in the brain, associating it with hippocampal function and memory. The main aim of this study was to elucidate whether NEIL3 impacts the functional plasticity of hippocampal neurons using electrophysiology strategies. To address the main aim, I (***i***) assembled microdrives with four intracranial tetrodes (16 electrodes) that were implanted in the mouse hippocampus and (***ii***) recorded place cells in the hippocampal CA1 and DG regions in behaving mice. I successfully recorded the activity of hippocampal place cells in four animals (two wildtype and two NEIL3-deficient). Cells from one wildtype and one NEIL3-deficient mice were clustered and analysed. Based on the analysis of two animals, I found that the NEIL3 deficient mouse exhibited fewer cells in the hippocampal CA1 with multiple place fields, bigger field size, and higher field peak firing rate compared to cells from the wildtype mouse, suggesting a disruption in the spatial specificity. Further, place cells recorded in the DG of the NEIL3-deficient mouse displayed signs of impaired remapping, as the mouse showed decreased ability to generate new functional representations when moved from a familiar environment to a novel one. However, NEIL3-deficient place cells in DG did not show impaired spatial stability. This contrasts with an earlier study that found impaired stability in CA1 place cells. These results suggest that the functional plasticity of DG place cells may deviate from the functional plasticity in CA1 of NEIL3-deficient mice. More cells and animals need to be included in the study to make a solid conclusion.

The secondary aim of this study was to elucidate whether NEIL3 impacts anxiety and spatial memory. To address the secondary aim, I used three different behavioural experiments: the open field, the novel object location, and the y-maze. A total of 30 mice (nine young and six old wildtype mice, and nine young and six old NEIL3 deficient mice) were tested in these experiments. The young NEIL3 deficient mice had tendencies towards anxious behaviour in an open field experiment, contrary to what has been previously described. Further, the young NEIL3 deficient mice also travelled a shorter distance at a lower speed, indicating reduced general locomotor activity. In the novel object location task, I tested both short-term and long-term spatial memory. The NEIL3 deficient mice showed indications of impaired memory in the long-term condition, but not in the short-term condition. In conclusion, the findings indicates that depletion of NEIL3 leads to increased anxiety-like behaviour and impaired long-term spatial memory.

Sammendrag

Endonuclease VIII-like 3 (NEIL3) DNA glycosylase er et enzym som spiller en rolle i initieringen av en viktig DNA reparasjonsprosess. I den siste tiden har det kommet frem nye funn som fremhever rollene NEIL3 spiller utenom DNA reparasjon, og blant disse rollene er en interaksjon med hukommelsessystemet i hjernen. Hovedmålet med denne studien var å finne ut om NEIL3 påvirker den funksjonelle plastisiteten av plass celler i CA1 og DG i hippocampus. For å adressere hovedmålet, implanterte jeg fire mikrodrivere med fire intrakranielle tetroder (16 elektroder) i hippocampus på mus, og målte nevral aktivitet i CA1 og DG. Jeg målte fire mus (to villtyper og to som manglet genet for NEIL3). Celler fra en villtype og en som manglet genet for NEIL3 ble gruppert og analysert. Basert på analyser av disse cellene fant jeg at musa som manglet NEIL3 hadde færre celler som hadde flere en ett plassfelt, større plassfelt, og høyere nevral aktivitet innad i plassfeltene. Dette er en indikasjon på at spesifisiteten til plass cellene er påvirket av NEIL3. Videre fant jeg tegn på svekkelse i evnen til å danne nye mentale representasjoner av rommet i plass cellene i DG når mus som manglet NEIL3 ble introdusert til et nytt område. Jeg fant også at stabiliteten til plass cellene i DG ikke viste tegn til forstyrrelser, i motsetning av tidligere funn fra CA1. Disse resultatene indikerer at den funksjonelle plastisiteten til plass celler i DG kan være forskjellige fra den funksjonelle plastisiteten i CA1. Flere celler og dyr er nødvendig for å kunne gjøre solide konklusjoner.

Det sekundære målet med denne studien var å belyse om NEIL3 påvirker angst og romlig hukommelse. For å adressere det sekundære målet brukte jeg tre forskjellige adferseksperimenter: open field, ny objektlokasjon, og y-labyrinten. Totalt ble 30 mus (ni unge og seks gamle villtyper, og ni unge og seks gamle mus uten *Neil3* genet) testet i disse eksperimentene. Unge mus som manglet NEIL3 hadde tendenser til angst i open field eksperimentet, i motsetning til tidligere funn fra eldre mus som manglet NEIL3. Når musene ble testet med en hukommelsestest fant jeg indikasjon på hukommelsessvikt når musene ble testet i en langtidsbetingelse, men ikke i en korttidsbetingelse. Jeg konkluderer at funnene indikerer at NEIL3 spiller en rolle i funksjonell plastisitet i hippocampus, angst, og i romlig hukommelse.

Preface

I want to extend a warm thanks to everyone that has helped me through this process. First, thanks to my supervisors, Jing and Magnar, for allowing me to work with such an interesting project over the last year. Especially Jing, who has helped me every step of the way, but still allowing me to work independently. It has been an fun and rewarding learning experience. I also want to thank the research group for the good and fun discussions we have had. Especially thanks goes out to Marion for the training, reading my thesis, and providing constructive critisism. I also want to thank the nice people of IKOM and Comed for their help and interesting conversations. Further, I want to thank my family for all the support they have given me though my studies. Finally I want to thank my girlfriend Elizabeth for all the love and support I have received during this process.

Table of Contents

List of Figures

List of Tables

List of Abbreviations

BER	Base excision repair
CA	Cornu ammonis
DG	Dentate Gyrus
DNA	Deoxyribonucleic acid
EC	Entorhinal cortex
GCL	Granule cell layer
HD	Head direction
LTM	Long-term memory
mEC	Medial entorhinal cortex
ML	Molecular layer
NEIL	Endonuclease VIII Like
NEIL3	NEIL3 glycosylase
Neil3$^{-/-}$	Nullizygous *Neil3*
NOL	Novel Object Location
PCL	Polymorphic cell layer
SGZ	Subgranular zone
STM	Short-term memory

1 Introduction

In recent years, new knowledge about the DNA glycosylases has appeared, implicating its role in cognitive functions outside its established role in DNA repair. This study will investigate the relationship between a specific DNA glycosylase, the endonuclease VIII-like 3 (NEIL3), and spatial memory, with a focus on the functional plasticity of hippocampal neurons in the Cornu Ammonis 1 (CA1) and the dentate gyrus (DG). This introductory section will first outline the canonical and non-canonical roles of NEIL3, then introduce spatial memory, and finally describe the interaction between NEIL3 and spatial memory.

1.1 NEIL3

1.1.1 DNA Repair and the BER Pathway

The canonical role of NEIL3 is related to DNA repair through the base excision repair (BER) pathway. The energy required by cells is obtained through various metabolism processes, which can occur in presence or absence of oxygen. If there is oxygen present, the chemical reactions will produce reactive oxygen species. These reactive oxygen species constitute a major source of oxidative stress, which Sies (2015) defines as "An imbalance between oxidants and antioxidants in favour of the oxidants, leading to a disruption of redox signalling and control and/or molecular damage". Oxidative stress is also involved in neurogenerative disorders like Alzheimer's, Parkinson's, and Huntington's disease (Chen and Zhong, 2014; Watts, Pocock and Claudianos, 2018).

The deoxyribonucleic acid (DNA) is a molecule that resides within the nucleus of nearly all the cells in our bodies and, albeit in much less quantity, in the mitochondria (Dhruve, 2021). The DNA molecule is made up by nucleotides, which consist of three parts: a nitrogen base, a sugar molecule (deoxyribose), and a phosphate group. DNA is exposed to noxious agents from endogenous and exogenous sources throughout the life of an organism which threatens both the genome and the epigenome (Agarwal and Miller, 2017). In fact, DNA reactivity results in between 10000 and 20000 damaged bases in every cell every day (Lindahl and Barnes, 2000). This damage to the DNA requires repair mechanisms to protect the structural integrity of the DNA. Such DNA repair mechanisms require a series of specialised enzymes, and one of these enzymes is NEIL3. The NEIL3 DNA glycosylase belongs to the endonuclease VIII-like (NEIL) glycosylases family and has been implicated in DNA repair through the BER pathway (Anindya, 2020; Krokan and Bjørås, 2013). The

molecular damage caused by oxidative stress can impact the nucleotide bases of the DNA, both in the nucleus and in the mitochondria. It is essential to maintain genomic stability in order to preserve optimal cellular functioning and genetic transfer (Wilson, 2017). Nucleotide bases that are damaged by oxidative stress are repaired by the BER pathway (Cadet and Davies, 2017). BER is essential for the functioning of a range of different organisms, including mammals. BER has been shown to play a role in normal ageing, neurodegenerative diseases, and resilience to cancer and other diseases (Wilson, 2017).

The BER pathway is executed by the action of one of multiple different glycosylases, excising a nucleotide base. There are six important glycosylases that are involved in the repair of oxidatively damaged bases: Nei-like DNA glycosylases 1–3 (NEIL1–3), 8-oxoguanine DNA glycosylase (OGG1), adenine-DNA glycosylase (MUTYH), endonuclease III-like protein 1 DNA glycosylase (NTH1/NTHL1). The NEIL glycosylases have a bifunctional role in DNA repair. The first is to recognise the abasic site, and the second is to cleave it, making it available for repair (de Sousa *et al.*, 2021). These two roles of the NEIL glycosylases are considered canonical (Ha, Lin and Yan, 2020). The different NEIL proteins have developed specialized functions, where NEIL1 is associated with replication-associated repair, NEIL2 is associated with transcription-coupled repair, and NEIL3 is associated with post-replication telomere maintenance (Wilson, 2017). It is important to note that while these six glycosylases have been identified as catalysts for the BER pathway, there might be additional proteins that play important roles, either alone or in interaction with these glycosylases (Wilson, 2017). NEIL3 is only found in brain regions that have neural stem and progenitor cells during embryogenesis and in neonatal mice (Wilson, 2017; Rolseth *et al.*, 2008). Nullizygous *Neil*3 mice (*Neil*3$^{-/-}$) show disrupted DNA repair function (Regnell *et al.*, 2012), but no cancer predispositions or increased mutation rate (Rolseth *et al.*, 2017). The BER pathway has been implicated in a number of different biological processes in addition to DNA repair, such as governing embryonic neural stem cells (Reis and Hermanson, 2012) and predispositions to autoimmunity (Massaad *et al.*, 2016).

1.1.2 Non-Canonical Role of NEIL3

NEIL3 has been shown to influence a number of processes outside of its bifunctional cannonical role of preserving genomic integrity. These non-canonical functions include neurogenesis, anxiety, memory, gene expression, brain maturation, and hippocampal functional representations.

Using a NEIL3 deficient rat model, Reis and Hermanson (2012) found a decreased ability of neural stem cells to differentiate. Further, they found a molecular marker of premature senescence that was highly expressed in neural stem cells in their NEIL3 model.

When applying a hypoxia-ischemia experimental model to *Neil3*$^{-/-}$ mice, Sejersted *et al.* (2011) found a loss of proliferating progenitor cells in the striatum. Similarly, by utilizing an in vitro neurosphere assay, both Rolseth *et al.* (2013) and Regnell *et al.* (2012) found that NEIL3 depletion in mice inhibited proliferation, but the ability to differentiate was intact. These findings demonstrate that the role NEIL3 plays in governing neurogenesis is complex.

While researching *Neil3*$^{-/-}$ mice, Regnell *et al.* (2012) found issues with spatial navigation in a Morris water maze, where the *Neil3*$^{-/-}$ mice learned to find the way out of the maze similarly to the wildtype mice in the short-term condition, but when tested on long-term retention, they found a discrepancy with the *Neil3*$^{-/-}$ mice performing worse. The behavioural outcome of the Morris water maze is associated with hippocampal dependent learning and memory. Regnell *et al.* (2012) also found decreased anxiety of *Neil3*$^{-/-}$ mice in an elevated zero maze. Based on this finding, they further investigated the molecular basis of this deficit and found a differential expression of various subunits of both excitatory and inhibitory receptors. Later, Kunath *et al.* (2021) investigated the neurophysiological effects of the *Neil3*$^{-/-}$ mouse model. They found that almost 2000 genes were differentially expressed between the genotypes, and that many of these were related to synaptic plasticity, which is a process that is essential for memory formation (Martin, Grimwood and Morris, 2000). They also found spatially induced expression of the immediate early genes Arc and c-Fos was significantly impaired in *Neil3*$^{-/-}$ mice. Arc and c-Fos are thought to function as markers of neural activity during spatial learning (Guzowski *et al.*, 2001; Guzowski *et al.*, 2006). Further, they found differences in the transcriptome of CA1 during postnatal maturation, which caused delayed maturation in the *Neil3*$^{-/-}$ mice. Finally, Kunath *et al.* (2021) found two functional differences of CA1 place cells, the specificity, and the long-term stability of spatial representations. This will be discussed later in the text in relation to place cells.

1.2 Spatial memory

Spatial cognition is a basic and important function of the brain that allows animals to explore and learn the layout of an area. Ever since the seminal surgery of patient HM (Scoville and Milner, 1957), evidence has accumulated indicating that both spatial and episodic memory is reliant on encoding in the hippocampal region (Moser, Moser and McNaughton, 2017; Zemla and Basu, 2017). This section will describe some of the anatomical and functional underpinnings of the spatial navigation system.

1.2.1 The Hippocampal Region

The hippocampal region consists of the hippocampal formation and the parahippocampal region (Andersen *et al.*, 2006). The hippocampal region manages large amounts of data simultaneously and connects through complex bidirectional connections with the associative regions of the neocortex.

1.2.1.1 Anatomy of the Hippocampal Formation

The hippocampal formation consists of the dentate gyrus (DG), subiculum, and hippocampus proper, which is a three layered allocortical lamina called Cornu Ammonis (CA). The CA can be subdivided into three fields: CA1, CA2, and CA3 (Andersen *et al.*, 2006). Anatomically, the mouse hippocampus has an elongated structure, extending from the septal nuclei of the basal forebrain, around the diencephalon and into the temporal parts of the brain (Witter, 2012), and is a structure that is largely evolutionarily conserved across species (Manns and Eichenbaum, 2006). The anatomical structure of the hippocampus can be understood on several axes. The longitudinal axis (also called dorsoventral axis) of the hippocampal formation is the longest and runs from the ventral to dorsal pole, the transverse axis (also called the orthogonal axis) is orthogonal to the longitudinal axis (Witter, 2012) with the proximal closest to the DG and the distal furthest away from DG. Finally, the radial axis runs from superficial to deep. An illustration of these axes is found in Figure 1. The anatomical organisation of the parahippocampal input to the hippocampus has led to a hypothesis that there are major circuits that run in parallel to each other, conveying signals from distinct cortical areas. These input signals terminate at different transverse locations in CA1, but not in the other subregions of the hippocampus (Witter *et al.*, 2000).

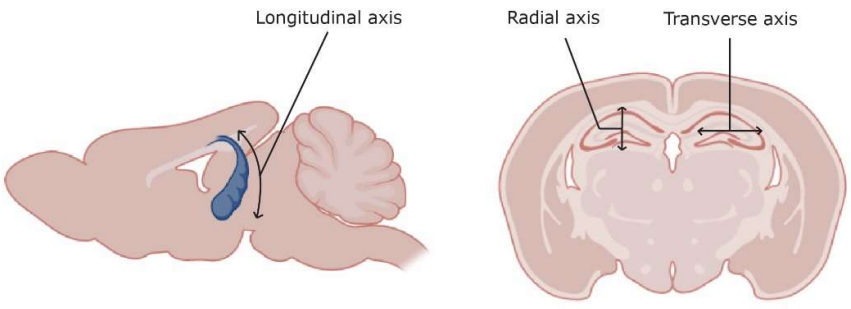

Figure 1. Illustration of the anatomical axes.
The figure was created in BioRender.

1.2.1.2 Anatomy of the Parahippocampal Region

The parahippocampal region consists of five sub-regions: entorhinal, perirhinal, postrhinal, presubiculum, and parasubiculum (Andersen *et al.*, 2006). The entorhinal cortex (EC) is the sub-region that has the most connections with the hippocampal formation, and at the same time has strong connections with the other parahippocampal sub-regions (Witter, 2012). The EC has bidirectional connections with the subiculum and the CA1 and has unidirectional projections to all the other regions of the hippocampal formation (Witter *et al.*, 2017).

1.2.1.3 Information Flow in the Hippocampal Region

The EC receives afferent projections from many cortical structures and represents a structure with great convergence of sensory signals. Furthermore, the EC-hippocampal circuit has been suggested as an integrator for higher order multimodal signals (Li, Arleo and Sheynikhovich, 2020). The classical view of hippocampal information flow postulated that neocortical information converged in the EC, before it continued to the DG, then to the CA3, then to the CA1 and finally back to the EC (Witter, 2018). This view does not fully capture the complexities of the hippocampal region. A functional division between the lateral and medial EC (mEC) has been made, as the mEC mainly processes spatial information (Hardcastle *et al.*, 2017), whereas the lateral EC processes other types of information, such as olfaction (Li *et al.*, 2017; Xu and Wilson, 2012) and time (Tsao *et al.*, 2018; Montchal, Reagh and Yassa, 2019). More recent evidence showcases the interactivity of these two processing streams, and suggests that these two streams might integrate information from each other (Nilssen *et al.*, 2019). A modern view of the information flow in the hippocampus includes connections from the EC to all sub-regions of the hippocampus and interactions between them.

There are three major fibre bundles associated with the hippocampal formation (Andersen *et al.*, 2006). The first, which contains the fibres that go between the EC and the sub-regions of the hippocampus, is called the angular bundle. The second, which contains fibres that go between the basal forebrain, the brain stem, and the hypothalamus, is called the fimbra-fornix pathway. The third, which contains fibres that connect the hippocampus in one hemisphere to its contralateral counterpart, is called the dorsal and ventral commissures (Andersen *et al.*, 2006). There is evidence that lesions to the two first of these fibre bundles causes learning and memory deficits (Benear, Ngo and Olson, 2020; Poulos, Christian and Thompson, 2008), but evidence is lacking for the dorsal and ventral commissures (Postans *et al.*, 2020).

1.2.1.4 Spatially Selective Cells

Some of the cells in the hippocampal region exhibit spatial selectivity. This means that the cells have a receptive field that corresponds to a location in space. The first spatially selective cells were found by O'Keefe and Dostrovsky (1971), who dubbed these cells place cells. The locations in space of which it is tuned is dubbed place fields. These cells were non-topographically organized, meaning that neighbouring cells' place fields were not correlated to eachother. Spatially selective cells have been found in all the sub regions of the hippocampal formation. Spatially selective cells have also been found in the EC by Hafting *et al.* (2005). These cells, dubbed grid cells, have regularly spaced fields that cover the environment in a tessellating fashion.

1.2.2 CA1

The CA1 is the most researched of all the sub-regions of the hippocampus. It is responsible for much of the output of the hippocampus with its projection to layer 5 of the EC, and thus an important region where highly processed spatial information passes through. There has also been a lot of investigation into the synaptic plasticity of the CA1 pyramidal cells.

1.2.2.1 Neuroanatomy and Cell Types of the CA1

The CA1 is situated between the subiculum and CA2. It has four layers: Stratum oriens, the pyramidal layer, stratum radiatum, and alveum. The main intrahippocampal output from the CA1 is to the striatum. This projection is topographically organized in its targets, forming a column in the transverse axis (Witter, 2012). The CA1 receives intrahippocampal input both ipsilaterally and contralaterally from the CA3, called the Schaffer collaterals, alongside with smaller input from the subiculum. Furthermore, the CA1 receives input from a variety of cortical and subcortical sources (Witter, 2012). The cortical input mainly comes through the EC. The CA1 also receives inputs from the ventral tegmental area, locus coerulus, lateral supramamilary region, and the raphe complex (Witter, 2012). Further, the CA1 projects to a range of extrahippocampal regions such as retrosplenial cortex, nucleus accumbens, ventral taenia, anterior olfactory nucleus, hypothalamus, and the amygdalaliod region (Witter, 2012). Even though the hippocampus shares connections with a range of other regions, the most prominent are the ones that arise from within the hippocampus (Andersen *et al.*, 2006).

The pyramidal layer contains the principal pyramidal cell, which often exhibits spatial selectivity. The pyramidal cells are the most numerous cells of the CA1. Compared to the pyramidal cells in the other sub-regions, the CA1 pyramidal cell is smaller in size. The cells usually have one or two apical dendrites. By investigating the gene-expression

properties of pyramidal cells, it becomes apparent that the population within the CA1 is heterogeneous, and that the most prominent heterogeneity is found on the longitudinal axis (Cembrowski *et al.*, 2016). Furthermore, by investigating the functional properties using calcium imaging, it has been shown that there are differences in the firing properties in the radial axis of the CA1 (Danielson *et al.*, 2016). The heterogeneity is also illustrated by the differential projection from the EC. The lateral EC targets cells in the distal CA1 selectively, whereas the mEC projects to the proximal CA1 selectively (Witter, 2018).

Within all the layers of the CA1, heterogeneous populations of gamma-amino-butyric acid (GABA) secreting interneurons exist. One of these populations, the pyramidal basket cell, resides in proximity to the pyramidal cells. These cells receive projections from many pyramidal cells and innervate the dendrites of many pyramidal cells. Another population of interneurons in the CA1 is the chandelier cell. They also innervate many pyramidal cells, but their synapses terminate on the initial segment of the axon rather than the dendrites.

1.2.2.2 Electrophysiological and Functional Properties of Cells in the CA1

The electrophysiological properties of pyramidal cells in the CA1 are not homogenous. One study showed that there is a linear gradual increase in input resistance and resting membrane potential from ventral to dorsal (Malik *et al.*, 2016). Whereas another study showed a difference in excitability in the dorsal and ventral hippocampus, with the ventral cells being most excitable (Milior *et al.*, 2016). Further, the same study concluded that the long-term potentiation, a central mechanism in synaptic plasticity, was most pronounced in the dorsal hippocampus. Summarized, these findings indicate that cells in the ventral parts of CA1 are more likely to be active than their dorsal counterparts.

1.2.3 Dentate Gyrus

The DG has been proposed as a central structure for the transfer of information into the CA areas of the hippocampus. The DG is also one of the few brain regions that supports adult neurogenesis, making it an interesting area for investigating the functional consequences of the disrupted neurogenesis found in the *Neil3*$^{-/-}$ mouse model.

1.2.3.1 Neuroanatomy and Cell Types of the DG

Like the CA areas of the hippocampus proper, the DG consists of three layers. The layer that is closest to the hippocampal fissure and the EC is called the molecular layer (ML).

The layer deeper to the ML is the granule cell layer (GCL). The third and deepest layer is the polymorphic cell layer (PCL), which is sometimes called the hilus (Andersen *et al.*, 2006). The ML can further be divided into the inner, intermediate, and outer molecular layer (Rovira-Esteban *et al.*, 2020).

The DG consists of many different types of cells, and the most abundant glutamatergic cell is called granule cell. Granule cells exists in multiple different brain areas, but for the remainder of this text granule cells refers to the granule cells found in the DG. Granule cells are thought to be important to the formation of spatial memories based on the memory deficit that arises when these cells are abolished (Colicos and Dash, 1996). Granule cells are approximately 10 µm wide and 18 µm high and are tightly packed within the GCL. The dendrites of granule cells often extend into the ML(Witter, 2012). The input to the granule cells mainly originates in the EC, but they also receive some projections from the PCL, CA3, and the medial septum (Sun *et al.*, 2017). The Granule cell axons are called mossy fibres which are unmyelinated and terminate in the PCL and in the stratum lucidum, just above the pyramidal cell layer in CA3 (Senzai, 2019). An interesting, and somewhat controversial aspect of these mossy fibres is that they seem to be able to corelease both GABA and glutamate, and that the target synapses of these cells display synaptic plasticity depending on the layer they terminate in (Galván and Gutiérrez, 2017; Beltrán and Gutiérrez, 2012).

Within the inner ML exists a cell that has a striking similarity to granule cells, named semilunar granule cells. These cells project locally within the ML, and have large dendritic arborizations within the ML (Williams *et al.*, 2007).

Within the PCL, the most common glutamatergic cell type is called the mossy cell. This cell type receives the mossy fibres from the granule cells onto their complex spines (Witter, 2012), as well as inhibitory input from local interneurons (Sun *et al.*, 2017). Further, these cells receive both excitatory and inhibitory input from proximal CA3 (Sun *et al.*, 2017). A minor part of their input comes from areas outside of the hippocampal region, especially from the medial septum and the septofimbrial nucleus (Sun *et al.*, 2017). The mossy cells project back into the ML where they create synapses with the dendrites of granule cells, and it is thought that they play an important modulatory function (Houser *et al.*, 2021). In addition to the excitative function they have on granule cells, the mossy cells innervate interneurons which has an inhibitory effect on granule cells (Scharfman, 2018). The mossy cell constitutes the third glutamatergic cell type in the DG. This marks a striking difference from the CA fields, which only have one glutamatergic cell type.

There are also several sub-types of GABAergic interneurons in the DG. One of these is the chandelier cell that projects onto the initial segment of the axon of granule cells

(Houser, 2007). Another of these are the basket cells which project onto the soma of granule cells. Both of these two sub-populations can be identified through parvalbumin expression, and predominantly reside within the inner ML and the GCL (Rovira-Esteban *et al.*, 2020). Supressing the activity of parvalbumin expressing interneurons can decrease the coupling between the entorhinal cortex and CA1 (Aery Jones *et al.*, 2021). Somatostatin-expressing interneurons are often found in the PCL, and project both ipsilaterally within the PCL and to the contralateral medial septum (Eyre and Bartos, 2019), where they might have a role in modulating theta oscillations in the hippocampus (Colgin, 2016). Interestingly, supressing these interneurons has the opposite effect of supressing the parvalbumin expressing interneurons (Aery Jones *et al.*, 2021). These findings highlight the importance of interneurons in regulating the information flow in the hippocampus.

1.2.3.2 Electrophysiological and Functional Properties of Cells in the DG

A large proportion of the granule cells receive input with spatial tuning, but a much smaller proportion show spatial tuning themselves (Zhang, Schlögl and Jonas, 2020). This might be an indication that the granule cells encode and process the spatial information but are very selective in what information they send onto the CA3. This is further highlighted by the study of Stefanini *et al.* (2020), where they employed a machine learning algorithm to investigate the relative importance of various non-spatially tuned cells in the DG for position encoding. They found that they could decode precise position from non-spatially tuned cells. Further, they found similar results in the CA1. This indicates that if a cell has spatial tuning or not is not the most important in deciding if it plays a role in the spatial navigation system.

How many place fields the spatially selective cells have might be a defining factor of different cell types and different stages of the neuronal development. Neunuebel and Knierim (2012) propose that cells with single place fields are mature granule cells, whereas cells with multiple place fields might be mossy cells or newly born granule cells. Many of the granule cells fire more sparsely than other cells in the hippocampus, and it is hypothesized that the sparsity is strongest in the mature ones (Alme *et al.*, 2010). An interesting difference between the granule cells and the mossy cells is the position they fire in relation to the neural oscillations. Compared to mossy cells, granule cells are more strongly phase modulated, fire on earlier phases of gamma waves, and on later phases of theta waves.

1.2.3.3 Neurogenesis in the Dentate Gyrus

The DG is one of the few areas of the brain where adult neurogenesis happens (Abbott and Nigussie, 2020). Neurogenesis is the process by which neurons are produced by neural stem cells. Granule cells are generated in the subgranular zone of the DG, which is an area between the GCL and the PCL and get functionally incorporated to local neural circuits (Muramatsu *et al.*, 2007). The process of adult neurogenesis is similar to the neurogenesis that happens in prenatal and early postnatal development, with some cells continuously undergoing cell divisions, and others differentiating through several steps to become mature granule cells (Abbott and Nigussie, 2020). Adult born granule cells tend to be positioned deeper within the GCL than pre and postnatally born granule cells (Kempermann *et al.*, 2003).

NEIL3 is the primary DNA glycosylase used for the repair of hydantoin lesions of single-stranded DNA in neural stem cells, which is a factor in maintaining adult neurogenesis. As explained earlier, neural stem cells from older *Neil3*$^{-/-}$ mice showed impaired ability to undergo cell divisions (Regnell *et al.*, 2012), but the differentiation was not affected (Rolseth *et al.*, 2013), resulting in fewer adult born granule cells.

The continued supply of new neurons into the granule cell layer of DG during adult hippocampal neurogenesis suggests that neurogenesis has a role in learning and memory. Experimental evidence shows that silencing these newly born granule cells can impair memory retrieval (Gu, Janoschka and Ge, 2013). Further, newly born granule cells have increased ability to undergo synaptic plasticity, compared to older granule cells (Ernst and Frisén, 2015; Lopez-Rojas, Heine and Kreutz, 2016) .

1.2.4 Synaptic Plasticity

Synaptic plasticity refers to the change in properties of communication at the level of synapses, where experience generates neural activity that alters brain function through modifications of synaptic transmission. Synaptic plasticity is an important mechanism in shaping the neural pathways during development, and for encoding memories within neural structures. There are multiple forms of synaptic plasticity, such as facilitation, augmentation, sensitization, potentiation, and depression. These forms of synaptic plasticity can work on both a short and long time frame. For this text I will focus on long term potentiation (LTP).

LTP was first described by Bliss and Lømo (1973) and is a long-lasting increase in synaptic strength. Several properties of LTP make it important in encoding memories. The induction of LTP is quick and can last for a long time, it can select which synapses get strengthened together, and it can specify which synapses gets strengthened and which do

not. All these properties are important in creating the neural structures that are memories. LTP can work on both short and long timeframes, with different molecular mechanisms governing them (Pastalkova *et al.*, 2006). Short-LTP, which can account for the synaptic plasticity that happens within one or two hours after the experience, relies on implementing new receptors in already existing synapses, while long-LTP, which can account for the synaptic plasticity that happens later and can last for years, relies on creating new synapses (Baltaci, Mogulkoc and Baltaci, 2019).

LTP is reliant on the glutamatergic receptors N-metyl-D-aspartat (NMDA), α-amino-3-hydroxy-5-methyl-4-isoxazolepropionic (AMPA) and metabotropic glutamate receptor 5 (mGluR5). NMDA has an important function in initiating LTP by being selectively permeable to Ca^{2+}, which induces an intracellular signalling cascade that leads to either the insertion of additional AMPA receptors into the synapse or activates transcription factors that results in the creation of new synapses (Baltaci, Mogulkoc and Baltaci, 2019). When AMPA receptors are inserted into the synapse, the synapse is strengthened. mGluR5 has a mediating role in LTP by regulating the intracellular levels of Ca^{2+} (Bikbaev *et al.*, 2008).

1.2.5 Place Cells

Place cells demonstrate specificity, remapping, and stability. The spatial specificity of the place cells refers to the focality, multiplicity, and frequency of the place field in an unchanged environment. Remapping refers to the observation that when an animal moves to a novel environment, the place cells reorganise their place fields. The spatial stability of the place cells refers to the temporal stability of the place field when the animal returns to a known environment.

1.2.5.1 Specificity

Although it is most common with a single place field, CA1, CA3 and DG all display cells with multiple irregularly spaced fields (Park, Dvorak and Fenton, 2011). When the size of the recording enclosure is increased, the probability of multiple place fields increases (Park, Dvorak and Fenton, 2011). Neunuebel and Knierim (2012) propose that in the DG, cells with single place fields are mature granule cells, whereas cells with multiple place fields might be mossy cells or immature granule cells.

The place field size is variable between the place cells, but in an unchanged environment it is stable. The place field size is generally larger at the ventral pole of the hippocampus than it is at the dorsal pole, and the increase from dorsal pole to ventral pole is close to linear (Kjelstrup, K. B. *et al.*, 2008). To investigate the place field size, Hussaini

et al. (2011) used a cation channel knockout mouse model. The cation channel is highly expressed in both grid cells and CA1 place cells. They found that the knockout mice had an increase in place field size in the CA1, while CA3 was only moderately affected. This might be an indication that place field size in the CA1 place cells is more reliant on local circuitry than it is on the spatial information transfer from the grid cells. When using a genetic approach to specifically inhibit the release of vesicles from CA3 terminals, Davoudi and Foster (2019) found that the place field size increased in the CA1. Place field size is also influenced by optic flow, which is related to path integration. When Lu and Bilkey (2010) increased the optic flow information experimentally, they observed a decrease in the place field size. The place field size might also be related to the number and quality of local cues available. When Sharif *et al.* (2021) tested the difference in spatial representations in environments that were either enriched with cues or lacked cues, they found that the amount of cues had a negative correlation with the place field size.

The peak firing rate within the place fields are often stable when in an unchanged environment. The peak firing rate does not seem to be related to the place field size, as experimental manipulations of the place field size did not affect the place field peak firing rate (Hussaini *et al.*, 2011). Similarly, when Davoudi and Foster (2019) disrupted the signaling from the CA3 place cells, the CA1 place cells retained their place field peak firing rate.

1.2.5.2 Remapping

Remapping can happen at both a local scale, remapping just a subset of place cells, or at a global scale, remapping all the place cells (Muller and Kubie, 1987; Latuske *et al.*, 2017). These different remapping types are called partial and global remapping, respectively. A third type of remapping, called rate remapping, can modulate the firing rate of the place cells in response to sensory input through the EC (Rennó-Costa, Lisman and Verschure, 2010).

The cause of remapping in place cells remains to be determined. Much of the research into this has focused on the role of the medial EC. One line of inquiry has focused on determining if the mEC is detrimental to remapping. In a study by Schlesiger *et al.* (2018) where they lesioned the mEC, the place cells retained their ability to remap while changing environments. Another study by Jun *et al.* (2020) utilized Alzheimer knockin mice. In this animal model, the input cells from the mEC deteriorate faster than the place cells. They found that the place cells kept their ability to remap, even after the input from the mEC was disrupted. Another line of inquiry investigates whether there is a functional relationship between the mEC and place cells. Fyhn *et al.* (2007) found that global

remapping in place cells correlated with reorientation of grid fields in mEC. The input from mEC seems to modulate place cell remapping. Miao *et al.* (2015) did an experiment where they inactivated parts of the mEC both pharmacologically and optogenetically and found that this inactivation correlated with increased remapping of place cells in the CA3. Similarly, Rueckemann *et al.* (2016) found that inactivating the mEC optogenically caused partial remapping in CA1. A bit surprisingly, Kanter *et al.* (2017) found that activation of neurons in the mEC also correlated with remapping in CA1.

It is interesting that both the inactivation and activation of mEC neurons caused remapping but removing the input from mEC did not cause abnormal remapping. This might indicate that input from the mEC has a stabilizing role on the place cells, possibly as a function to synchronize the input from the mEC to the hippocampal place cells, so that large changes in the activity pattern of mEC cells can force remapping in the place cells. This idea is supported by the findings of Rennó-Costa and Tort (2017) who modelled the hippocampal-entorhinal circuit in silico. In the model, the input from the mEC performed as a stabilizer for the place cells, enhancing their ability to handle unstable sensory input and filter out noise. The model also showed that grid realignment can be explained in terms of place cell remapping as opposed to the reverse, in line with the observations made by Fyhn *et al.* (2007). The researchers also predicted that the mEC-hippocampus circuit is interacting in the formation of cognitive maps.

Remapping might be influenced by anxiety. Using a fear conditioning methodology, Moita *et al.* (2004) found that many of the place cells in CA1 remapped, even though the environment was unaffected. Similarly, by introducing an anxiogenic robot to the environment, Kim *et al.* (2015) found that many CA1 place cells underwent remapping. Additionally, this anxiogenic remapping was disrupted when they lesioned the amygdala.

1.2.5.3 Stability

Place cells have been shown to remain stable over long time periods. Thompson and Best (1990) showed stability that lasted up to 153 days. Place cells are reliant on protein synthesis for long-term stability, much like LTP. Agnihotri *et al.* (2004) did an experiment with injections of protein synthesis inhibitors in the CA1 while they were electrically recording place cells in the same area. They found that this intervention did not affect the short-term stability of the place fields, but the long-term stability was severely disrupted. Interestingly, this intervention did not affect the recall of already established spatial representations, indicating that protein synthesis is exclusively important in the encoding of the spatial memory. Another interesting aspect of place field stability is that it seems to

be sublayer specific, at least in the CA1. Danielson *et al.* (2016) showed that the stability of spatial representations varied considerably along the radial axis of the CA1. The deeper place cells had better stability when the mice were engaged in a goal-oriented exploration task than during normal exploration. This finding indicates that the deeper place cells of CA1 encode salient features of the environment, whereas the more superficial ones encode a stable spatial representation.

The stability of the place fields can be disrupted by perturbing different brain areas. When Jacob *et al.* (2020) lesioned the mEC of rats, and reduced the available sensory input such that the rats had to rely on self-motion cues, they found that the place field stability was significantly reduced in CA1 place cells. Similarly, when Mallory *et al.* (2018) blocked the HCN1 channels of the mEC, causing an increase in the grid scale but sparing the ability to send spatial signals, the long-term stability of place fields was disrupted. Other areas of the brain have also been shown to have an influence on place field stability. Cholvin *et al.* (2018) lesioned the reuniens and rhomboid nuclei of the ventral midline thalamus and found it produced a strong and long-lasting disruption of place field stability in CA1.

1.2.6 NEIL3 and Place Cells

Kunath *et al.* (2021) explored the functional characteristics of place cells in *Neil*3$^{-/-}$ mice. They found that there was no significant difference regarding spatial information content, spatial coherence, or within-trial spatial stability between *Neil*3$^{-/-}$ and wildtypes. Minor changes in peak firing rate, mean firing rate, and mean field size was observed between the genotypes. Further they found that the *Neil*3$^{-/-}$ mice had a higher proportion of cells that displayed multiple place fields, indicating a minor disruption of spatial specificity.

Kunath *et al.* (2021) also investigated both the long-term and short-term stability of the place fields. They found a significant difference in the place field stability between the genotypes when sessions with 3-minutes, 5-minutes, and 24-hour time gap between them were compared, with the most pronounced difference in the 24 hours stability condition. Together, these findings indicate that the stability of the place cells' spatial representation is compromised in *Neil*3$^{-/-}$ mice. They also investigated the remapping ability in *Neil*3$^{-/-}$ mice. By using a similar experimental setup as will be explained in the methods section of this text, they found that there was no major difference between the genotypes in their remapping capabilities.

1.2.7 Head Direction, Speed, and Conjunctive Cells

The cells in the hippocampus are tuned to more features than space. Sensorimotor information that is related to the path of the animal is also found in all parts of the hippocampus, but in much lower quantities than in the mEC. This text will focus on head direction, speed, and conjunctive cells, but cells that are tuned to other stimuli are also found.

Head direction (HD) cells are tuned to the HD of the animal, meaning that the cells fire preferentially in one direction (Taube, Muller and Ranck, 1990). HD cells are usually found outside of the hippocampus, but the information transfer from the mEC carries part of the HD information (Winter and Taube, 2014).

Speed cells are tuned to the speed of the animal, meaning that the firing of the cells is correlated with the speed of the animal. Speed cells are found both in the mEC and in the hippocampus (Ye *et al.*, 2018).

Some of the cells in the hippocampus are tuned to several stimuli. These conjunctive cells might have an integrative role in the hippocampal circuit, where representations of space get updated by the path integration signals (Moser, Moser and McNaughton, 2017).

1.2.8 Grid cells

Grid cells are principal neurons found in the mEC which have receptive fields much like place cells, but these fields have regular spacing and are organized in a tessellating, grid like fashion. As the grid cells are responsible for the main input to the hippocampus, an impairment in their functioning can perturb the function of the hippocampus.

The activity of grid cells is thought to provide an intrinsic metric for space (Stensola and Moser, 2016). The grid cells are organised in modules, which are sets of cells that are activated with the same spacing and orientation within the grid, but that are activated at different locations within the environments (Stensola *et al.*, 2012). The size of the receptive fields is stable within an environment, but when the environment's size and shape is changed experimentally, a similar change is seen in the receptive fields' size (Barry *et al.*, 2007).

1.3 Theories of Hippocampal Function

There have been several theories that focus on what specific function the hippocampus plays in a broader context. The theories can be broadly divided into those pertaining to episodic and declarative memory, and those pertaining to spatial navigation and spatial memory (Schiller *et al.*, 2015). These two sets of theories are not mutually exclusive, and neither provides us with a complete understanding of hippocampal function. In this text, the focus will be on the theories pertaining to spatial navigation and spatial memory as they are the ones relevant to my research questions.

1.3.1 Cognitive Map Theory

Edward Tolman (1948) postulated that the internal representation of space was reliant of a cognitive map. Cognitive maps are the mental representations of external environments. Utilizing this map, or this mental framework for familiar space, facilitates efficient and flexible navigation through the mapped space.

O'Keefe and Dostrovsky (1971) managed to pin the cognitive map to the hippocampus through a series of electrophysiological experiments. Their discovery of the place cell provided the cognitive map with a neurophysiological substrate. Later, O'Keefe and Nadel (1978) extended Tolman's cognitive map theory. The new theory included two different navigational systems: the locale and the taxon. The locale system uses allocentric information, which relates to the spatial relationship between objects or landmarks within the space. They proposed that the place cell was central in this navigational system. The taxon system uses egocentric information, which relates to the spatial relationship between the actor and the objects or landmarks. This idea of separate sub systems that process specific types of data was important for the further development of the cognitive map theory.

Modern renditions of the cognitive map theory have expanded on the function of the mapping mechanism in the hippocampus to cognitive areas such as social space (Tavares *et al.*, 2015; Park, Miller and Boorman, 2021), or abstract value space (Knudsen and Wallis, 2021), highlighting the hippocampus as an important region for higher-order cognition.

1.3.2 Pattern Separation, Completion, and Attractor Dynamics

There is a proposed mechanism responsible for separating and completing different patterns of cortical inputs that is thought to be integral in creating and differentiating

discrete memories (Leutgeb *et al.*, 2007). The pattern separating ability is thought to arise in the DG, and might be related to the sparse firing properties of the granule cells (Scharfman and Myers, 2016). When Madar, Ewell and Jones (2019) investigated the electrophysiological properties in both the input and the output of granule cells, they found that there were large temporal differences in their firing properties, indicating that the cells were indeed performing pattern separation. Others have highlighted the interconnectedness between proximal CA3 and the DG as important circuitry in the pattern separation process (Lee, Goodsmith and Knierim, 2020). Pattern completion is though to be supported by the autoassociative properties of the CA3 pyramidal cells (Leutgeb *et al.*, 2007). The autoassociative properties of the CA3 are thought to enable attractor dynamics (Rennó-Costa, Lisman and Verschure, 2014).

Attractor dynamics have been part of many models explaining the function of the spatial navigation system and memory (Knierim and Zhang, 2012; Wills *et al.*, 2005). Attractor networks can offer insights into how attractor dynamics work. Attractor networks are artificial neural networks consisting of nodes that are interconnected, often recurrently (Amit, 1989). These networks dynamically gravitate towards a stable pattern given a set input (Amit, 1989). The stable pattern is called an attractor, and the points from which the input gravitates is called an attraction basin (Hopfield, 1982). It can do so because the patterns are stored in the connections between the nodes in the network (Amit, 1989). When the network is encoding a new pattern, the connections between the nodes change, much like the synaptic strength between neurons can change through synaptic plasticity as a function of the activity in an organic neural network. Attractor dynamics is then the ability of the network activity to converge into stored patterns.

The remapping of place cells in the hippocampus implies that there are several maps stored somewhere within the spatial navigation system (Wills *et al.*, 2005). Furthermore, evidence suggests that there can be multiple stable maps stored of the same environment that changes between visits (Kentros *et al.*, 2004; Sheintuch *et al.*, 2020). There are several findings that suggest that attractor dynamics in the hippocampal networks might play a role in the encoding and retrieval of these maps. First, the fact that the place fields tend to remain stable while in a unchanging environment suggests that the network settles into a stable state, much like an attractor network would (Sheintuch *et al.*, 2020). Second, the fact that remapping often occurs on a global scale indicates that this happens at a meso level, as attractor dynamics do. Third, as attractor networks often are, some of the connectivity in parts of the hippocampus is recurrent (Miles *et al.*, 2014; Núñez-Ochoa *et al.*, 2021; Jensen *et al.*, 2021). Attractor networks also offer a possible explanation to how multiple maps of the same environment can co-exist. An attractor network can sometimes converge on an alternative pattern if the input has high variability.

The input to the hippocampal network can have high variability as a result of a range of factors, such as the biophysical processes inherent in neurons (Faisal, Selen and Wolpert, 2008), or attention, which has been shown to influence place field stability (Kentros *et al.*, 2004). If the input has a high degree of noise, the network might converge on an alternative pattern, and thus show a different neural activity pattern as a representation of the same space.

Many of the classical models of the functional relationship between mEC and hippocampal place cells propose a feedforward mechanism where entorhinal activity drives hippocampal activity or vice versa. Agmon and Burak (2020) propose a model based on joint attractor dynamics. One part of this model relates to how the reciprocal connectivity between grid cells and place cells can function as an error correcting mechanism, similar to the stabilizing role of the grid cell input suggested by Rennó-Costa and Tort (2017). This mechanism can eliminate drifts in the representation of position by distinct grid cell modules, independent of sensory inputs. They found that this model had good performance compared to other models, and that it could account for findings such as those of Kanter *et al.* (2017), who found that both hyperpolarizing and depolarizing grid cells lead to remapping of place cells, which is a finding that can't easily be explained by classical models.

1.4 Research Questions and Hypotheses

The main aim of this study is to elucidate whether NEIL3 impacts the functional plasticity of hippocampal place cells in the CA1 and DG. The secondary aim of this study is to investigate if NEIL3 impacts spatial memory and anxiety. Five research questions are asked, and they are as follows:

Question 1: Whether NEIL3 impacts the spatial specificity of hippocampal place cells.

Question 2: Whether NEIL3 impacts the spatial remapping of hippocampal place cells.

Question 3: Whether NEIL3 impacts the spatial stability of hippocampal place cells.

Question 4: Whether NEIL3 impacts anxiety.

Question 5: Whether NEIL3 impacts spatial memory.

2 Methods

To address the aims of this study, a series of electrophysiological and behavioural experiments were conducted. This methods section will first describe the animals I used and how they were treated, then the electrophysiological experiments will be described, and finally the behavioural experiments will be described.

2.1 Animal work

All the animal work has been performed in compliance with *The Norwegian Animal Welfare Act* and *The Norwegian Regulation on Animal Research.* All animal work was performed at an approved animal facility managed by the Comparative Medicine Core (CoMed) at NTNU. This masters project is a part of a larger project that has been approved by the Food Safety Authority (FOTS: 23840). The project has been evaluated to moderate severity due to the intra-cranial surgery which might cause distress during recovery. The mice were housed in the specific pathogen free unit with a 12-hour light/dark cycle (light 18:00-06:00) at 55-65% relative humidity and 23±2°C. The mice had free access to food (Ssniff) and water.

2.1.1 Ethics

Overall, the benefits of the findings are considered to outweigh the harm to the animals. This is ensured by utilizing the three R's. The three R's are guiding principles meant to promote ethical use of research animals. These principles were first published by Russell and Burch (1959). The three R's stand for Replacement, Reduction, and Refinement. Replacement is about finding alternatives to using research animals. Reduction is about reducing the number of animals used. Refinement is about making the lives of research animals as good and as pain free as possible.

I consider there to be no other alternatives to using research animals, as there is not enough data on the effects of this glycosylase on the hippocampal system to simulate experiments. Mice are widely used experimental animals and have been extensively used in comparative medicine, making them a fitting model organism. To reduce the number of animals used, I extracted as much data from each animal as possible. In addition to this I took measures to avoid that the experiments resulted in bad data, such as keeping surgeries as sterile as possible and keeping the animals healthy. Further, the animals used

in this study will contribute to other studies on the NEIL glycosylases. To optimize the well-being of the animals I gave them enhanced housing with extra shelter, gnawing sticks, and nesting materials. The animals were also housed with siblings as much as possible. After any surgical procedure, the animals were inspected daily to ensure that their well-being was satisfactory.

2.1.2 Mouse Models

As a mouse model the C57BL/6N strain with a knockout of the *Neil*3 gene (*Neil*3$^{-/-}$) was used. This is the same strain as used by Sejersted *et al.* (2011). The same mouse strain without the knockout was used as a control (Wildtype). All the mice included in this study were male.

2.2 Electrophysiology

The electrophysiological experiments were done to investigate the main aim of the of this study, whether NEIL3 impacts the functional plasticity of hippocampal place cells in the CA1 and DG.

2.2.1 Microdrives

MDR-xx Microdrives from Axona (Axona) were wired with four tetrodes (sixteen electrodes). The electrodes were made of a platinum and 10% iridium alloy wire (California Fine Wire Co., USA). Each connection between the electrode and the drive was coated with electrically conductive silver paint (Electrolube) and insulated with nail polish. The tetrodes were then cut to between six and seven millimetres and plated with platinum (Neuralynx) by applying an electric pulse generated with a 10Mhz pulse generator (Thurlby Tandar Instruments), amplified by Axona DasqUSB stimulus isolator (Axona), by as much as was required to get the impedance of the electrode to around Z = 200kΩ, measured with a multimeter (Escort Instruments Corporation).

2.2.2 Surgical Implantation

The surgery was performed by a colleague in the research group, with me assisting and doing parts of the surgery. The mice were first anaesthetised with isoflurane and secured to a stereotaxic instrument. The isoflurane dosage (around 0.6% in pure oxygen) was regulated during the surgery by observing the breathing rate of the mice. A subcutaneous

dose of Marcain (diluted 1:5 with saline solution, making the dose 0.5 mg/ml, and given 1,0 mg/kg) was injected over the cranium for local analgesia. Temgesic (diluted 1:10 with saline solution, making the dose 0.03 mg/ml, and given 0,6 mg/kg) and Metacam (diluted 1:10 with saline solution, making the dose 5 mg/ml, and given 1,0 mg/kg) were administered intraperitoneally for systemic analgesia. The eyes of the mice were protected by a layer of moisturising eye gel (Viscotears) during the surgery. A 2 cm incision was made with a scalpel to expose the skull and the remaining skin covering the skull was removed with surgical scissors. The tissue and any piece of debris covering the skull was removed with sterile Q-tips. Then two holes were drilled in the skull. The first hole was for the grounding screw and was located at approximate stereotactic coordinates: AP[Bregma]: 0.2 mm, ML: 0.5 mm. The second hole was for the tetrodes and was located at stereotactic coordinates: AP[Bregma]: -2 mm, ML: -1.8 mm. After the holes were made, the grounding screw was inserted with the help of a sterile screwdriver. The tetrode hole was covered with an absorbable haemostatic gelatine sponge (ETHICON) soaked in saline solution. With the bigger hole protected, the surface of the skull was scratched with a 19G needle and covered with histoacryl (B|BRAUN) which was allowed to set. After this the microdrive was mounted to the stereotaxic instrument, the sponge was removed, the dura mater was pierced inside the hole, and the tetrode was implanted at stereotactic coordinates: AP[Bregma]: -2 mm, ML: -1.8 mm, DV: -0.8 mm. A protective outer cannula was then lowered to cover the exposed tetrodes, and a protective layer of sponge was spread around the outer cannula. For the last part of the procedure, the skull was covered with dental cement which provided a secure foundation for the Microdrive. The dry cement and drive were covered with a thin layer of surgical tape to prevent tearing or pulling.

After the surgery the mice were administered antibiotics (Baytril, Bayer Animal Health GmbH, at a dose of 2 mg/kg) and analgesics (Metacam) for three days. They were housed in a custom cage which had higher ceiling so that the microdrive would not crash. The mice were given wet food during the recovery phase. They were also checked daily for pain and infection symptoms for the rest of their life.

2.2.3 Electrophysiological Recording

All the recordings were done in a recording room, which was a dimly lit soundproofed room in the animal facility. The recording space was on a table inside this room, surrounded by lightproof curtains. All recordings were done during the dark cycle, and the mice had spent at least one week in this cycle before the experiments began. All the equipment that came in contact with the mice were washed with a lemon scented soap between trials to reduce olfactory cues. The recording box (50L x 50W x 30H cm) that had black walls and a black

antistatic floor mat. The box had a white cue card on one of the walls. There was a counterbalanced cable suspended above the recording area for connecting the headstage (Axona) with the microdrive. The headstage was fitted with two different LEDs, making it possible to record head direction and position. This LED signal was captured by a camera (CBC Co. Ltd). The electric signal was routed through a preamplifier (Axona) and a system unit (Axona) before it was recorded in the software DacqUSB (Axona). The mice were recorded for 20 mins while they were scavenging for crumbs of a chocolate flavoured cereal (Weetabix) and for small deposits of vanilla sugar (Freia).

To clean up the single unit signal, a bandpass filter was employed, including only frequencies between 300 and 7000 Hz. The gain and threshold were set on a case-to-case basis based on the signal. For the EEG, a Bessel lowpass filter allowing frequencies under 1000 Hz was employed. A channel without neural activity was chosen for reference before every recording session. The reference channel was used to remove the noise and make the signal more apparent.

During the recording phase, the tetrode was gradually lowered through turning a nut on the drive. The tetrodes were lowered in 25 µm increments to find new cells. Each recording session was registered in a recording journal, so that I had control over the depth.

2.2.4 Remapping and Stability

To investigate remapping capabilities of the place cells, I utilized two open field boxes. The first box, henceforth called box A, was the same box used for the regular recordings. The second box, henceforth called box B, had the same size as box A, but had white walls and a black cue card fixed to a different position than box A. Box B was the same box used for the behavioural experiments. The mice were recorded in box A first for 20 minutes, then in box B for 20 minutes, then in box B again for 20 minutes, then lastly in box A again for 20minutes. All these sessions had a three-minute break between them where mice waited in their housing cage while the box was cleaned. A graphical overview of this procedure is presented in Figure 2A. Short term stability was assessed by comparing the A1 and A2 recordings.

To investigate the long-term stability of the spatial representation I recorded in the same box at the same recording depth with a 24-hour break between. A graphical overview of this procedure is presented in Figure 2B.

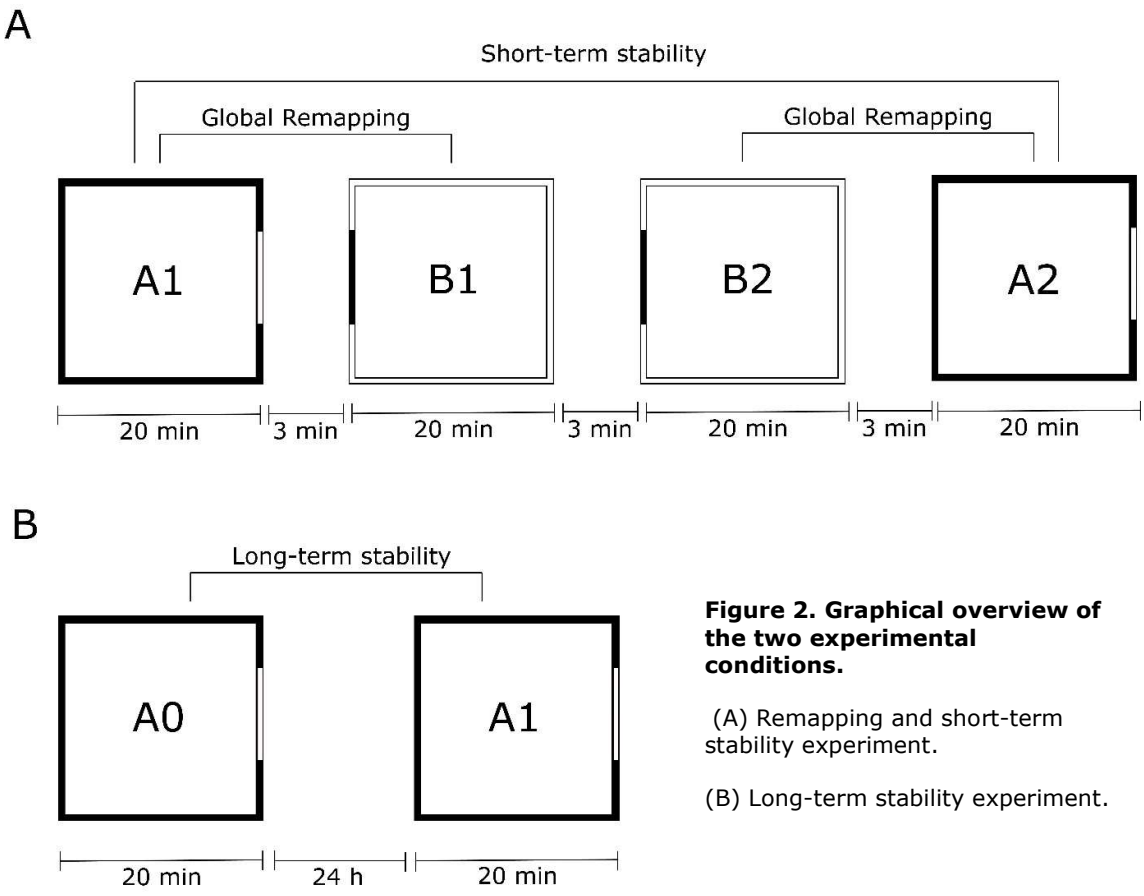

Figure 2. Graphical overview of the two experimental conditions.

(A) Remapping and short-term stability experiment.

(B) Long-term stability experiment.

2.3 Behavioral Testing

Three behavioural experiments were conducted to address the secondary aim of this study. All the experiments were recorded in the ANY-maze software (Stoelting) with a mounted optical camera over the recoding area. The recording room was the same room used for the electrophysiological recordings. The recording space was on a table inside this room, surrounded by lightproof curtains. All behavioural experiments were done during the dark cycle, and the mice had spent at least one week in this cycle before the experiments began. All the equipment that came in contact with the mice was washed with a lemon scented soap between trials to reduce olfactory cues. The cage locations in the dark room were randomized as much as possible to account for effects of light and sound pollution as well as effects of feeding and bedding sequence. The order the mice were tested in was also randomized.

2.3.1 Handling and Acclimation

Before the experiments started, the mice were habituated to handling. I handled the mice by lifting them by their tails several times. After each tail lifting session, the mice were put on a light proof transportation trolley and moved to the recording room to habituate them to the transportation. In the dimly lit recording room, they were split from their shared housing into individual resting cages and left there for at least 5 minutes. After this they were taken back into the dark room. This habituation procedure was repeated for three days. Before the experiment started, the mice were acclimatised to the recording room by sitting in their resting cages for 30 minutes.

2.3.2 Open Field

A modified protocol (Seibenhener and Wooten, 2015) of the open field experiment (Hall and Ballachey, 1932) was used to assess the anxiety and general locomotor activity of the mice. To assess anxiety, I considered time spent in the corners, time spent in the centre, and the time it took before the centre zone was entered for the first time. To assess general activity levels, I considered the total distance travelled, the average speed, and the number of times the mice crossed the borders between zones. This method has previously been validated for measuring anxiety (Carola *et al.*, 2002). The recording enclosure was 50L x 50W x 30H cm with white walls made of PVC plastic and a white floor. A black proximal cue card was placed inside the recording box. An area in the middle (33.3L x 33.3W cm) was defined as the centre zone. The mice were placed into the releasing corner of the box by tail handling, facing the corner. They were then allowed to freely explore the box for 10 minutes. A graphical overview of this procedure is presented in Figure 3.

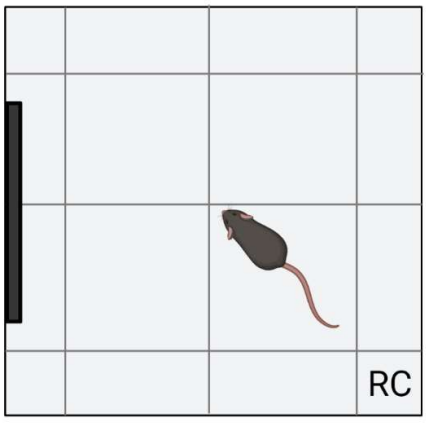

Figure 3. Graphical overview of the open field task.
RC = Releasing corner.
The figure was created in BioRender.

2.3.3 Novel Object Location

A modified protocol of the novel object location (NOL) experiment (Denninger, Smith and Kirby, 2018) was used to assess long-term memory (LTM) and short-term memory (STM). The novel object location experiment evaluates hippocampal dependent spatial learning (Denninger, Smith and Kirby, 2018). It does so by habituating the mice to the placement of two objects within an enclosure for the habituating phase, and then moving one of the objects for the test phase to see if the mice showed renewed interest for the moved object. The enclosure is the same as in the open field experiment. In the habituation phase, which lasts for three sessions, the mice are allowed to freely explore the box and objects for 10 minutes. In the test phase, I recorded if the mice spent more time exploring the object in the novel location compared to the object in the familiar location. The recording time was 10 minutes for the habituation periods with 24-hour intervals between each session for the LTM condition and with five-minute intervals for the STM condition. The recording for the test phase was finalised when the mouse had spent an accumulative time of 30 seconds in the novel and familiar quadrants. A graphical overview of this procedure is presented in Figure 4.

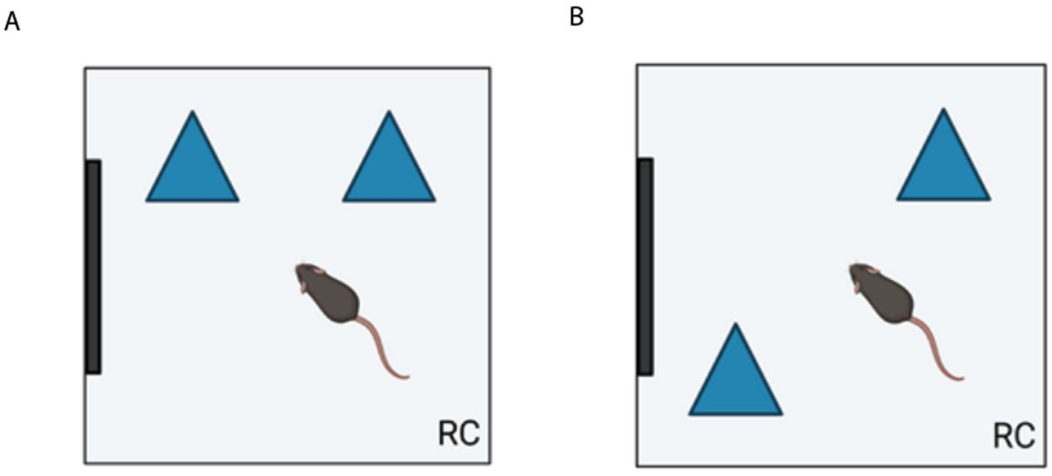

Figure 4. Graphical overview of the NOL task.
RC = Releasing corner. A = habituation phase, B = test phase. The thick black line illustrates the proximal cue card. The triangles illustrate the objects. The figure was created in BioRender.

2.3.4 Y-maze

A modified protocol of the Y-maze experiment was used to assess LTM (Sanderson *et al.*, 2009). The Y-maze experiment utilizes the inherent exploratory behaviour of mice to assess hippocampal dependent spatial reference memory (Kraeuter, Guest and Sarnyai, 2019). It does so by habituating the mice to a y-shaped maze which has one of the arms closed off. Two distal cue cards with different symbols were placed on the surrounding curtains to help the mice orient themselves. After a six-day habituation phase, where the mice are left to freely explore the restricted maze for five minutes, the mice are tested in the maze with both the arms open for five minutes. If the mouse remembered the maze, it should spend more time exploring the novel arm compared to the familiar arm. The recording time was five minutes with 24 hours intervals between each session for the LTM and with five minutes intervals for the STM. A graphical overview of this procedure is presented in Figure 5.

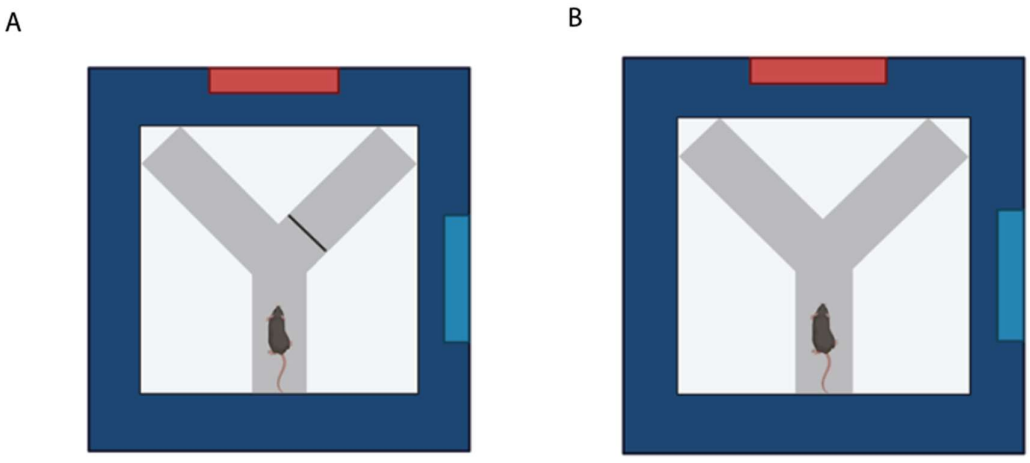

Figure 5. Graphical overview of y-maze task.
A = habituation phase, B = test phase. The dark blue surrounding illustrates the light proof curtains, while the red and blue lines illustrate the distal cue cards that are fixed to the curtains. The figure was created in BioRender.

2.4 Perfusion

To perfuse the mice which were not implanted with a microdrive, they were first anaesthetised with isoflurane, and then administered intraperitoneal pentobarbital (Norges Apotekerforening, 100mg/ml, 0.01ml/g) for a strong analgesic effect. They were then fixed in a supine position. Then an incision was made from the neck to the abdomen, and the rib cage cut open, exposing the heart. The descending aorta was clamped shut with a haemostatic clamp, the right atrium was punctured, and 60ml of 0.9% saline was injected into the left ventricle of the heart. After the profusion, the mice were decapitated, and the scalp and scull were removed so the brain could be extracted. The brain was then extracted and divided down the fissura longitudinalis cerebri. The right hemisphere was fixated in 4% paraformaldehyde/ phosphate-buffered saline (PBS) solution, whereas the left hemisphere was micro-dissected into CA1, CA3, and DG before it was deep frozen with liquid nitrogen. The micro-dissected sections were used in a different study.

To perfuse the mice which were implanted with a microdrive, a perfusion almost identical to the one done by non-implanted mice was done, but the whole head was suspended in 4% paraformaldehyde/PBS solution for 24 hours before I unscrewed the tetrode nut, removed the external tissue and skull bones starting ventrally, and extracted the brain. The whole brain was fixated in 4% paraformaldehyde/PBS solution.

2.5 Cryo-Sectioning

After the brains of the tetrode implanted mice had been fixated for minimum 48 hours, I performed cryo-sectioning on them using a cryostat. First, I sectioned the brain through the fissura longitudinalis cerebri with a scalpel. Each hemisphere was then mounted to the cryo-stat metal socket with the use of a mounting medium. The hemisphere was then put in the cryostat for deepfreezing while I sprayed it with Cold spray at -55ºC (Taerosol). I cut the brains in 30 µm thick saggital sections, half of which were mounted on histological glass slides, while the other half were put into a 24 well plate with ProClin300 (Sigma-Aldrich)/PBS (VWR chemicals) (at a ratio of 500µl of ProClin300 per 1L of PBS) solution.

2.6 Histology

The brain sections that were mounted on the histological glass slides were stained shortly after cutting them. This was done with a modified cresyl violet procedure. First, I soaked the slides in distilled water for 2 minutes, and then I dehydrated them by dipping them 10 times up and down into 70% - 80% - 90% - 100% ethanol sequentially. The ethanol

solutions were made by diluting absolute ethanol (VWR Chemicals) with distilled water. Then the slides were put into pure xylene (Sigma-Aldrich) for 2 minutes before it was rehydrated in 100% - 90% - 80% - 70% ethanol and put in differentiation solution (consisting of 0.5% acetic acid in 70% ethanol) for 5 minutes. After this the slides were rinsed in distilled water and stained in cresyl violet solution (made by mixing 30ml of a stock solution consisting of 0.2g cresyl violet-acetate (Sigma-Aldrich) in 150 ml distilled water and 300ml pH 3.5 buffer solution consisting of 282 ml of 0.1 M acetic acid (Sigma-Aldrich) and 18 ml of 0.1 M sodium acetate (Sigma-Aldrich)) for 8 minutes. After the staining, the slides were washed in water and differentiation solution until the colour of the sections was appropriate. Then the slides were dehydrated in 70% - 80% - 90% - 100% ethanol and put in xylene for 10 minutes before it was finally sealed with cover glass on the slides using Eukitt mounting oil.

The slides where then scanned in an Axioscan microscope (Zeiss) that rendered high resolution images of the whole brain section. All the images were inspected for traces of the tetrodes. The images with a visible trace were edited in photoshop (Adobe) where I cropped the irrelevant parts, adjusted the angle so the pictures were easier to compare, and adjusted the contrast so that the trace was easier to see.

2.7 Analyses

The data for both the cell physiology and behavioural parts were organised using Microsoft Excel. All pre-processing of the cell physiology data were done in Matlab (Mathworks) using the Behavioural Neurology Toolbox (BNT) toolbox developed by the Kavli Institute of Systems Neuroscience at NTNU. All pre-processing of the behavioural data were done in ANY-maze (Stoelting). All statistical analyses were performed in R (The R Foundation), using Rstudio (Rstudio, PBC) as an integrated development environment.

BNT was used for extracting spatial information content, spatial information rate, average firing rate, spatial stability, head direction scores, speed scores, place field size, place field peak firing, number of fields for each cell, rate maps, shuffling, and correlation of rate maps between sessions. Statistical analyses in R were performed using the library rstatix (Kassambara, 2021) and the figures were created using the library ggplot2 (Pedersen, 2022).

2.8 Key Resources

Table 1. Summary of used resources

RESOURCE	SOURCE	IDENTIFIER
Chemicals		
Acetic acid	Sigma-Aldrich	CAS 64-19-7
Cresyl Violet Acetate	Sigma-Aldrich	CAS 10510-54-0
Ethanol absolute	VWR chemicals	CAS 64-17-5
Eukitt Mounting Medium	Sigma-Aldrich	CAS 25608-33-7
PBS	VWR chemicals	E404-100TABS
Sodium acetate	Sigma-Aldrich	CAS 6131-90-4
Xylene	Sigma-Aldrich	REACH 01-2119488216-32-XXXX
Mouse Models		
C57Bl6N wildtype mice	Janvier Labs	Bx 239294
Neil3$^{-/-}$ mutant mice	Own breed	Gene ID 234258
Software		
ANY-maze	Stoelting Co.	https://www.any-maze.com/
BioRender	BioRender	https://biorender.com/
dacqUSB	Axona	https://www.axona.com
Excel v.2201	Microsoft	https://www.microsoft.com/en/
Illustrator	Adobe	https://www.adobe.com/
MATLAB R2021a	Mathworks	https://se.mathworks.com/
Photoshop	Adobe	https://www.adobe.com/
R 4.1.2 - Bird Hippie	The R Foundation	https://www.r-project.org/
Rstudio build 382 - Ghost Orchid	Rstudio, PBC	https://www.rstudio.com/
Tint graphical clustering software	Axona	https://www.axona.com
Hardware		
Axioscan	Zeiss	https://www.zeiss.com/
dacqUSB Preamp	Axona	https://www.axona.com
dacqUSB System Unit	Axona	https://www.axona.com
Elc-131d LCR meter	Escort Instruments Co.	
GANZ CCD color camera	CBC Co. Ltd	
Headstage	Axona	https://www.axona.com
MDR-xx Microdrives	Axona	https://www.axona.com
Platinum and 10% iridium alloy wire	California Fine Wire Co.	https://calfinewire.com/
Pulse Generator TGP110 10MHz	Thurlby Tandar Instruments	https://www.ttid.co.uk/pulse-generators/aim-tti/tgp110
Stimulus isolator	Axona	https://www.axona.com
Surgery materials		
Eye Gel	Viscotears®	https://www.medicines.org.uk/emc/product/2310/smpc
Haemostatic gel sponge	Ethicon	https://www.jnjmedtech.com/en-EMEA/product/spongostan-absorbable-haemostatic-gelatin-sponge
Histoacryl	B|Braun	https://www.bbraun.com/en/products/b/histoacryl.html
MELIODENT Rapid repair liquid	Kulzer GmbH	https://www.kulzer.com/int2/en/products/meliodent-rr.html
MELIODENT Rapid repair powder	Kulzer GmbH	https://www.kulzer.com/int2/en/products/meliodent-rr.html

Platinum plating solution	Neuralynx	https://neuralynx.com/hardware/platinum-black-plating-solution
Saline 0.9%	BBraun	https://www.bbraun.com/en/products/b0/nacl-0-9-b-braun.html
Silver Conductive paint	Electrolube	https://electrolube.com/
Drugs		
Baytril	Bayer Animal Health GmbH	https://www.felleskatalogen.no/medisin-vet/baytril-vet-bayer-animal-health-gmbh-546731
Isoflurane	Baxter	ATC N01A B06
Marcain	Aspen Pharma	https://www.felleskatalogen.no/medisin/pasienter/pil-marcain-aspen-561225
Metacam	Boehringer Ingelheim	https://www.boehringer-ingelheim.com/animal-health/livestock-products/metacam
Pentobarbital NAF	Norges Apotekerforening	ATC QN51AA01
Temgesic	Indivior	https://www.felleskatalogen.no/medisin/temgesic-indivior-564488
Other materials		
Cold spray	Taerosol	101 Cold spray Green Non-flammable - Taerosol
V1536	Ssniff	https://www.ssniff.com/index.php?pcid=9&pdid=15
Vanilla sugar	Freia	https://www.freia.no/
Wheetos Choco	Weetabix	https://weetabix.no/our-products/weetos/weetos/

3 Results

A series of analyses were conducted to investigate the influence of NEIL3 on memory, anxiety, and hippocampal functional plasticity. The first part of this section appertains to the electrophysiological experiments, while the second part appertains to the behavioural experiments.

3.1 Cell Physiology

To investigate whether NEIL3 impacts the functional characteristics of hippocampal cells, I recorded the activity of hippocampal CA1 and DG cells in behaving mice and conducted a series of analyses on the recorded electrophysiological data. A total of four mice were implanted successfully, where two were *Neil3*$^{-/-}$ mice and two were wildtype mice. Cells from one wildtype and one *Neil3*$^{-/-}$ mouse were included in the analysis due to time constraints.

3.1.1 Clustering

I used offline graphical clustering software Tint (Axona) to separate cell clusters in the recorded animals. The recording data are represented in a two-dimensional feature space, and I clustered cells based on parameters such as the distance between the peak and the trough of the waveform, voltage as a function of time, amplitude of the peak, amplitude of the trough, time of peak, time of trough, or principal components based on a principal components analysis. An example of this clustering procedure is seen in Figure 6A-B.

Based on this feature space, I manually grouped the recording data into cell categories. These cell categories were then inspected for diverging waveforms and subsequently cleaned up if they were found. The temporal characteristics of the electric activity was also inspected. A neuron has an absolute refractory period, in which it cannot fire another action potential within 2 ms. Because of this, a cell category with spikes that were less than 2 ms apart required more cleaning. An example of the waveforms that were extracted through this clustering process is presented in Figure 6C. Once the spike activity of a cell was clustered, a rate map, a trajectory map and a polar map were generated by Tint, which allows for a visual indication of whether the cell is spatially tuned (Figure 6D

and 6E). In total, I clustered 408 cells in one wildtype mouse and 211 cells in one *Neil3*$^{-/-}$ mouse and these cells were analysed further.

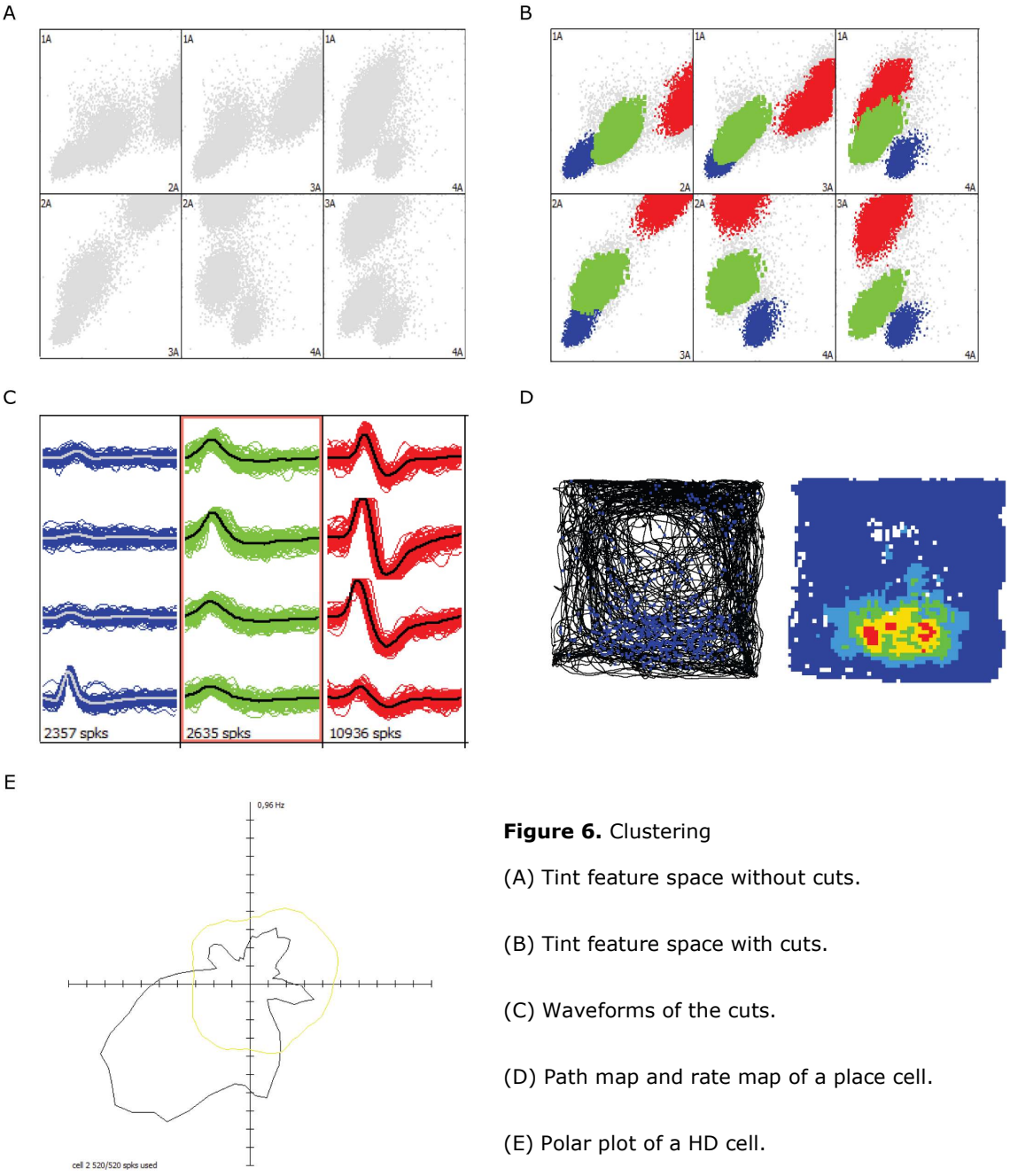

Figure 6. Clustering

(A) Tint feature space without cuts.

(B) Tint feature space with cuts.

(C) Waveforms of the cuts.

(D) Path map and rate map of a place cell.

(E) Polar plot of a HD cell.

3.1.2 Determining Location

The tetrode trace was visualized by cresyl-violet staining. Long tetrode traces passing through hippocampal CA1 and DG regions of the *Neil3*$^{-/-}$ mouse were detected, confirming the location of recorded cells in these animals. I could not find a clear trace through the CA1 for the wildtype (Figure 7), but it is visible through the DG. To further separate the recorded CA1 and DG cells, I grouped the cells recorded from DV1050 to DV1250 in the wildtype and DV1200 to DV1300 in the *Neil3*$^{-/-}$, as CA1 cells based on the detection of dramatic cell activity and θ-modulated EEG. When the tetrodes passed the CA1 pyramidal region, a gap of about 300 µm was found with less cell activity. When the tetrodes reached the DG granular layer, more active cells emerged. I grouped the cells recorded from DV1550 to DV1750 in the wildtype and DV1575 to DV1850 in the *Neil3*$^{-/-}$ as DG cells. In total, I recorded 246 cells in CA1 and 162 cells in DG of the wildtype mouse and 106 cells in CA1 and 105 cells in DG of the *Neil3*$^{-/-}$ mouse. These cells were analysed further.

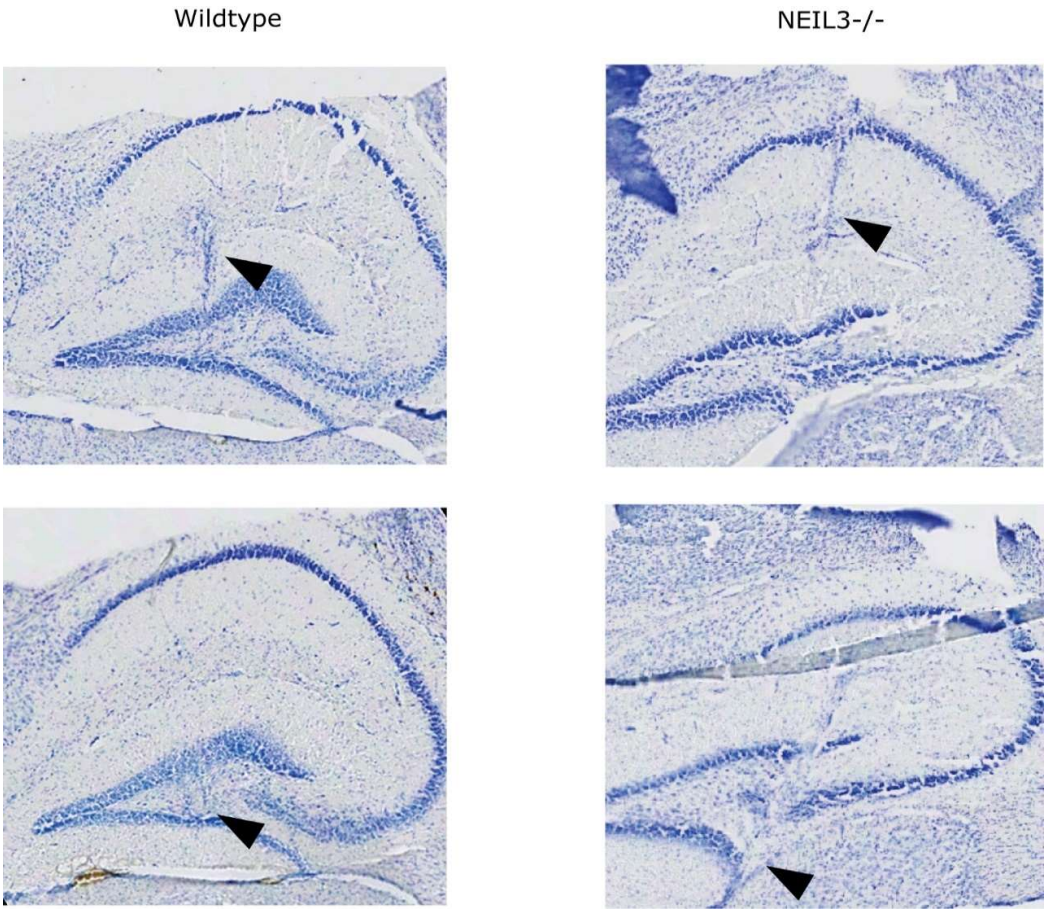

Figure 7. Cresyl-violet stained brain sections.
The black arrow points at the trace.

3.1.3 Classification of Cell Types

A total of 619 cells were included in the analysis, with 246 belonging to the wildtype in CA1, 162 belonging to the wildtype in DG, 106 belonging to the *Neil3*$^{-/-}$ in CA1, and 105 belonging to the *Neil3*$^{-/-}$ in DG. To classify the different cell types a series of different variables were calculated and used as criteria for the inclusion to each category. Cells from wildtype CA1 and wildtype DG, *Neil3*$^{-/-}$ CA1 and *Neil3*$^{-/-}$ DG were analysed in separate populations. A summary of relevant statistics for the classification of cell types is found in Table 2.

To classify place cells I first calculated the spatial information content based on the information theoretic approach described by Skaggs, McNaughton and Gothard (1992). The information content equation is:

$$I = \sum p_x \left(\frac{\lambda(x)}{\lambda}\right) \log_2 \left(\frac{\lambda(x)}{\lambda}\right)$$

where I is the information content in bits per spike for each cell, x is the bin number, $P(x)$ is the probability for the mouse being at bin x, $\lambda(x)$ is the mean firing rate when the mouse is at x, and λ is the total mean firing rate of the cell. The spatial information content is a measure of the amount of information about the location of the animal that is carried by the firing properties of the cell. I then shuffled the data by redistributing the spikes of a cell randomly across the path of the animal. Each shuffle iteration was done 100 times. The shuffled and observed values for spatial information content is presented in Appendix A and B. Further, I filtered out the cell activity in which the mouse was moving less than 2 cm/s and above 100 cm/s, cells that had less than 100 spikes, cells that did not have a clear place field, the cells that had less than 0.1 Hz firing rate, the cells that had more than 7Hz firing rate, and the cells that displayed a spatial correlation less than 0.5 between the first and second half of the recording. After these filters, the cells passing the criteria of a 95th percentile cut-off for the spatial information content were classified as place cells. Further, rate maps were calculated by adding up the spikes in each location in the recording arena and dividing that by the time the mouse spent in this location. The locations were binned into 2.5 cm bins. The map was then smoothed with a gaussian distribution in the centre of each bin. A total of 178 (29% of the total cell number) cells were classified as place cells, where 84 (54% of the total cells in this condition) belonged to the wildtype mouse in the CA1, 13 (12% of the total cells in this condition) belonged to the *Neil3*$^{-/-}$ mouse in the CA1, 49 (30% of the total cells in this condition) belonged to the wildtype mouse in the DG, and 32 (30% of the total cells in this condition) belonged to the *Neil3*$^{-/-}$ mouse in the DG, as shown in Table 2.

To classify HD cells, I first calculated head direction from the relative angle between the LEDs on the headstage. Then the head direction scores were computed by binning the head direction as a function of the action potential into 3-degree bins, creating a total of 120 bins. Then the mean length of the HD modulated neural activity vector was used as the head direction score. The head direction score indicates how well the spikes are tuned to the cells preferred angle. I then shuffled the head direction scores identically to the information content shuffling. A 99th percentile cut-off on the shuffled data was used to classify HD cells. The shuffled and observed values for the head direction score is presented in Appendix C and D. A total of 39 (6% of the total cell number) cells were classified as HD cells, where 24 (10% of the total cells in this condition) belonged to the wildtype mouse in the CA1, 5 (5% of the total cells in this condition) belonged to the *Neil3*$^{-/-}$ mouse in the CA1, 8 (5% of the total cells in this condition) belonged to the wildtype mouse in the DG, and 2(2% of the total cells in this condition) belonged to the *Neil3*$^{-/-}$ mouse in the DG, as shown in Table 2.

To classify speed cells, I first calculated the speed score by binning the recorded speed between 5 and 100 cm/s into 2 cm/s bins. These bins were then correlated with the firing rate. I then shuffled the data identically to the information content and head direction score. A 99th percentile cut-off on the shuffled data was used to classify speed cells. The shuffled and observed values for the speed score is presented in Appendix C and D. A total of 224 (36% of the total cell number) cells were classified as speed cells, where 80 (33% of the total cells in this condition) belonged to the wildtype mouse in the CA1, 44 (42% of the total cells in this condition) belonged to the *Neil3*$^{-/-}$ mouse in the CA1, 64 (40% of the total cells in this condition) belonged to the wildtype mouse in the DG, and 36 (34% of the total cells in this condition) belonged to the *Neil3*$^{-/-}$ mouse in the DG, as shown in Table 2.

Conjunctive cells were classified by their belonging to multiple of these cell groups. A total of 20 (3% of the total cell number) cells were classified as place and HD conjunctive cells, where 12 (5% of the total cells in this condition) belonged to the wildtype mouse in the CA1, 2 (2% of the total cells in this condition) belonged to the *Neil3*$^{-/-}$ mouse in the CA1, 4 (3% of the total cells in this condition) belonged to the wildtype mouse in the DG, and 2 (2% of the total cells in this condition) belonged to the *Neil3*$^{-/-}$ mouse in the DG, as shown in Table 2. A total of 58 (9% of the total cell number) cells were classified as place and speed conjunctive cells, where 31 (13% of the total cells in this condition) belonged to the wildtype mouse in the CA1, none belonged to the *Neil3*$^{-/-}$ mouse in the CA1, 19 (12% of the total cells in this condition) belonged to the wildtype mouse in the DG, and 8 (8% of the total cells in this condition) belonged to the *Neil3*$^{-/-}$ mouse in the DG, as shown in Table 2. There were 3 (0.5% of the total cell

number) cells that were classified as conjunctive place, HD and speed cells, and they all belonged to the wildtype mouse in the CA1 (1% of the total cells in this condition).

In summary, I classified the cells into six categories: place cells, HD cells, speed cells, conjunctive place and HD cells, conjunctive place and speed cells, and conjunctive place, HD, and speed cells. Of particular importance is the place cells, in which there was a low population of in the CA1 of the *Neil3*$^{-/-}$ mouse.

Table 2. Summary for Cell Classification.

	CA1		DG	
	WT	***Neil3*$^{-/-}$**	**WT**	***Neil3*$^{-/-}$**
Total Cells	246	106	162	105
Spatial Information Content Shuffled (P95)	0.404	0.394	0.502	0.639
Spatial Information Content Shuffled (P99)	0.616	0.586	0.758	1.456
Number of place cells (% of total)	84 (54%)	13 (12%)	49 (30%)	32 (30%)
Spatial Stability half and half (mean±SEM)	0.57±0.02	0.70±0.05	0.65±0.04	0.77±0.02
Head Direction Score Shuffled (P99)	0.223	0.208	0.280	0.372
Number of head direction cells (n, % of total)	24 (10%)	5 (5%)	8 (5%)	2 (2%)
Speed Score Shuffled (P99)	0.149	0.155	0.158	0.085
Number of Speed Cells (n, % of total)	80 (33%)	44 (42%)	64 (40%)	36 (34%)
Conjunctive Place and Head Direction Cells (n, % of total)	12 (5%)	2 (2%)	4 (3%)	2 (2%)
Conjunctive Place and Speed Cells (n, % of total)	31 (13%)	0	19 (12%)	8 (8%)
Conjunctive Place, Head Direction and Speed Cells (n, % of total)	3 (1%)	0	0	0

Note. The *% of the total cells* refers to the proportion of relevant cells compared to the total number of cells in that condition.

3.1.4 Place cells

To investigate if there were any apparent differences in the place cells, a series of inferential analyses were conducted on the spatial information content, the spatial information rate, and the speed filtered average firing rate.

The mean spatial information content was higher and more variable in the CA1 for the *Neil3*$^{-/-}$ mouse (*M* = 0.89 ± 0.16 bits/spike, *SD* = 0.59) compared to the wildtype in CA1 (*M* = 0.71 ± 0.06 bits/spike, *SD* = 0.55). The same pattern was found in the DG with the *Neil3*$^{-/-}$ mouse (*M* = 1.18 ± 0.14 bits/spike, *SD* = 0.79) having higher mean scores than the wildtype (*M* = 0.91 ± 0.07 bits/spike, *SD* = 0.51), as shown in Table 3. A two-way ANOVA revealed that there was not a statistically significant interaction between the effects of location and genotype $F(1, 174) = 0.18$, $p = .678$. Simple main effects analysis showed that location had a statistically significant effect on the spatial information content of the place cells $F(1, 174) = 5.34$ $p = .022$, and so did genotype $F(1, 174) = 9.19$, $p = .003$. A post-hoc Tukey test revealed that there was a significant interaction effect between the wildtype mouse in CA1 and the *Neil3*$^{-/-}$ mouse in DG $p = .001$. Further, I calculated the spatial information rate, which is related to the spatial information content. This was done with the equation:

$$I = \int_x \lambda(\mathrm{x}) \log_2 \frac{\lambda(\mathrm{x})}{\lambda} p(x)\, dx$$

where I is the information rate in bits per second for each cell, x is location in space, $p(x)$ is the probability for the mouse being at x, $\lambda(x)$ is the mean firing rate when the mouse is at x, and $\int_x \lambda(x)p(x)dx$ is the total mean firing rate of the cell. The spatial information rate is a measure of how much information about location the cell transmits per second. The *Neil3*$^{-/-}$ mouse (*M* = 0.58 ± 0.18 bits/sec, *SD* = 0.65) had a higher mean spatial information rate than the wildtype (*M* = 0.47 ± 0.04 bits/sec, *SD* = 0.38) in CA1, but in the DG the *Neil3*$^{-/-}$ mouse (*M* = 0.67 ± 0.10 bits/sec, *SD* = 0.59) and the wildtype (*M* = 0.67 ± 0.09 bits/sec, *SD* = 0.62) were similar, as shown in Table 3. A two-way ANOVA revealed that there was not a statistically significant interaction between the effects of location and genotype $F(1, 174) = 0.33$, $p = .565$. Simple main effects analysis showed that location had a statistically significant effect on the spatial information rate $F(1, 174) = 4.69$, $p = .032$, but genotype did not $F(1, 174) = 1.42$, $p = .235$.

To investigate the average firing rate, a speed filter of 2 cm/s was applied to exclude firing in which the mouse was not moving. There were no apparent differences in the speed filtered average firing rate among the wildtype (*M* = 0.90 ± 0.07 Hz, *SD* = 0.61) in CA1, *Neil3*$^{-/-}$ mouse (*M* = 0.93 ± 0.21 Hz, *SD* = 0.76) in CA1, wildtype (*M* = 0.97 ± 0.11 Hz, *SD*

= 0.77) in DG, or the *Neil3*$^{-/-}$ mouse (*M* = 1.07 ± 0.17 Hz, *SD* = 0.98) in DG, as shown in Table 3. The sample had a small deviation from normality, but not enough to warrant a non-parametric test. A two-way ANOVA revealed that there was not a statistically significant interaction between the effects of location and genotype $F(1, 174) = 0.07$, $p = .795$. Simple main effects analysis showed that location did not have significant effect on the speed filtered average firing rate $F(1, 174) = 0.97$, $p = .326$, and neither did genotype $F(1, 174) = 0.29$, $p = .590$.

In summary, the spatial information content was higher in both CA1 and DG of the Neil3$^{-/-}$ mouse, the information rate was higher in the CA1 of the Neil3$^{-/-}$ mouse, and the average firing rate was higher in the CA1 and DG of the Neil3$^{-/-}$ mouse. This result suggests that there is a difference in the mutual information carried by the place cells, both between the locations and the genotypes.

Table 3. Summary statistics for the place cells

	CA1		DG	
	WT	***Neil3*$^{-/-}$**	**WT**	***Neil3*$^{-/-}$**
Spatial Information Content (bits/spike, mean±SEM)	0.71±0.06	0.89±0.16	0.91±0.07	1.18±0.14
Spatial Information Rate (bits/sec, mean±SEM)	0.47±0.04	0.58±0.18	0.67±0.09	0.67±0.10
Speed Filtered Average Firing Rate (Hz, mean+-SEM,)	0.90±0.07	0.93±0.21	0.97±0.11	1.07±0.17

3.1.4.1 Specificity

To investigate the specificity of place cells, I investigated the number of cells with multiple fields, average size of the place fields, and the peak firing rate within the fields. Selected statistics are presented in Table 4.

A count was performed on the cells that had more than one place field. This count revealed that a smaller proportion of cells in the DG of the *Neil3*$^{-/-}$ mouse (3, 14% of place cells) had multiple place fields compared to the CA1 of the *Neil3*$^{-/-}$ mouse (4, 31% of place cells) and to the wildtype in both CA1 (22, 26% of place cells) and DG (16, 33% of place cells), as shown in Table 4. The number of place fields were not significantly different between the genotypes or the locations. This was investigated with a two-way ANOVA. The ANOVA revealed that there was not a statistically significant interaction between the effects of location and genotype $F(1, 174) = 2.71$, $p = .101$. Simple main effects analysis showed that location did not have a statistically significant effect on number of place fields $F(1, 174) = 0.05$ $p = .943$), nor did genotype $F(1, 174) = 1.79$ $p = .182$.

The place field size was different between both the genotypes and the locations. The mean place field size was smaller in CA1 for the *Neil3*$^{-/-}$ mouse (M = 478 ± 83.2 mm^2, SD = 300) than it was for the wildtype (M = 755 ± 43.9 mm^2, SD = 402). The mean place field size was also smaller in DG for the *Neil3*$^{-/-}$ mouse (M = 448 ± 46.5 mm^2, SD = 265) than it was for the wildtype (M = 554 ± 42.5 mm^2, SD = 297). A two-way ANOVA revealed that the interaction between the effects of location and genotype was not significant $F(1, 174) = 1.74$, $p = .189$. Simple main effects analysis showed that location had a statistically significant effect on place field size $F(1, 174) = 15.6$ $p < .001$, and so did genotype $F(1, 174) = 7.27$ $p = .007$. A post hoc Tukey test showed that the genotypes were significantly different in CA1 ($p = .038$), but not in DG ($p = .531$). The test also showed that the wildtype had significant differences in place field sizes between CA1 and DG ($p = .008$), whereas *Neil3*$^{-/-}$ mouse did not ($p = .993$). A boxplot figure of the place field size is presented in Figure 8.

The mean place field peak firing rates were different with the *Neil3*$^{-/-}$ mouse having higher peak firing rates in the CA1 (M = 5.77 ± 1.83 Hz, SD = 6.58) and in the DG (M = 6.34 ± 0.94 Hz, SD = 5.34) compared to the wildtype in CA1 (M = 4.53 ± 0.33 Hz, SD = 3.04) and DG (M = 5.75 ± 0.62 Hz, SD = 4.32), as shown in Table 4. A two-way ANOVA revealed that there was not a statistically significant interaction between the effects of location and genotype $F(1, 174) = 0.17$, $p = .678$. Simple main effects analysis showed that location had a statistically significant effect on the peak firing rate of place fields $F(1, 174) = 4.13$ $p = .043$, but genotype did not $F(1, 174) = 1.17$ $p = .279$.

In summary, the *Neil3*$^{-/-}$ mouse had lower proportion of cells with multiple fields in the DG, the place field size was smaller in both CA1 and DG, and the field peak firing rate was higher. This might be an indication of impaired spatial specificity.

Table 4. Summary statistics for the place cell specificity.

	CA1		DG	
	WT	***Neil3*$^{-/-}$**	**WT**	***Neil3*$^{-/-}$**
Number of Place Cells with Multiple Fields (mean (% of place cells))	22 (26%)	4 (31%)	16 (33%)	3 (14%)
Field Size (mm2, mean (SD))	755 (402)	478 (300)	554 (297)	448 (265)
Field Peak Firing Rate (Hz, mean (SD))	4.53 (3.04)	5.77 (6.58)	5.75 (4.32)	6.34 (5.34)

Note. The *% of place cells* refers to the proportion of relevant cells compared to the total number of place cells in that condition. SD = standard deviation.

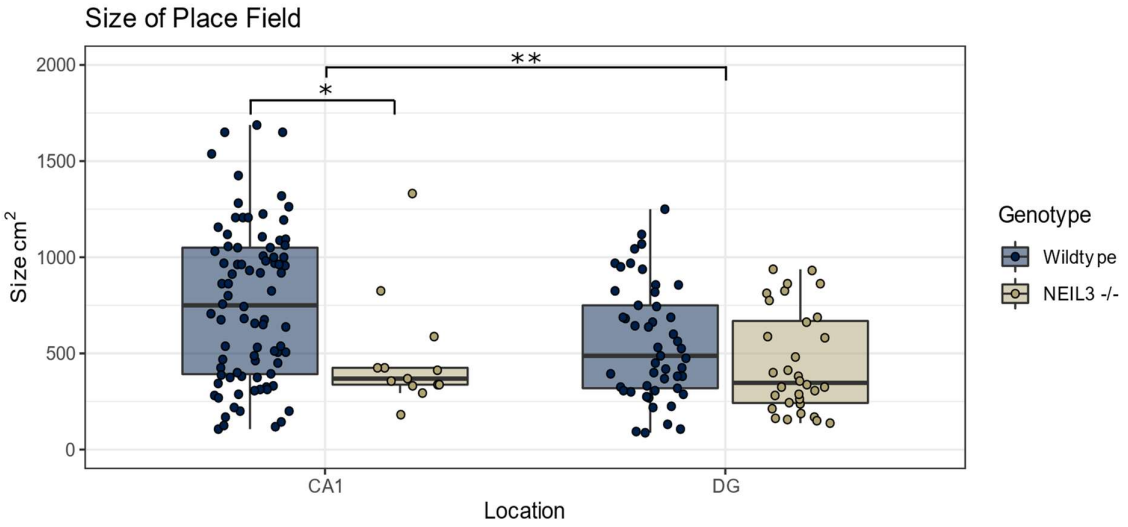

Figure 8. Boxplot for the size of place fields.
* = $p < 0.05$, ** = $p < 0.01$

3.1.4.2 Remapping

To investigate the remapping capabilities of the place cells, I did a correlation analysis on the rate maps between the two boxes in the two remapping conditions (A1 to B1 and B2 to A2, see Figure 2 in section 2.2.4). All the remapping experiments were performed while recording cells in the DG. To calculate the correlations between the rate maps, the whole map was binned into 2cm bins. I then correlated the summed value of the bins for each value on the y-axis. The iterations over the y-axis resulted in an averaged total Pearson correlation coefficient for the whole map. I then calculated descriptive and inferential statistics for the correlation coefficients. If the cells remap as normal, we expect to see correlation coefficients close to 0. The wildtype mouse partook in 7 recording sessions, while the *Neil3*$^{-/-}$ mouse partook in 8 recording sessions. A total of 39 place cells were analysed for the A1 to B1 condition, where 29 belonged to the wildtype mouse and 10 belonged to the *Neil3*$^{-/-}$ mouse. A total of 33 place cells were analysed in the B2 to A2 condition, where 24 belonged to the wildtype mouse and 9 belonged to the *Neil3*$^{-/-}$ mouse. The difference in cell numbers between these two conditions stem from losing the cells during the experiments. The result of the descriptive analysis is presented in Table 5.

In the A1 to B1 condition, the wildtype mouse (M = -0.03 ± 0.05, SD = 0.37) remapped as expected, but the *Neil3*$^{-/-}$ mouse (M = 0.34 ± 0.10, SD = 0.44) had higher mean correlation coefficients, as seen in in Table 5. The distributions of coefficients showed slight deviations from normality, but not enough to warrant non-parametric tests, The genotypes were significantly different from each other $t(37)$ = -2.65, p = .012. The *Neil3*$^{-}$

$^{/-}$ mouse's correlation coefficients were significantly different from 0, $t(9) = 2.49$, $p = .035$. A boxplot of the two groups is presented in Figure 9. A figure of rate maps from selected cells from the analysis is presented in Appendix E.

In the B2 to A2 condition, like the A1 to B1 condition, the wildtype mouse (M = 0.00 ± 0.05, SD = 0.33) remapped as expected, but the *Neil3*$^{-/-}$ mouse (M = 0.34 ± 0.10, SD = 0.44) had higher mean correlation coefficients, as seen in in Table 5. This difference was significant $t(31) = -2.41$, $p = .022$. The *Neil3*$^{-/-}$ mouse's correlation coefficients were significantly different from 0, $t(8) = 2.31$, $p = .049$. A boxplot of the two groups is presented in Figure 10. A figure of rate maps from selected cells from the analysis is presented in Appendix F.

In summary, the wildtype mouse showed low correlation coefficients when moved to a new environment, whereas the *Neil3*$^{-/-}$ mouse showed higher correlation coefficients. This was true for both the remapping conditions, indicating that the *Neil3*$^{-/-}$ mouse had an impairment in his remapping capabilities of place cells in the DG.

Table 5. Descriptive statistics for the global remapping conditions.

Genotype	M	SD	SE	Median	Range	Skewness	Kurtosis
A1B1							
Wildtype	-0.03	0.37	0.05	-0.17	[-0.54 – 0.92]	1.13	0.71
Neil3$^{-/-}$	0.34	0.44	0.10	0.35	[-0.25 – 0.85]	-0.17	-1.75
B2A2							
Wildtype	0.00	0.33	0.05	-0.09	[-0.51 – 0.84]	0.61	-0.28
Neil3$^{-/-}$	0.34	0.44	0.10	0.43	[-0.45 – 0.78]	-0.54	-1.39

Note. M = Mean, *SE* = Standard Error, *SD* = Standard Deviation.

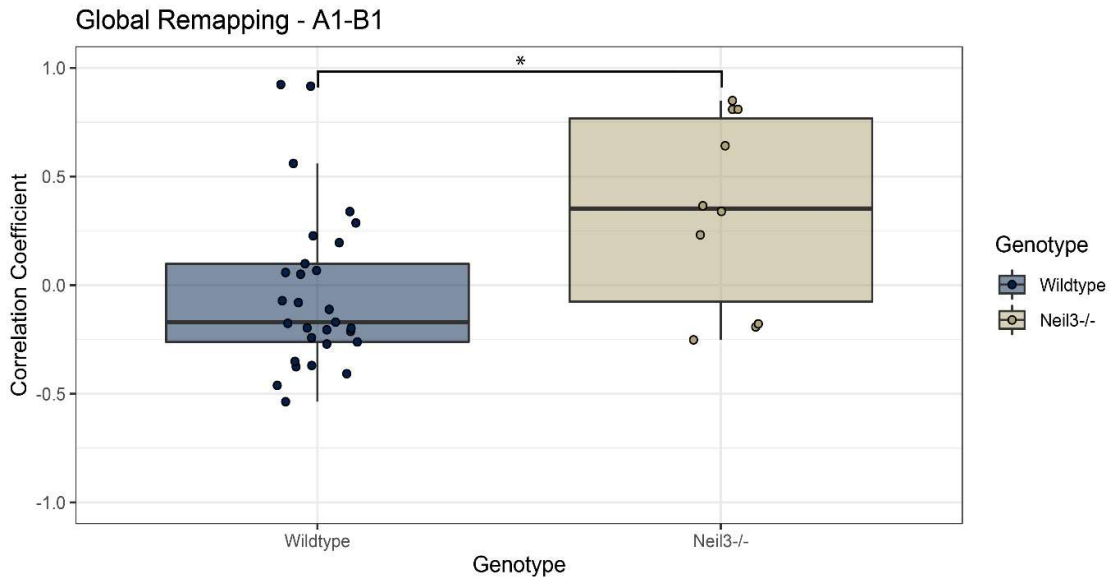

Figure 9. Boxplot for the A1 to B1 global remapping condition. Comparison of the distributions of the correlation coefficients.
* = $p < .05$

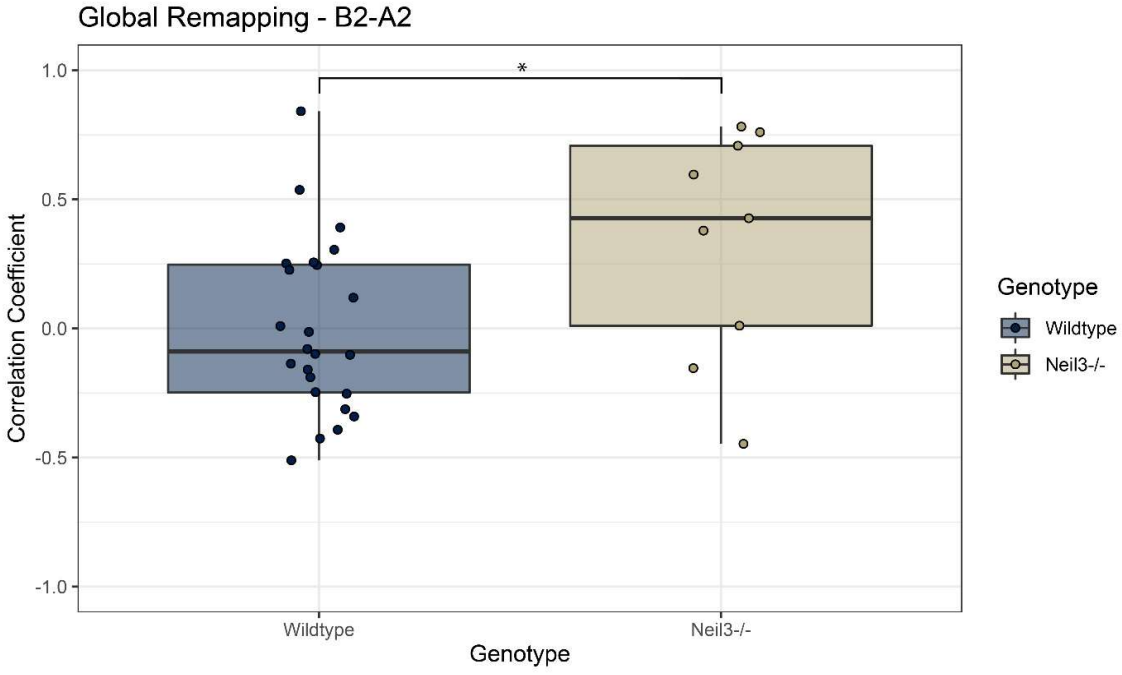

Figure 10. Boxplot for the B2 to A2 global remapping condition. Comparison of the distributions of the correlation coefficients.
* = $p < .05$

3.1.4.3 Short-term Stability

To investigate the short-term stability of the spatial representations, I did a similar analysis of the rate maps as I did for the global remapping condition. A total of 60 cells were included in the short-term stability condition, where 38 were from the wildtype and 22 were from the *Neil3*$^{-/-}$. To investigate the short-term stability, I compared the correlation coefficients between the A1 and A2 box (see Figure 2 in section 2.2.4). If short-term stability is normal, we can expect to see strong correlations between the maps. A descriptive analysis was conducted and is presented in Table 6.

Both the wildtype (M= 0.72 ± 0.05, SD = 0.31) and the *Neil3*$^{-/-}$ (M= 0.83 ± 0.04, SD = 0.17) had strong mean correlation coefficients, as seen in Table 6. Both the mice had significant deviations from normality, so a Wilcoxon rank sum test was conducted. The test revealed that the group distributions were not statistically significantly different from each other W = 525, p = .103. A boxplot of the two groups is presented in Figure 11. A figure of rate maps from selected cells from the analysis is presented in Appendix G.

In summary, both the mice had high correlation coefficients, which suggests that both the mice had preserved short-term stability of the place cell spatial representation in the DG.

Table 6. Descriptive statistics for the short-term stability condition.

Genotype	*M*	*SD*	*SE*	Median	Range	Skewness	Kurtosis
Wildtype	0.72	0.31	0.05	0.81	[-0.51 – 0.97]	-2.28	5.38
Neil3 -/-	0.83	0.17	0.04	0.91	[0.40 – 0.98]	-1.42	0.38

Note. M = Mean, *SE* = Standard Error, *SD* = Standard Deviation.

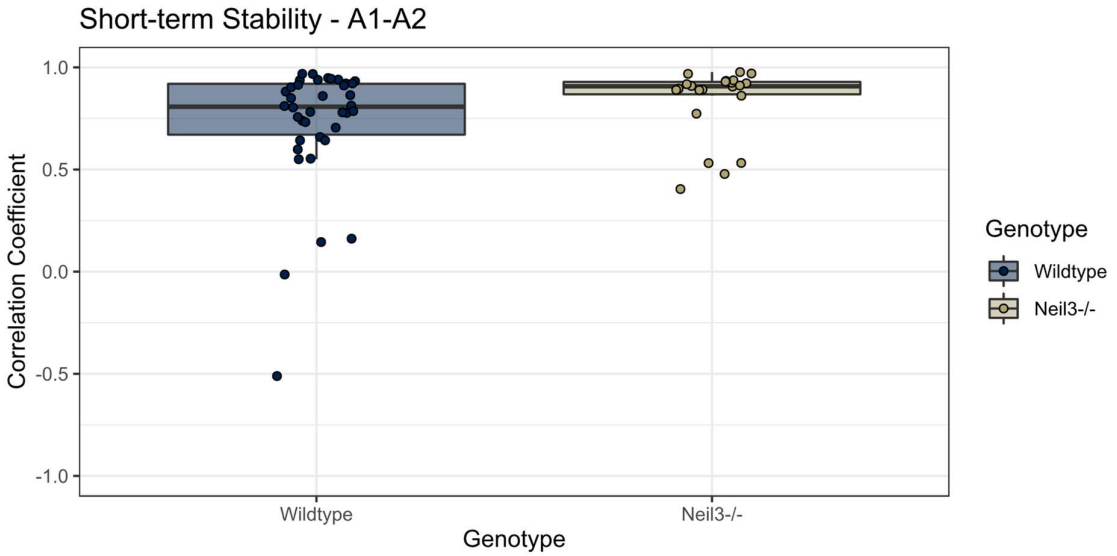

Figure 11. Boxplot for the short-term stability condition.
Comparison of the distributions of the correlation coefficients.

3.1.4.4 Long-term Stability

To investigate the long-term stability of the spatial representations, I did a similar analysis to the rate maps as I did in the short-term stability and global remapping condition. A total of 48 cells were included in the long-term stability condition, where 33 were from the wildtype and 15 were from the *Neil3*$^{-/-}$. To investigate the long-term stability, I compared the correlation coefficients between the A0 and A1 box (see Figure 2 in section 2.2.4). If long-term stability is normal, we can expect to see strong correlations between the maps. A descriptive analysis was conducted and is presented in Table 7.

The wildtype mouse (M= 0.53 ± 0.07, SD = 0.38) had lower mean correlation coefficients than the *Neil3*$^{-/-}$ mouse (M= 0.85 ± 0.04, SD = 0.16), as seen in Table 7. The samples had significant deviations from normal distribution, so a Wilcoxon rank sum test was conducted. The test revealed that the group distributions were significantly different from each other W = 92, p < .001. A boxplot of the two groups is presented in Figure 12. A figure of rate maps from selected cells from the analysis is presented in Appendix H.

In summary, both the mice had high correlation coefficients, which suggests that both the mice had preserved long-term stability of the place cell spatial representations in the DG.

Table 7. Descriptive statistics for the long-term stability condition.

Genotype	*M*	*SD*	*SE*	Median	Range	Skewness	Kurtosis
Wildtype	0.53	0.38	0.07	0.64	[-0.41 – 0.95]	-0.83	-0.38
Neil3-/-	0.85	0.16	0.04	0.91	[0.40 – 0.99]	-1.67	-1.73

Note. M = Mean, *SE* = Standard Error, *SD* = Standard Deviation.

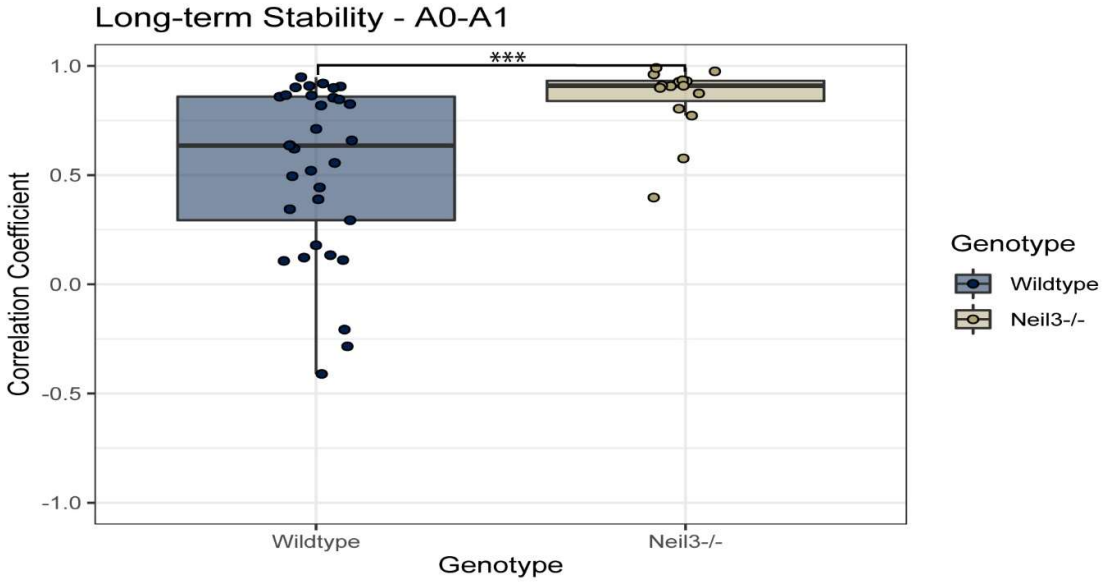

Figure 12. Boxplot for the long-term stability condition.
Comparison of the distributions of the correlation coefficients.
*** = $p < .001$.

3.2 Behavioural

The behaviour experiments were conducted to investigate the secondary aim of this study, whether NEIL3 impacts the brain's cognitive functions such as anxiety and spatial memory. The alpha levels for all the behavioural analyses are set to $\alpha = 0.05$. The alpha level determines the certainty that the null hypothesis is not a false positive. Assumptions for all tests were checked before they were performed. Parametric tests were chosen where it was appropriate. The data collection was done together with colleagues.

3.2.1 Open field

The open field experiment was used to determine general anxiety levels of the mice. A total of 30 mice were included in the analysis. These mice belonged to one of four groups: young wildtype, old wildtype, young *Neil3*$^{-/-}$, or old *Neil3*$^{-/-}$. One mouse (old *Neil3*$^{-/-}$) was excluded from the analysis due to being a multivariate outlier. Of these, 9 were young wildtypes, 6 were old wildtypes, 9 were young *Neil3*$^{-/-}$, and 6 were old *Neil3*$^{-/-}$. The young mice were 3-4 months old, and the old mice were 18-20 months old. A descriptive analysis, and a series of inferential analyses were conducted on selected variables of all the mice in the open field experiment. The result of the descriptive analysis is presented in Table 8.

The variable *total distance* describes how far the mice travelled in meters for the whole duration of the experiment. The mean (*M*) distance travelled and associated standard deviation (*SD*) was lower for the young *Neil3*$^{-/-}$ mice ($M = 29.1$ m, $SD = 5.58$) than the older *Neil3*$^{-/-}$ mice ($M = 37.3$ m, $SD = 18.1$), the young wildtype mice ($M = 33.1$ m, $SD = 5.88$) and the old wildtype mice ($M = 36.5$ m, $SD = 8.63$), as shown in Table 8. This might be an indication of increased anxiety. A two-way ANOVA revealed that the interaction effect was not statistically significant $F(1,26) = 0.05$, $p = .819$. The main effects were not statistically significant for genotype $F(1,26) = 2.90$, $p = .101$ or for age $F(1,26) = 1.08$, $p = .307$. A boxplot for this variable is presented in Figure 13A.

The variable *average speed* describes the mean speed in meters per second for the whole duration of the experiment. On average, the young *Neil3*$^{-/-}$ mice were slower ($M = 0.048$ m/s, $SD = 0.009$) than the older *Neil3*$^{-/-}$ ($M = 0.062$ m/s, $SD = 0.030$), the young wildtype ($M = 0.055$ m/s, $SD = 0.010$) and the old wildtype ($M = 0.061$ m/s, $SD = 0.015$), as shown in Table 8. This also might be an indication of increased anxiety. A two-way ANOVA revealed that the interaction was not statistically significant $F(1,26) = 0.48$, $p = .829$, neither was the effect for genotype $F(1,26) = 3.08$, $p = .091$, or the effect for age $F(1,26) = 1.10$, $p = .302$. A boxplot for this variable is presented in Figure 13B.

The variable *number of zone crossings* describes the number of times the mice crossed the border between two zones for the whole duration of the experiment. On average, the young *Neil3*$^{-/-}$ (M = 297, SD = 31.9) mice crossed the zone borders less than the older *Neil3*$^{-/-}$ (M = 366, SD = 120), the young wildtype (M = 361, SD = 43.5) and the old wildtype (M = 363, SD = 58.8), as shown in Table 8. This might be an indication of increased anxiety. A two-way ANOVA revealed that the interaction was not statistically significant $F(1,26) = 0.65$, $p = .428$. The effect for genotype was significant $F(1,26) = 10.2$, $p = .003$, but the effect for age was not $F(1,26) = 0.67$, $p = .419$. A boxplot for this variable is presented in Figure 13C.

The variable *time in corner* describes the cumulative time spent in the corner zones measured in seconds. On average, the young *Neil3*$^{-/-}$ mice (M = 187 s, SD = 65.1) spent more time in the corners than the older *Neil3*$^{-/-}$ (M = 131 s, SD = 120), the young wildtype (M = 144 s, SD = 75) and the old wildtype (M = 122 s, SD = 91.9), as shown in Table 8. This might be an indication of increased anxiety. A two-way ANOVA revealed that the interaction was not statistically significant $F(1,26) = 0.55$, $p = .467$. neither was the effect for genotype $F(1,26) = 0.53$, $p = .472$, or the effect for age $F(1,26) = 1.97$, $p = .172$. A boxplot for this variable is presented in Figure 13D.

The variable *entries to centre* describes how many times the mice entered the centre zone on average. The young *Neil3*$^{-/-}$ mice (M = 48.2, SD = 8.76) entered the centre zone less frequently than the older *Neil3*$^{-/-}$ (M = 52, SD = 10.2), the young wildtype (M = 60.4, SD = 10.4) and the old wildtype (M = 57, SD = 11.6), as shown in Table 8. This might be an indication of increased anxiety. A two-way ANOVA revealed that the interaction was not statistically significant $F(1,26) = 0.88$, $p = .357$. The effect for genotype was significant $F(1,26) = 6.13$, $p = .020$, but the effect for age was not $F(1,26) = 0.01$, $p = .966$. A boxplot for this variable is presented in Figure 13E.

Table 8. Descriptive statistics for selected variables in open field.

Genotype	Age	*M*	*SE*	*SD*	Range	Skewness	Kurtosis
Total Distance (m)							
Wildtype	Young	33.1	1.96	5.88	[22.8 – 40.5]	-0.39	-1.35
Wildtype	Old	36.5	3.52	8.63	[22.9 – 46.6]	-0.42	-1.57
Neil3$^{-/-}$	Young	29.1	1.86	5.58	[22.2 – 38.1]	0.30	-1.51
Neil3$^{-/-}$	Old	37.3	6.83	18.1	[16.8 – 83.4]	0.88	-0.47
Average Speed (m/s)							
Wildtype	Young	0.055	0.003	0.010	[0.038 – 0.068]	-0.40	-1.32
Wildtype	Old	0.061	0.006	0.015	[0.038 – 0.078]	-0.42	-1.55
Neil3$^{-/-}$	Young	0.048	0.003	0.009	[0.037 – 0.063]	0.28	-1.53
Neil3$^{-/-}$	Old	0.062	0.011	0.030	[0.028 – 0.122]	0.88	-0.47
Number of Zone Crossings							
Wildtype	Young	361	14.5	43.5	[278 – 409]	-0.72	-1.04
Wildtype	Old	362	24.0	58.8	[274 – 448]	-0.03	-1.37
Neil3$^{-/-}$	Young	297	10.6	31.9	[264 – 354]	0.50	-1.39
Neil3$^{-/-}$	Old	366	45.3	120	[268 – 614]	1.11	-0.26
Time in Corner (s)							
Wildtype	Young	144	25.0	75	[44.4 – 241]	-0.15	-1.77
Wildtype	Old	122	37.5	91.9	[10.6 – 229]	-0.22	-1.97
Neil3$^{-/-}$	Young	187	21.7	65.1	[59.9 – 267]	-0.47	-0.88
Neil3$^{-/-}$	Old	131	45.5	120	[1.70 – 287]	-0.01	-2.04
Entries to Centre							
Wildtype	Young	60.4	3.5	10.4	[45 – 81]	0.38	-0.60
Wildtype	Old	57.0	4.7	11.6	[44 – 76]	0.43	-1.47
Neil3$^{-/-}$	Young	48.2	2.9	8.76	[34 – 66]	0.36	-0.25
Neil3$^{-/-}$	Old	52.0	3.8	10.2	[35 – 70]	0.12	-0.48
Latency to Centre (s)							
Wildtype	Young	3.29	2.03	6.08	[0 – 18.9]	1.81	1.87
Wildtype	Old	9.28	2.07	5.07	[1.40 – 15.8]	-0.31	-1.51
Neil3$^{-/-}$	Young	5.59	3.54	10.6	[0 – 32.1]	1.66	1.35
Neil3$^{-/-}$	Old	9.17	6.07	16.1	[0 – 44.6]	1.46	0.42

Note. M = Mean, *SE* = Standard Error, *SD* = Standard Deviation.

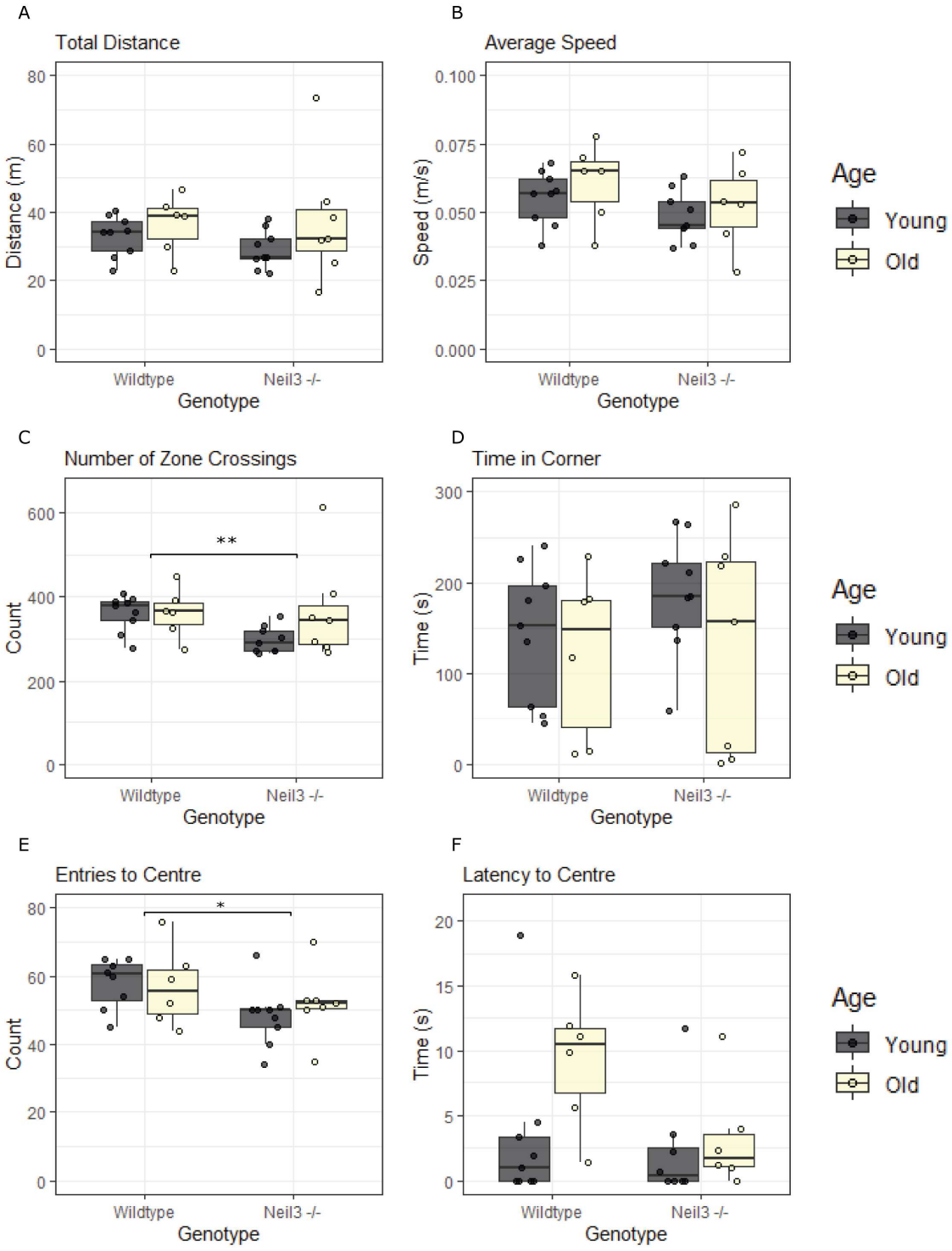

Figure 13. Boxplots for the variables in the open field analysis.
* = $p < 0.05$, ** = $p < 0.01$

The variable latency to centre describes the time it took the mice to enter the centre zone for the first time measured in seconds. On average, the young *Neil3*$^{-/-}$ mice (*M* = 5.59 s, *SD* = 10.6) entered the centre zone for the first time later than the young wildtypes (*M* = 3.29 s, *SD* = 6.08), but both the old wildtypes (*M* = 9.28 s, *SD* = 5.07) and old *Neil3*$^{-/-}$ (*M* = 9.17 s, *SD* = 16.1) were later than the young mice, as shown in Table 8. The dependent variable was not normally distributed, thus breaking one of the assumptions of ANOVA. The observed difference in means is largely due to two univariate outliers. When these two mice are excluded, the data fulfils the ANOVA assumptions. The two-way ANOVA revealed that the interaction was not statistically significant $F(1,24) = 1.36$, $p = .255$. The effect for genotype was not significant $F(1,24) = 2.15$, $p = .156$, and neither was the effect for age $F(1,24) = 3.92$, $p = .059$. A boxplot for this variable is presented in Figure 13F.

In summary, young *Neil3*$^{-/-}$ mice spent more time in the corners and entered the centre less than the other groups, indicating increased anxiety. The young *Neil3*$^{-/-}$ mice travelled a shorter distance at a lower speed, and with less crossings between the zones, indicating reduced general activity.

3.2.2 Novel Object Location

The NOL experiment was used to determine the memory capabilities of the mice. A total of 47 mice were included in the NOL analysis. To investigate memory in the NOL experiment I calculated the discrimination index as:

$$Discrimination\ index = \frac{t(novel) - t(familiar)}{t(novel) + t(familiar)}$$

Where *t(novel)* is the time spent in close proximity to the novel object location and *t(familiar)* is the time spent in close proximity to the familiar object location. A higher discrimination index means that the mice discriminate the novel location from the familiar location. A discrimination index of 0.4 indicates that the mouse spent 40% more time with the novel object compared to the familiar object. A discrimination index below 0 means that the mice preferred the familiar object. A high and positive discrimination index is thus an indication of preserved memory capabilities.

3.2.2.1 Short-term Memory

A total of 21 mice were included in the STM condition. Of these, 3 were young wildtype mice, 7 were old wildtype mice, 2 were young *Neil3*$^{-/-}$ mice, and 9 were old *Neil3*$^{-/-}$ mice. A descriptive analysis was conducted on the variables and is presented in Table 9.

There was no clear difference in the means of the discrimination index among young wildtypes (M = 0.44 ± 0.08, SD = 0.13), old wildtypes (M = 0.52 ± 0.08, SD = 0.22), young *Neil3*$^{-/-}$ (M = 0.46 ± 0.44, SD = 0.62), or old *Neil3*$^{-/-}$ (M = 0.43±0.08, SD = 0.25), as seen in Table 9. A two-way ANOVA revealed that the interaction was not statistically significant $F(1,17) = 0.16$, $p = .689$. The effect for genotype was not significant $F(1,17) = 0.36$, $p = .556$, nor was the effect for age $F(1,17) = 0.05$, $p = .821$. A boxplot figure of this variable is presented in Figure 14.

The groups were tested for significant deviations from the chance level. One sample t-test revealed that the young wildtype, $t(2) = 5.84$, $p = .028$, the old wildtype, $t(6) = 6.44$, $p < .001$, and the old *Neil3*$^{-/-}$, $t(8) = 5.10$, $p < .001$, groups were all significantly different from chance level. The young *Neil3*$^{-/-}$ group, $t(1) = 1.05$, $p = .483$, was not significantly different from chance level.

In summary, the mean discrimination indices were all positive, indicating that the memory capabilities were intact. However, the sample size for the young mice were small and the young *Neil3*$^{-/-}$ mice had high variance, thus making the results unreliable.

Table 9. Descriptive statistics for the STM condition of NOL.

Genotype	Age	M	SE	SD	Range	Skewness	Kurtosis
Wildtype	Young	0.44	0.08	0.13	[0.33 – 0.59]	0.28	-2.33
Wildtype	Old	0.52	0.08	0.22	[0.31 – 0.89]	0.68	-1.43
Neil3$^{-/-}$	Young	0.46	0.44	0.62	[0.02 – 0.90]	0.00	-2.75
Neil3$^{-/-}$,	Old	0.43	0.08	0.25	[0.08 – 0.69]	-0.42	-1.84

Note. Statistics of the discrimination index. M = Mean, SE = Standard Error, SD = Standard Deviation.

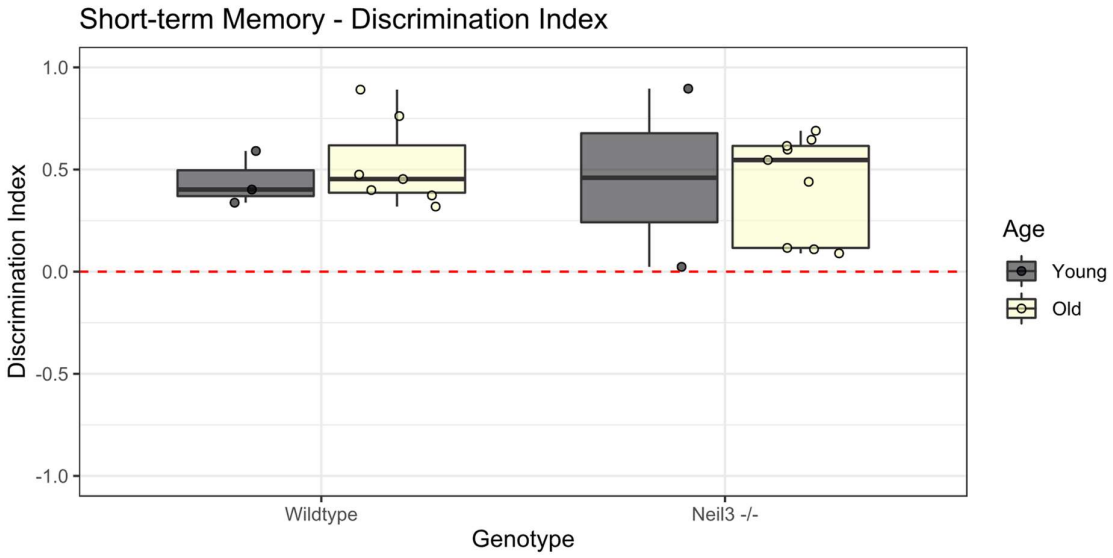

Figure 14. Boxplot for the discrimination index for the STM condition.
The x axis differentiates genotype, and the colours differentiates age. The red dotted line illustrates the chance level.

3.2.2.2 Long-term Memory

A total of 26 mice were included in the LTM condition. Of these, 9 were young wildtype mice, 4 were old wildtype mice, 9 were young *Neil3*$^{-/-}$ mice, and 4 were old *Neil3*$^{-/-}$ mice. A descriptive analysis was conducted on the variables and is presented in Table 10.

In the long-term memory condition, a pattern emerged with the young *Neil3*$^{-/-}$ mice (M = 0.16 ± 0.11, SD = 0.33) and the old *Neil3*$^{-/-}$ mice (M = 0.15 ± 0.22, SD = 0.44) showing lower mean scores on the discrimination index than the young wildtypes (M = 0.40 ± 0.12, SD = 0.35), and the old wildtypes (M = 0.29 ± 0.09, SD = 0.19), as seen in Table 10. A two-way ANOVA revealed that the interaction was not statistically significant $F(1,22) = 0.13$, $p = .718$. The effect for genotype was not significant $F(1,22) = 2.504$, $p = .020$, and neither was the effect for age $F(1,22) = 0.15$, $p = .701$. A boxplot figure of this variable is presented in Figure 15.

The groups were tested for significant deviations from the chance level. One sample t-test revealed that the young wildtype, $t(8) = 3.41$, $p < .001$, was the only significant group. the old wildtype group, $t(3) = 3.12$, $p = .053$, was close to significant. The young *Neil3*$^{-/-}$ group, $t(8) = 1.42$, $p = .192$ and the old *Neil3*$^{-/-}$group, $t(3) = 0.69$, $p = .539$, were not significantly different from chance level.

In summary, the mean discrimination indices for the wildtype mice were positive, indicating that the memory capabilities were intact. However, the *Neil3*$^{-/-}$ mice showed

tendencies to not discriminate the objects as well, indicating impaired memory in the long-term condition.

Table 10. Descriptive statistics for the LTM condition of NOL.

Genotype	Age	*M*	*SE*	*SD*	Range	Skewness	Kurtosis
Wildtype	Young	0.40	0.12	0.35	[-0.11 – 0.96]	0.31	-1.22
Wildtype	Old	0.29	0.09	0.19	[0.02 – 0.43]	-0.68	-1.73
Neil3$^{-/-}$	Young	0.16	0.11	0.33	[-0.21 – 0.67]	0.49	-1.50
Neil3$^{-/-}$	Old	0.15	0.22	0.44	[-0.28 – 0.77]	0.43	-1.83

Note. Statistics of the discrimination index. *M* = Mean, *SE* = Standard Error, *SD* = Standard Deviation.

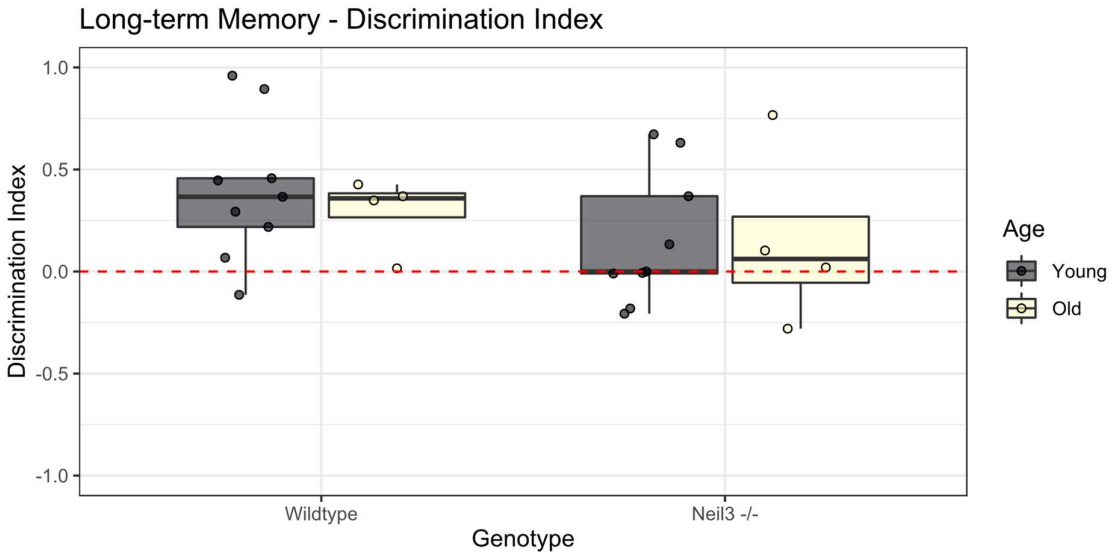

Figure 15. Boxplot for the discrimination index for the LTM condition.
The x axis differentiates genotype, and the colours differentiates age. The red dotted line illustrates the chance level.

3.2.3 Y-maze

A total of 27 mice were included in the y-maze analysis, where 9 were young wildtypes, 9 were young *Neil3*$^{-/-}$, 5 were old wildtypes, and 4 were old *Neil3*$^{-/-}$. There were not enough animals in the STM condition, so all the results are from the LTM condition. To investigate memory in the y-maze experiment, I compared the discrimination index for entries to, and time spent in, the novel arm. The discrimination index was calculated in the same way as was done for the NOL. A low or negative discrimination index indicates that the mice did not prefer the novel arm. A descriptive analysis was conducted on the discrimination indices for all the included mice in the y-maze experiment. The result of this analysis is presented in Table 11.

There was a difference in the discrimination index of entries, where the young *Neil3*$^{-/-}$ mice (M = -0.25 ± 0.05, SD = 0.14) had a higher negative score than the young wildtypes (M = -0.09 ± 0.06, SD = 0.17), the old wildtypes (M = -0.12 ± 0.11, SD = 0.26), and the old *Neil3*$^{-/-}$ mice (M = -0.03 ± 0.13, SD = 0.26), as seen in Table 11. A boxplot figure of this variable is presented in Figure 16. A two-way ANOVA revealed that the interaction was not statistically significant $F(1,23) = 2.55$, $p = .124$. The effect for genotype was not statistically significant $F(1,23) = 1.23$, $p = .278$, and neither was the effect for age $F(1,23) = 1.21$, $p = .282$. The young *Neil3*$^{-/-}$ mice preferred to enter the familiar arm, and this difference was statistically significant $t(8) = -5.42$, $p < .001$. The effects for the young wildtypes $t(8) = -1.52$, $p = .167$, the old wildtypes $t(4) = -1.02$, $p = .367$, or the old *Neil3*$^{-/-}$ mice $t(3) = -0.24$, $p = .829$ were not statistically significant.

There was a difference in the mean discrimination index of time, where the young wildtype mice (M = -0.16± 0.07, SD = 0.21) and the young *Neil3*$^{-/-}$ mice (M = -0.21 ± 0.06, SD = 0.18) spent longer in the familiar arm, whereas the old wildtype mice (M = 0.15 ± 0.13, SD = 0.30) and the old *Neil3*$^{-/-}$ mice (M = 0.18. ± 0.18, SD = 0.36) spent more time in the novel arm, as seen in Table 11. A boxplot figure of this variable is presented in Figure 17. A two-way ANOVA revealed that the interaction was not statistically significant $F(1,23) = 0.18$, $p = .679$. The effect for genotype was not statistically significant $F(1,23) = 0.07$, $p = .799$, but the effect for age was statistically significant $F(1,23) = 12.5$, $p = .002$. The difference from zero for the young wildtype mice $t(8) = -2.33$, $p = .049$ and the young *Neil3*$^{-/-}$ mice $t(8) = -3.60$, $p = .007$ were statistically significant, whereas the difference from zero for the old wildtype mice $t(4) = 1.12$, $p = .324$ and the old *Neil3*$^{-/-}$ mice $t(3) = 1.00$, $p = .389$ was not statistically significant.

In summary, the discrimination indices for both time and entries for all the animals were close to zero, indicating that they did not discriminate between the familiar

and novel arm well. The young mice, especially the *Neil3*$^{-/-}$, showed a tendency to prefer the familiar arm.

Table 11. Descriptive statistics for the y-maze.

Genotype	Age	*M*	*SE*	*SD*	Range	Skewness	Kurtosis
Discrimination index of entries							
Wildtype	Young	-0.09	0.06	0.17	[0.30 – 0.18]	0.11	-1.66
Wildtype	Old	-0.12	0.11	0.26	[-0.29 – 0.33]	0.98	-1.03
Neil3 -/-	Young	-0.25	0.05	0.14	[-0.44 – -0.06]	0.03	-1.74
Neil3 -/-	Old	-0.03	0.13	0.26	[-0.27 – 0.33]	0.49	-1.80
Discrimination index of time							
Wildtype	Young	-0.16	0.07	0.21	[-0.47 – 0.10]	-0.19	-1.79
Wildtype	Old	0.15	0.13	0.30	[-0.18 – 0.60]	0.39	-1.67
Neil3 -/-	Young	-0.21	0.06	0.18	[-0.54 – 0.03]	-0.30	-1.16
Neil3 -/-	Old	0.18	0.18	0.36	[-0.07 – 0.72]	0.69	-1.72

Note. M = Mean, *SE* = Standard Error, *SD* = Standard Deviation.

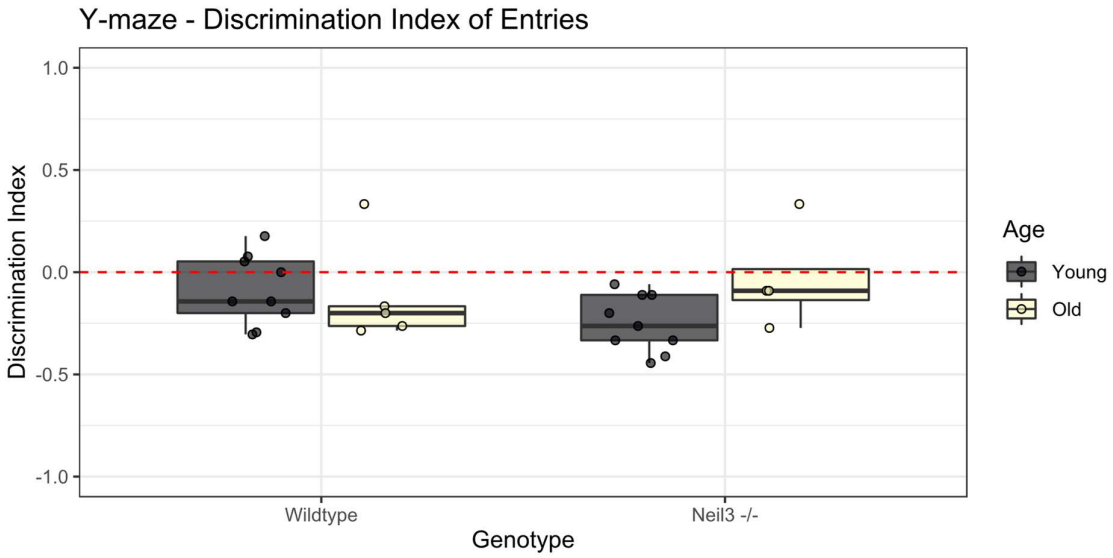

Figure 16. Boxplot for the discrimination index of entries in the y-maze. The x axis differentiates genotype, and the colours differentiates age.

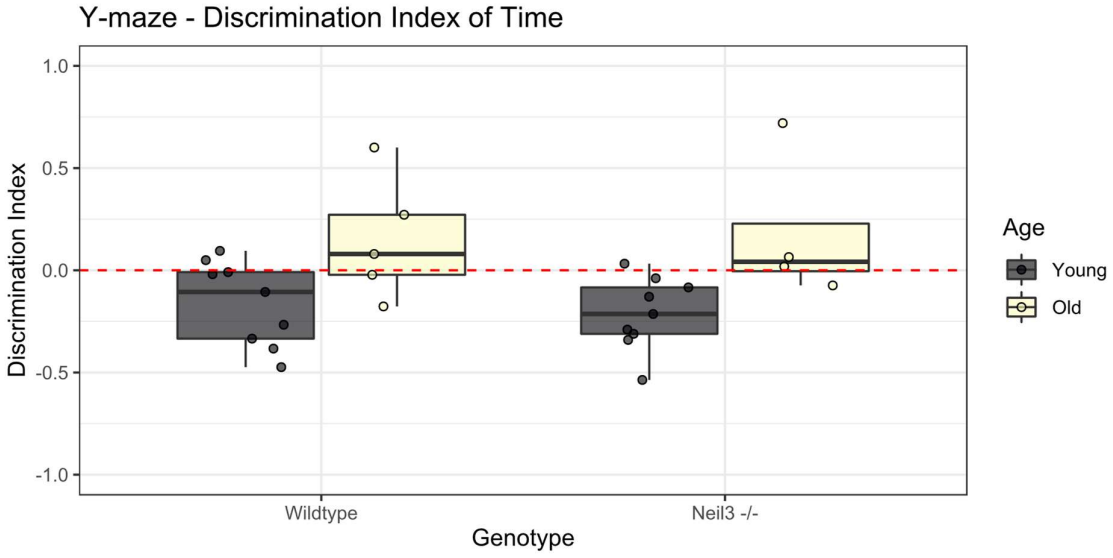

Figure 17. Boxplot for the discrimination index of time in the y-maze. The x axis differentiates genotype, and the colours differentiates age.

4 Discussion

The main aim of this study was to elucidate whether NEIL3 impacts the functional plasticity of hippocampal place cells in the CA1 and DG. The findings indicate that NEIL3 does impact the functional plasticity of cells in the DG. No relevant differences were found for CA1, but the most relevant findings for DG, long-term stability and remapping, were not tested for CA1. The secondary aim of this study is to investigate if NEIL3 impacts spatial memory and anxiety. The findings indicate a memory impairment in the *Neil3*$^{-/-}$ mice for the LTM condition of the NOL, but no clear differences between the genotypes emerged in the STM or in the y-maze experiment. The results of the open field experiment suggest that young *Neil3*$^{-/-}$ mice display increased anxiety. Knowledge about the functional and behavioural correlates of a NEIL3 depletion can give us further insight into the mechanisms that govern the DNA glycosylases. Further, if the molecular correlates of a NEIL3 depletion is elucidated, these findings in function and behaviour can give us insight into the spatial navigation system and spatial memory in general.

A significant limitation of this study is the small and uneven sample size, and the addition of data might significantly change the results. The first part of the discussion appertains to the cell physiology, and the second part appertains to the behavioural testing. Limitations and recommendations for further studies are discussed in the end.

4.1 Cell Physiology

To determine the recording location, I used a combination of histology and the characteristics of the electric signal. Even though there were no clear histological markers for where the tetrode passed the CA1, we can impose a straight line onto the picture and assume the location in which the tetrode passed the CA1. The tetrode trace looks similar on the transverse axis, but it is hard to determine location on longitudinal axis. As the most prominent differences are found on the longitudinal axis (Cembrowski *et al.*, 2016), this might be a cause of the observed differences.

A total of 619 cells were clustered. There are some possible issues with the cell clustering. First, if the cell cluster contains spikes that originates from a different cell, the cells characteristics becomes less valid. Second, if the cell cluster lack spikes from the cell, the cells characteristics becomes less valid. Third, it is possible that I missed some of the granule cells while clustering the data from the DG. As the granule cells often have very

sparse firing, and thus has less data points in the clustering feature space, there could have been instances where the spikes of these cells were not clustered. A possible remedy for clustering is to use two independent experimenters to cluster the data, and then look at the internal consistency of the clustered data.

4.1.1 Cell Classification

The cells were classified into six categories: place cells, HD cells, speed cells, conjunctive place and HD cells, conjunctive place and speed cells, and conjunctive place, HD, and speed cells. Of particular importance were the place cells, of which there was a low population in the CA1 of the *Neil3*$^{-/-}$ mouse.

A smaller proportion of place cells were found in CA1 in the *Neil3*$^{-/-}$ mouse, similar to what Kunath *et al.* (2021) found, but more profound. It is possible that the number of place cells are different between the genotypes, and that there does in fact exist a smaller proportion of place cells in the *Neil3*$^{-/-}$ mice. This might be due to them having disruptions in the amount of mutual information they carry, meaning that the number of principal neurons is the same in the genotypes, but the spatial information carried by the cells is impeded. If this is the case, it points to a disruption in the spatial information processing between the DG and the CA1, as the proportion of place cells is the same between the genotypes in the DG. It is also possible that the more stringent filtering procedure that was done on this dataset to classify place cells had a stronger effect on the amount of place cells in the *Neil3*$^{-/-}$ than it had on the wildtype, which lead to the more profound differences compared to what was found by Kunath *et al.* (2021). Especially the intrasession spatial stability of the cells might have an influence, as Kunath *et al.* (2021) found indications of impaired spatial stability in the CA1 of *Neil3*$^{-/-}$ mice. Finally, it is possible that the total number of cells had an influence on how many of the cells were place cells. If there is a low sample size, random deviations from normal have a more profound effect.

A smaller proportion of HD cells were found in the *Neil3*$^{-/-}$ mouse, both in CA1 and DG, and A higher proportion of speed cells were found in the *Neil3*$^{-/-}$ mouse in CA1, but not in the DG. In the DG the *Neil3*$^{-/-}$ mouse had a smaller proportion of speed cells. In the CA1, the wildtype mouse had 13% of the cells classified as conjunctive place and speed cells, whereas the *Neil3*$^{-/-}$ mouse had none. This might be due to the low sample size. It might also stem from the input from the mEC being perturbed, as HD is integrated in the mEC.

4.1.2 Place Cells

To my knowledge, this is the first time the spatial representations of DG cells has been investigated in the *Neil3*$^{-/-}$ mouse model.

There was a difference in spatial information content of place cells in both CA1 and DG, with the *Neil3*$^{-/-}$ mouse place cells carrying more spatial information. Similarly, a difference in spatial information rate was in CA1, but not in the DG, with *Neil3*$^{-/-}$ mouse having a higher spatial information rate. This might be due to differences in sample size. Kunath *et al.* (2021) did not find a difference between the genotypes in content in CA1.

In summary, the spatial information content was higher in both CA1 and DG of the Neil3$^{-/-}$ mouse, the information rate was higher in the CA1 of the Neil3$^{-/-}$ mouse, and the average firing rate was higher in the CA1 and DG of the Neil3$^{-/-}$ mouse. This result suggests that there is a difference in the mutual information carried by the place cells, both between the locations and the genotypes.

4.1.2.1 Specificity

A series of analyses were conducted to investigate whether NEIL3 impacts the spatial specificity of hippocampal place cells. To investigate specificity, I investigated the number of cells that had multiple place fields, the size of the place fields, and the peak firing rate within the place fields.

Regarding multiple fields, there were a smaller proportion of cells in the DG of the *Neil3*$^{-/-}$ mouse that had multiple place fields compared to the other conditions. This difference might be due to the difference in sample size. It might also be due to the lack of adult born granule cells in the *Neil3*$^{-/-}$ mouse. Neunuebel and Knierim (2012) propose that cells with single place fields are mature granule cells, whereas cells with multiple place fields might be mossy cells or newly born granule cells. If there is a lack of adult born granule cells in the *Neil3*$^{-/-}$ mouse, we can expect to see a reduced number of cells with multiple place fields in the DG. Another possibility is that the scale of the hippocampal representation is disrupted in some way. When Fenton *et al.* (2008) compared place cell representations in a small area and in a larger area, they found a higher proportion of place cells and more cells with multiple fields in the larger area. If this is the case, it might be due to either a difference in recording location on the longitudinal axis, as the scale increases on the longitudinal axis of the hippocampus (Kjelstrup *et al.*, 2008), or it might be due to a disruption in the input from the mEC. In the mEC, the scale of the grid representations increases on the dorsoventral axis (Kjelstrup *et al.*, 2008), and if there is a disruption in this system, the scale transfer to the hippocampus might be affected.

Regarding the size of the place fields, there was a difference between both the genotypes and the location. The place fields in CA1 of the *Neil3*$^{-/-}$ mouse were smaller than the other conditions. This might be due to the sample size, where the *Neil3*$^{-/-}$ mouse had a considerably smaller number of place cells recorded in the CA1. It might also be due to different recording locations, but if this was the case, there should have been observed differences in the DG too. It is also possible that the observed difference is due to scale difference and disruption in mEC as discussed in the previous paragraph. The difference in scale could become more pronounced downstream in the hippocampal circuit.

Regarding the peak firing rate within the place fields, there was no apparent difference between the genotypes. The peak firing rate within the place fields is not necessarily related to the field size and might be unaffected by a disruption of the scale.

4.1.2.2 Remapping

A series of analyses were conducted to investigate whether NEIL3 impacts the spatial remapping capabilities of hippocampal place cells. In this study, some of the place cells of the *Neil3*$^{-/-}$ mouse maintained their place fields when moved to a new environment. The findings indicate that NEIL3 influences the remapping capabilities in the DG, contrary to the findings of Kunath *et al.* (2021), who found preserved remapping capabilities in the CA1 in *Neil3*$^{-/-}$ mice.

The observed difference in remapping capabilities might stem from a heterogeneous and low sample size. The findings might also be due to an issue in the experimental setup. However, if it was an issue with the experimental setup, it should have been for both the mice, as they were exposed to the exact same experimental conditions and analyses. Anxiety might be a confounding variable, but anxiety has been shown to cause remapping in CA1 (Kim *et al.*, 2015; Moita *et al.*, 2004), not impeding it as observed in this study. It is possible however, that anxiety influences remapping differentially in the DG and in the CA1.

Issues with remapping might be related to the observed memory deficits. An issue with remapping indicates that the population of cells that represent the different spaces are not unique. If a subset of the place cell does not remap when introduced to a new environment, there is a chance that parts of the memory code get written onto the wrong substrate, corrupting parts of the memory. In terms of cognitive map theory, the phenomenon can be explained in terms of writing the memory coordinates onto the wrong map, and thus the maps become scrambled in terms of their content. However, as will be discussed in the next section, the spatial representation remains stable over time.

The difference in remapping between the genotypes might stem from an issue in a sub-population of place cells in the DG. The DG place cells can be divided into three different classes: mature granule cells, adult-born granule cells, and mossy cells. These cells have different properties and functional significance in the hippocampal circuitry, and the lack of some of these cells might have an influence on remapping. It has previously been reported that the neural progenitor cells of the *Neil3*$^{-/-}$ mice have reduced proliferative capabilities, resulting in the lack of adult-born granule cells in NEIL3 deficient mice. However, more advanced analyses are needed to investigate the contribution of specific cell types in the DG.

The impaired remapping might indicate issues with pattern separation. If the DG local microcircuits enable pattern separation, which decides what pattern gets completed in the CA3, and this pattern separation process is partially disrupted, we can expect to see impaired remapping. It is possible that the lack of adult born granule cells makes the pattern separation process weaker. This phenomenon can also be explained in in terms of attractor dynamics. If the pattern separation process in the DG controls which point attractors in the CA3 get activated, then an impairment in the microcircuit governing pattern separation could lead to the wrong point attractors being converged upon.

The pattern separation and completion can also be influenced by the input from the mEC. If the mEC functions as a noise reducer, as suggested by Rennó-Costa and Tort (2017) and Agmon and Burak (2020), and this function is somehow impaired, we could expect to see the network activity converging on an alternative set of attractors, leading to impaired remapping. This impairment might stem from either a functional disruption in the local circuitry of the mEC, in the input to the mEC, or in parvalbumin expressing interneurons in the DG. Supressing the activity of parvalbumin expressing interneurons have been shown to decrease the coupling between the EC and the hippocampus (Aery Jones *et al.*, 2021), and an disruption in this cell class might impede the information transfer to the hippocampus.

There might be a difference in the strength of the attractors, stemming from a difference in synaptic plasticity. Kunath *et al.* (2021) found many differentially expressed genes related to synaptic plasticity between the genotypes. As attractors are created by manipulating the synaptic strength between the cells, an impairment in synaptic plasticity could make the attractors form and stabilize slower.

There was a difference in familiarity between the two recording boxes, where the mice were recorded many more times in box A, whereas box B was only used for the remapping experiments. This means that the cells had more time to consolidate the neural representation of the space in box A, possibly leading to stronger attractors. This could

also possibly be influenced by noise reduction impairments of the mEC, as a noisy signal might be more likely to converge onto the stronger attractors.

4.1.2.3 Stability

A series of analyses were conducted to investigate whether NEIL3 impacts the spatial stability of hippocampal place cells. The findings indicate that NEIL3 does not impair the stability capabilities in the DG, contrary to the findings of Kunath *et al.* (2021), who found disrupted long-term stability of *Neil3*$^{-/-}$ mice in the CA1. The findings suggest that the spatial stability of DG cells in the *Neil3*$^{-/-}$ mouse outperforms the wildtype, with many of the cells having almost perfectly preserved spatial representations in the long-term condition. As with the other experiments, these results might be strongly influenced by the small sample size.

If the stability is impaired in CA1 and not in the DG, it might indicate that there is some issue downstream from DG. This might indicate a possible issue with pattern completion in CA3, which might be due to synaptic plasticity being affected by the lack of NEIL3. It is possible that lack of NEIL3 causes a downregulation or a functional impairment in the intracellular molecular cascade of the metabotropic glutamate receptor 5 (mGluR5), which has been shown to mediate LTP. mGlur5 has been shown to be related to the late phase of LTP (Bikbaev *et al.*, 2008; Naie and Manahan-Vaughan, 2004) and long-term stability of spatial representations (Manahan-Vaughan and Braunewell, 2005). mGlur5 is also highly expressed during development (Romano, Van den Pol and O'Malley, 1996), and an impairment in the expression or functioning of these receptors might explain the delayed maturation in *Neil3*$^{-/-}$ mice found by Kunath *et al.* (2021). Further, mGlur5 is highly expressed in progenitor cells (Xu *et al.*, 2012), which might be related to the impaired ability of *Neil3*$^{-/-}$ mice to differentiate properly, as found by Rolseth *et al.* (2013).

It is possible that the discrepancy between remapping and stability is because the stability was investigated using a very familiar box. As discussed in the previous section, the attractors for box A might be stronger than the attractors for box B. This is also related to a difference between this study and the study by Kunath *et al.* (2021), where they found impaired long-term stability. They only recorded cells in the CA1, whereas in this study cells from both CA1 and DG was recorded, resulting in an overall higher number of recording sessions for the mice in this study.

4.2 Behavioral Testing

The main research questions that were tested with the behavioural tests were whether NEIL3 impacts spatial memory and whether NEIL3 impacts anxiety. There were indications of both spatial memory impairments and increased anxiety for the *Neil3*$^{-/-}$ mice. To my knowledge this is the first study to investigate the *Neil3*$^{-/-}$ model organism using the NOL and Y-Maze experiments. The behavioural data collection was part of a bigger project of establishing behavioural protocols.

4.2.1 Open Field

The open field experiment was used to answer if NEIL3 influences anxiety. A series of variables were extracted from the open field experiment to assess anxiety. There were several indications of increased anxiety in *Neil3*$^{-/-}$ mice, such as more time spent in the corner, and less entries to the centre zone.

These findings are contrary to the findings presented by Regnell *et al.* (2012). This discrepancy might be due to methodological differences between the two studies. Regnell *et al.* (2012) used exclusively 18-month-old mice, whereas the most apparent differences between the genotypes in this study were in mice that were 3-4 months old. Further, they primarily relied on a different test, the elevated zero maze, to assess anxiety which might influence the results. Carola *et al.* (2002) investigated the differences between anxiety measures on the open field and the elevated plus maze, which has similar characteristics to the elevated zero maze. They found that the tests sometimes give discrepant results when tested on the same genotypes. These differences might stem from differences in both testing and analysing. A possible remedy for this problem is to test the mice with both the elevated plus/zero maze and the open field, and then using a factor analysis to investigate anxiety levels accurately.

It is also possible that the *Neil3*$^{-/-}$ mice have increased baseline anxiety, but lower responsiveness to anxiogenic stimuli. The elevated zero maze is inherently more anxiogenic than the open field, and when the *Neil3*$^{-/-}$ mice are introduced to the elevated zero maze the differences in baseline anxiety are overshadowed by the differences in responsiveness.

Another interesting pattern emerged with the young *Neil3*$^{-/-}$ mice having lower activity levels than the other groups, measured by the total distance travelled, number of zone crossings and average speed. Regnell *et al.* (2012) also found indications that the *Neil3*$^{-/-}$ mice had lower activity levels. General activity level might be a mediating variable between the measured variables and anxiety.

4.2.2 Novel Object Location

The NOL experiment was used to answer if NEIL3 influences spatial memory. The NOL experiment had two different conditions: a STM condition, and a LTM condition. There was an indication that spatial memory was disrupted in the LTM condition, but not in the STM condition, both for the young and old *Neil3*$^{-/-}$ mice. These findings replicate the findings by Regnell *et al.* (2012), where they found impaired spatial LTM in old *Neil3*$^{-/-}$ mice when tested in the Morris water maze. It is important to note that the sample size in the STM condition was very low for the young animals.

Anxiety might be a possible confounding variable. As the young *Neil3*$^{-/-}$ mice were more likely to spend time in the corner zones, and less likely to enter the centre zone, the result might be influenced by this. Anxious mice are less likely to engage in exploratory behaviours (Heinz *et al.*, 2021). There is also the possible anxiogenic effect of being handled repeatedly. The effect of being subjected to repeated trials in a day also might influence anxiety. In the STM condition the mice were handled repeatedly and were introduced to the same box several times. In the STM condition the mice had a 5-minute interval between the phases, while in the LTM condition the mice had a 24-hour interval between each phase. It is hard to assess the influence of handling and testing frequency on anxiety. On the one hand, repeated handling by tail-lifting might be anxiogenic, whereas repeated exposure to the recording environment might have a habituating function, which might be anxiolytic.

The observed disruption of memory might be due to an issue with neurogenesis. As silencing adult-born granule cells leads to impaired long-term memory retrieval (Gu, Janoschka and Ge, 2013), the influence of NEIL3 on generating these cells might be the cause of the memory deficit.

4.2.3 Y-maze

The Y-maze experiment was used to answer if NEIL3 influences spatial memory. The Y-maze experiment was only conducted on the LTM condition. The results were inconclusive, with both the wildtype- and the *Neil3*$^{-/-}$ mice showing discrimination close to chance level. There was also a tendency of the young *Neil3*$^{-/-}$ mice to prefer the familiar arm. Three possible explanations are discussed for this finding.

First, the finding that wildtype mice did not discriminate between the familiar and novel arm indicates that there are some methodological issues, as we expect the wildtype mice to have preserved memory. If the wildtype mice had preserved spatial memory and the y-maze experiment measures spatial memory, we could expect the wildtype mice to

enter the novel arm more frequently and spend more time in the novel arm. These results thus indicates that the test lacks validity.

Second, as in the NOL task, anxiety might be a confounding variable. This might be related to the methodological issues. The Y-maze is inherently more anxiogenic than the NOL due to its narrow corridors and reduced visibility, which might result in less exploratory behaviour. The results might be confounded in the sense that *Neil3*$^{-/-}$ mice are more affected by the anxiogenic nature of the y-maze. There was a tendency of the young *Neil3*$^{-/-}$ mice to prefer the novel arm, whereas the wildtype mice tended to be closer to chance level. In response to this issue, the group obtained a new y-maze that had broader corridors.

Third, the narrow corridors of the Y-maze also might hinder the view to the distal cue cards, making it harder to orient themselves. There is a proposed difference between the use of proximal cues and local boundaries and the use of distal cues, where the proximal cues and local boundaries have a bigger influence on the hippocampal spatial representations, whereas proximal cues have an influence on the mEC dependent path integration (Knierim and Hamilton, 2011). If the cause of the spatial memory impairments in *Neil3*$^{-/-}$ mice originate in the mEC, we can expect the differences in memory to be attenuated when reducing the importance of the mEC dependent input.

4.3 Limitations and Suggestions for Further Research

A major limitation of this study is the non-homogenous and small sample size. This might influence the findings severely. This is true for both the behavioural and the cell physiology experiments. This is a particularly big problem for the cell physiology, as only two mice were included. Individual differences might play a significant role, which might overshadow the differences between the genotypes. This issue will be addressed further by the research group, as more data is ready to be analysed, and more experiments are planned for the future.

Another limitation is that I observed indications of increased anxiety in young *Neil3*$^{-/-}$ mice, and I do not know whether this increased anxiety affects the results of the other experiments. To better assess anxiousness in the mice, the elevated zero maze together with the open field could be used to delineate the effects of both general activity and anxiety. Further, additional variables could be extracted from the ANY-maze software and analysed through a dimension reduction method. Manually extracted variables from the open field, such as defecation, shivering, or gnawing, which have been shown to be signs of anxiety (Sestakova *et al.*, 2013), could also be used to determine anxiety levels.

To attenuate the possible effects of anxiety on the memory experiments, a food restriction paradigm could be used. Food restriction give a higher motivation to explore the recording area, as finding food is more important than avoiding anxiety (Heinz *et al.*, 2021). This does however warrant additional ethical considerations. Due to the possible effect anxiety might have on the outcomes of behavioural tests, tests that might influence anxiety, such as a fear conditioning paradigm, should be used with care as it might result in measuring differences in anxiety instead of differences in memory.

This study focused mainly on place cells, whereas non-spatially tuned principal cells and other cell types might also have an important influence on the representation of space in the hippocampus, as found by Stefanini *et al.* (2020). A future study that employs a recording technique with the possibility to investigate a higher number of cells simultaneously would be interesting. Further, finding a way to differentiate mossy cells and granule cells can elucidate effects of NEIL3 on the local circuitry of the DG. If there are issues with one of the cell types, pattern separation and/or completion could be compromised.

To my knowledge, the influence of NEIL3 on mGlur5 specifically has not been investigated. An impairment of mGlur5 downstream of DG might explain the discrepancy between the findings of long-term stability between the DG and CA1. As we already have collected transcriptome data for the different subfields of the hippocampus, we could check if the genes related to mGlur5 are differentially expressed. We could also test if the attractors are stronger for one of the environments by employing an unfamiliar recording area for the long-term stability experiment.

Further, the possible influence and disruption of mEC should be investigated. By investigating grid modules and their influence on the local circuit in DG, we could elucidate their influence on the hippocampal spatial representations. mEC and its connection to the hippocampus is hypothesized to act as an error correction / noise reducing function. A disruption in this system could be related to the observed deficits in remapping.

Finally, the severity of the genetic manipulation might be a limitation. We cannot say for sure that the observed differences are caused by hippocampal malfunction, general brain dysfunction, or if it is due to focal disruptions in other regions. The genetic knockout might influence other areas related to spatial memory.

5 Conclusion

The main aim of this study was to elucidate whether NEIL3 impacts the functional plasticity of hippocampal place cells in the CA1 and DG. To do this, microdrives were wired and implanted, and cell populations from the CA1 and DG were recorded, clustered, and analysed. A total of 619 cells were clustered and analysed. Some of these cells were further classified into six categories, where the place cell category was investigated further. Even though the sample size was very low, some tendencies were revealed. For the place cells, the spatial information content was higher in both CA1 and DG of the *Neil3*$^{-/-}$ mouse, the information rate was higher in the CA1 of the *Neil3*$^{-/-}$ mouse, and the average firing rate was higher in the CA1 and DG of the *Neil3*$^{-/-}$ mouse. To address the first research question, whether NEIL3 impacts the spatial specificity of hippocampal place cells, I extracted information about the place fields of the place cells. The *Neil3*$^{-/-}$ mouse had lower proportion of cells with multiple fields in the DG, the place field size was smaller in both CA1 and DG, and the field peak firing rate was higher. This might be an indication of impaired spatial specificity. To address the second research question, whether NEIL3 impacts the spatial remapping of hippocampal place cells, I employed a remapping experiment where the mice were recorded both in a familiar and a novel environment. The wildtype mouse showed low correlation coefficients when moved to a new environment, whereas the *Neil3*$^{-/-}$ mouse showed higher correlation coefficients. This was true for both the remapping conditions, indicating that the *Neil3*$^{-/-}$ mouse had an impairment in the remapping capabilities of place cells in the DG. To investigate the third research question, whether NEIL3 impacts the spatial stability of hippocampal place cells, I tested the mice in the same box with a short-term stability condition (50min) and a long-term condition (24h). In both the short-term and the long-term stability conditions, both the mice had high correlation coefficients, which suggests that both the mice had preserved stability of the place cell spatial representation in the DG.

The secondary aim of this study was to elucidate whether NEIL3 impacts anxiety and spatial memory. To address the fourth research question, whether NEIL3 influences anxiety, I performed an open field experiment. The young *Neil3*$^{-/-}$ mice spent more time on average in the corners and entered the centre less than the other groups in the open field experiment, indicating increased anxiety. The young *Neil3*$^{-/-}$ mice also travelled a shorter distance at a lower speed, and with less crossings between the zones, indicating reduced locomotor activity. To address the fifth research question, whether NEIL3 influences spatial memory, I performed the NOL experiment. In the NOL experiment the

mean discrimination indices were all positive in the STM condition, indicating that the memory capabilities were intact. In the LTM condition the *Neil3*$^{-/-}$ mice tended to discriminate the objects less well than the wildtype mice, indicating impaired memory. For the y-maze, the discrimination indices for both time and entries for all the animals were close to zero, indicating that they did not discriminate between the familiar and novel arm well. This indicates that there were some methodological issues with the y-maze experiment.

In summary, the results suggest that NEIL3 impacts the functional plasticity, anxiety, and spatial memory of mice.

6 References

Abbott, L. C. and Nigussie, F. (2020) Adult neurogenesis in the mammalian dentate gyrus, *Anat Histol Embryol*, 49(1), pp. 3-16. doi: 10.1111/ahe.12496.

Aery Jones, E. A. *et al.* (2021) Dentate gyrus and CA3 GABAergic interneurons bidirectionally modulate signatures of internal and external drive to CA1, *Cell Rep*, 37(13), pp. 110159. doi: 10.1016/j.celrep.2021.110159.

Agarwal, P. and Miller, K. M. (2017) Chapter 11 - Chromatin Dynamics and DNA Repair, in Göndör, A. (ed.) *Chromatin Regulation and Dynamics.* Boston: Academic Press, pp. 275-302.

Agmon, H. and Burak, Y. (2020) A theory of joint attractor dynamics in the hippocampus and the entorhinal cortex accounts for artificial remapping and grid cell field-to-field variability, *Elife*, 9. doi: 10.7554/eLife.56894.

Agnihotri, N. T. *et al.* (2004) The long-term stability of new hippocampal place fields requires new protein synthesis, *Proceedings of the National Academy of Sciences*, 101(10), pp. 3656-3661. doi: doi:10.1073/pnas.0400385101.

Alme, C. B. *et al.* (2010) Hippocampal granule cells opt for early retirement, *Hippocampus*, 20(10), pp. 1109-1123. doi: https://doi.org/10.1002/hipo.20810.

Amit, D. J. (1989) *Modeling brain function : the world of attractor neural networks*. Cambridge: Cambridge University Press.

Andersen, P. *et al.* (2006) *The hippocampus book*. New York, NY, US: Oxford University Press.

Anindya, R. (2020) Single-stranded DNA damage: Protecting the single-stranded DNA from chemical attack, *DNA Repair (Amst)*, 87, pp. 102804. doi: 10.1016/j.dnarep.2020.102804.

Baltaci, S. B., Mogulkoc, R. and Baltaci, A. K. (2019) Molecular Mechanisms of Early and Late LTP, *Neurochem Res*, 44(2), pp. 281-296. doi: 10.1007/s11064-018-2695-4.

Barry, C. *et al.* (2007) Experience-dependent rescaling of entorhinal grids, *Nat Neurosci*, 10(6), pp. 682-684. doi: 10.1038/nn1905.

Beltrán, J. Q. and Gutiérrez, R. (2012) Co-release of glutamate and GABA from single, identified mossy fibre giant boutons, *The Journal of Physiology*, 590(19), pp. 4789-4800. doi: https://doi.org/10.1113/jphysiol.2012.236372.

Benear, S. L., Ngo, C. T. and Olson, I. R. (2020) Dissecting the Fornix in Basic Memory Processes and Neuropsychiatric Disease: A Review, *Brain Connect*, 10(7), pp. 331-354. doi: 10.1089/brain.2020.0749.

Bikbaev, A. *et al.* (2008) MGluR5 mediates the interaction between late-LTP, network activity, and learning, *PLoS One*, 3(5), pp. e2155-e2155. doi: 10.1371/journal.pone.0002155.

Bliss, T. V. and Lømo, T. (1973) Long-lasting potentiation of synaptic transmission in the dentate area of the anaesthetized rabbit following stimulation of the perforant path, *J Physiol*, 232(2), pp. 331-356. doi: 10.1113/jphysiol.1973.sp010273.

Cadet, J. and Davies, K. J. A. (2017) Oxidative DNA damage & repair: An introduction, *Free Radical Biology and Medicine*, 107, pp. 2-12. doi: https://doi.org/10.1016/j.freeradbiomed.2017.03.030.

Carola, V. *et al.* (2002) Evaluation of the elevated plus-maze and open-field tests for the assessment of anxiety-related behaviour in inbred mice, *Behavioural Brain Research*, 134(1), pp. 49-57. doi: https://doi.org/10.1016/S0166-4328(01)00452-1.

Cembrowski, Mark S. *et al.* (2016) Spatial Gene-Expression Gradients Underlie Prominent Heterogeneity of CA1 Pyramidal Neurons, *Neuron*, 89(2), pp. 351-368. doi: https://doi.org/10.1016/j.neuron.2015.12.013.

Chen, Z. and Zhong, C. (2014) Oxidative stress in Alzheimer's disease, *Neuroscience Bulletin*, 30(2), pp. 271-281. doi: 10.1007/s12264-013-1423-y.

Cholvin, T. *et al.* (2018) Ventral Midline Thalamus Is Necessary for Hippocampal Place Field Stability and Cell Firing Modulation, *J Neurosci*, 38(1), pp. 158-172. doi: 10.1523/jneurosci.2039-17.2017.

Colgin, L. L. (2016) Rhythms of the hippocampal network, *Nature reviews. Neuroscience*, 17(4), pp. 239-249. doi: 10.1038/nrn.2016.21.

Colicos, M. A. and Dash, P. K. (1996) Apoptotic morphology of dentate gyrus granule cells following experimental cortical impact injury in rats: possible role in spatial memory deficits, *Brain Res*, 739(1-2), pp. 120-131. doi: 10.1016/s0006-8993(96)00824-4.

Danielson, N. B. *et al.* (2016) Sublayer-Specific Coding Dynamics during Spatial Navigation and Learning in Hippocampal Area CA1, *Neuron*, 91(3), pp. 652-665. doi: https://doi.org/10.1016/j.neuron.2016.06.020.

Davoudi, H. and Foster, D. J. (2019) Acute silencing of hippocampal CA3 reveals a dominant role in place field responses, *Nat Neurosci*, 22(3), pp. 337-342. doi: 10.1038/s41593-018-0321-z.

de Sousa, M. M. L. *et al.* (2021) Impact of Oxidative DNA Damage and the Role of DNA Glycosylases in Neurological Dysfunction, *Int J Mol Sci*, 22(23). doi: 10.3390/ijms222312924.

Denninger, Smith and Kirby (2018) Novel Object Recognition and Object Location Behavioral Testing in Mice on a Budget, *Journal of Visualized Experiments*, 2018. doi: 10.3791/58593.

Dhruve, J. J. (2021) *DNA : A Bridge Between Biochemistry and Biotechnology*. New India Publishing Agency NIPA.

Ernst, A. and Frisén, J. (2015) Adult neurogenesis in humans- common and unique traits in mammals, *PLoS Biol*, 13(1), pp. e1002045. doi: 10.1371/journal.pbio.1002045.

Eyre, M. D. and Bartos, M. (2019) Somatostatin-Expressing Interneurons Form Axonal Projections to the Contralateral Hippocampus, *Frontiers in Neural Circuits*, 13, pp. 56-56. doi: 10.3389/fncir.2019.00056.

Faisal, A. A., Selen, L. P. J. and Wolpert, D. M. (2008) Noise in the nervous system, *Nature reviews. Neuroscience*, 9(4), pp. 292-303. doi: 10.1038/nrn2258.

Fenton, A. A. *et al.* (2008) Unmasking the CA1 Ensemble Place Code by Exposures to Small and Large Environments: More Place Cells and Multiple, Irregularly Arranged, and Expanded Place Fields in the Larger Space, *The Journal of Neuroscience*, 28(44), pp. 11250-11262. doi: 10.1523/jneurosci.2862-08.2008.

Fyhn, M. *et al.* (2007) Hippocampal remapping and grid realignment in entorhinal cortex, *Nature*, 446(7132), pp. 190-194. doi: 10.1038/nature05601.

Galván, E. J. and Gutiérrez, R. (2017) Target-Dependent Compartmentalization of the Corelease of Glutamate and GABA from the Mossy Fibers, *The Journal of Neuroscience*, 37(3), pp. 701-714. doi: 10.1523/jneurosci.1915-16.2016.

Gu, Y., Janoschka, S. and Ge, S. (2013) Neurogenesis and hippocampal plasticity in adult brain, *Curr Top Behav Neurosci*, 15, pp. 31-48. doi: 10.1007/7854_2012_217.

Guzowski, J. F. *et al.* (2001) Experience-dependent gene expression in the rat hippocampus after spatial learning: a comparison of the immediate-early genes Arc, c-fos, and zif268, *J Neurosci*, 21(14), pp. 5089-5098. doi: 10.1523/jneurosci.21-14-05089.2001.

Guzowski, J. F. *et al.* (2006) Recent behavioral history modifies coupling between cell activity and Arc gene transcription in hippocampal CA1 neurons, *Proc Natl Acad Sci U S A*, 103(4), pp. 1077-1082. doi: 10.1073/pnas.0505519103.

Ha, A., Lin, Y. and Yan, S. (2020) A non-canonical role for the DNA glycosylase NEIL3 in suppressing APE1 endonuclease-mediated ssDNA damage, *J Biol Chem*, 295(41), pp. 14222-14235. doi: 10.1074/jbc.RA120.014228.

Hafting, T. *et al.* (2005) Microstructure of a spatial map in the entorhinal cortex, *Nature*, 436(7052), pp. 801-806. doi: 10.1038/nature03721.

Hall, C. and Ballachey, E. L. (1932) A study of the rat's behavior in a field. A contribution to method in comparative psychology, *University of California Publications in Psychology*.

Hardcastle, K. *et al.* (2017) A Multiplexed, Heterogeneous, and Adaptive Code for Navigation in Medial Entorhinal Cortex, *Neuron*, 94(2), pp. 375-387.e377. doi: 10.1016/j.neuron.2017.03.025.

Heinz, D. E. *et al.* (2021) Exploratory drive, fear, and anxiety are dissociable and independent components in foraging mice, *Translational Psychiatry*, 11(1), pp. 318. doi: 10.1038/s41398-021-01458-9.

Hopfield, J. J. (1982) Neural networks and physical systems with emergent collective computational abilities, *Proceedings of the National Academy of Sciences*, 79(8), pp. 2554-2558. doi: 10.1073/pnas.79.8.2554.

Houser, C. R. (2007) Interneurons of the dentate gyrus: an overview of cell types, terminal fields and neurochemical identity, *Prog Brain Res*, 163, pp. 217-232. doi: 10.1016/s0079-6123(07)63013-1.

Houser, C. R. *et al.* (2021) Mossy Cells in the Dorsal and Ventral Dentate Gyrus Differ in Their Patterns of Axonal Projections, *J Neurosci*, 41(5), pp. 991-1004. doi: 10.1523/jneurosci.2455-20.2020.

Hussaini, S. A. *et al.* (2011) Increased size and stability of CA1 and CA3 place fields in HCN1 knockout mice, *Neuron*, 72(4), pp. 643-653. doi: 10.1016/j.neuron.2011.09.007.

Jacob, P. Y. *et al.* (2020) Medial entorhinal cortex lesions induce degradation of CA1 place cell firing stability when self-motion information is used, *Brain Neurosci Adv*, 4, pp. 2398212820953004. doi: 10.1177/2398212820953004.

Jensen, K. R. *et al.* (2021) Multiple cannabinoid signaling cascades powerfully suppress recurrent excitation in the hippocampus, *Proc Natl Acad Sci U S A*, 118(4). doi: 10.1073/pnas.2017590118.

Jun, H. *et al.* (2020) Disrupted Place Cell Remapping and Impaired Grid Cells in a Knockin Model of Alzheimer's Disease, *Neuron*, 107(6), pp. 1095-1112. e1096. doi: https://doi.org/10.1016/j.neuron.2020.06.023.

Kanter, B. R. *et al.* (2017) A Novel Mechanism for the Grid-to-Place Cell Transformation Revealed by Transgenic Depolarization of Medial Entorhinal Cortex Layer II, *Neuron*, 93(6), pp. 1480-1492.e1486. doi: 10.1016/j.neuron.2017.03.001.

Kassambara, A. (2021) *rstatix*. Available at: https://www.rdocumentation.org/packages/rstatix/versions/0.7.0.

Kempermann, G. *et al.* (2003) Early determination and long-term persistence of adult-generated new neurons in the hippocampus of mice, *Development*, 130(2), pp. 391-399. doi: 10.1242/dev.00203.

Kentros, C. G. *et al.* (2004) Increased attention to spatial context increases both place field stability and spatial memory, *Neuron*, 42(2), pp. 283-295. doi: 10.1016/s0896-6273(04)00192-8.

Kim, E. J. *et al.* (2015) Alterations of hippocampal place cells in foraging rats facing a "predatory" threat, *Curr Biol*, 25(10), pp. 1362-1367. doi: 10.1016/j.cub.2015.03.048.

Kjelstrup *et al.* (2008) Finite Scale of Spatial Representation in the Hippocampus, *Science*, 321(5885), pp. 140-143. doi: doi:10.1126/science.1157086.

Kjelstrup, K. B. *et al.* (2008) Finite scale of spatial representation in the hippocampus, *Science*, 321(5885), pp. 140-143. doi: 10.1126/science.1157086.

Knierim, J. J. and Hamilton, D. A. (2011) Framing Spatial Cognition: Neural Representations of Proximal and Distal Frames of Reference and Their Roles in Navigation, *Physiological Reviews*, 91(4), pp. 1245-1279. doi: 10.1152/physrev.00021.2010.

Knierim, J. J. and Zhang, K. (2012) Attractor dynamics of spatially correlated neural activity in the limbic system, *Annual Review of Neuroscience*, 35, pp. 267-285. doi: 10.1146/annurev-neuro-062111-150351.

Knudsen, E. B. and Wallis, J. D. (2021) Hippocampal neurons construct a map of an abstract value space, *Cell*, 184(18), pp. 4640-4650.e4610. doi: https://doi.org/10.1016/j.cell.2021.07.010.

Kraeuter, A. K., Guest, P. C. and Sarnyai, Z. (2019) The Y-Maze for Assessment of Spatial Working and Reference Memory in Mice, *Methods Mol Biol*, 1916, pp. 105-111. doi: 10.1007/978-1-4939-8994-2_10.

Krokan, H. E. and Bjørås, M. (2013) Base excision repair, *Cold Spring Harbor perspectives in biology*, 5(4), pp. p.a012583-a012583. doi: https://doi.org/10.1101%2Fcshperspect.a012583.

Kunath, N. *et al.* (2021) DNA repair enzyme NEIL3 enables a stable neural representation of space by shaping transcription in hippocampal neurons, *iScience*, 24(12), pp. 103470. doi: 10.1016/j.isci.2021.103470.

Latuske, P. *et al.* (2017) Hippocampal Remapping and Its Entorhinal Origin, *Front Behav Neurosci*, 11, pp. 253. doi: https://doi.org/10.3389/fnbeh.2017.00253.

Lee, H., Goodsmith, D. and Knierim, J. J. (2020) Parallel processing streams in the hippocampus, *Curr Opin Neurobiol*, 64, pp. 127-134. doi: 10.1016/j.conb.2020.03.004.

Leutgeb, J. K. *et al.* (2007) Pattern Separation in the Dentate Gyrus and CA3 of the Hippocampus, *Science*, 315(5814), pp. 961-966. doi: doi:10.1126/science.1135801.

Li, T., Arleo, A. and Sheynikhovich, D. (2020) Modeling place cells and grid cells in multi-compartment environments: Entorhinal-hippocampal loop as a multisensory integration circuit, *Neural Netw*, 121, pp. 37-51. doi: 10.1016/j.neunet.2019.09.002.

Li, Y. *et al.* (2017) A distinct entorhinal cortex to hippocampal CA1 direct circuit for olfactory associative learning, *Nat Neurosci*, 20(4), pp. 559-570. doi: 10.1038/nn.4517.

Lindahl, T. and Barnes, D. E. (2000) Repair of endogenous DNA damage *Cold Spring Harbor Symposia on Quantitative Biology* (vol. 65, pp. 127-133): Cold Spring Harbor Laboratory Press. doi: 10.1101/sqb.2000.65.127.

Lopez-Rojas, J., Heine, M. and Kreutz, M. R. (2016) Plasticity of intrinsic excitability in mature granule cells of the dentate gyrus, *Sci Rep*, 6, pp. 21615. doi: 10.1038/srep21615.

Lu, X. and Bilkey, D. K. (2010) The velocity-related firing property of hippocampal place cells is dependent on self-movement, *Hippocampus*, 20(5), pp. 573-583. doi: 10.1002/hipo.20666.

Madar, A. D., Ewell, L. A. and Jones, M. V. (2019) Pattern separation of spiketrains in hippocampal neurons, *Sci Rep*, 9(1), pp. 5282. doi: 10.1038/s41598-019-41503-8.

Malik, R. *et al.* (2016) Mapping the electrophysiological and morphological properties of CA1 pyramidal neurons along the longitudinal hippocampal axis, *Hippocampus*, 26(3), pp. 341-361. doi: https://doi.org/10.1002/hipo.22526.

Mallory, C. S. *et al.* (2018) Grid scale drives the scale and long-term stability of place maps, *Nat Neurosci*, 21(2), pp. 270-282. doi: 10.1038/s41593-017-0055-3.

Manahan-Vaughan, D. and Braunewell, K. H. (2005) The metabotropic glutamate receptor, mGluR5, is a key determinant of good and bad spatial learning performance and hippocampal synaptic plasticity, *Cereb Cortex*, 15(11), pp. 1703-1713. doi: 10.1093/cercor/bhi047.

Manns, J. R. and Eichenbaum, H. (2006) Evolution of declarative memory, *Hippocampus*, 16(9), pp. 795-808. doi: https://doi.org/10.1002/hipo.20205.

Martin, S. J., Grimwood, P. D. and Morris, R. G. (2000) Synaptic plasticity and memory: an evaluation of the hypothesis, *Annu Rev Neurosci*, 23, pp. 649-711. doi: 10.1146/annurev.neuro.23.1.649.

Massaad, M. J. *et al.* (2016) Deficiency of base excision repair enzyme NEIL3 drives increased predisposition to autoimmunity, *J Clin Invest*, 126(11), pp. 4219-4236. doi: https://doi.org/10.1172/JCI85647.

Miao, C. *et al.* (2015) Hippocampal Remapping after Partial Inactivation of the Medial Entorhinal Cortex, *Neuron*, 88(3), pp. 590-603. doi: 10.1016/j.neuron.2015.09.051.

Miles, R. *et al.* (2014) Recurrent synapses and circuits in the CA3 region of the hippocampus: an associative network, *Frontiers in Cellular Neuroscience*, 7(262). doi: 10.3389/fncel.2013.00262.

Milior, G. *et al.* (2016) Electrophysiological Properties of CA1 Pyramidal Neurons along the Longitudinal Axis of the Mouse Hippocampus, *Scientific Reports*, 6(1), pp. 38242. doi: 10.1038/srep38242.

Moita, M. A. *et al.* (2004) Putting fear in its place: remapping of hippocampal place cells during fear conditioning, *J Neurosci*, 24(31), pp. 7015-7023. doi: 10.1523/jneurosci.5492-03.2004.

Montchal, M. E., Reagh, Z. M. and Yassa, M. A. (2019) Precise temporal memories are supported by the lateral entorhinal cortex in humans, *Nat Neurosci*, 22(2), pp. 284-288. doi: 10.1038/s41593-018-0303-1.

Moser, E. I., Moser, M.-B. and McNaughton, B. L. (2017) Spatial representation in the hippocampal formation: a history, *Nature neuroscience*, 20(11), pp. 1448 - 1464.

Muller, R. U. and Kubie, J. L. (1987) The effects of changes in the environment on the spatial firing of hippocampal complex-spike cells, *J Neurosci*, 7(7), pp. 1951-1968. doi: 10.1523/jneurosci.07-07-01951.1987.

Muramatsu, R. *et al.* (2007) Neonatally born granule cells numerically dominate adult mice dentate gyrus, *Neuroscience*, 148(3), pp. 593-598. doi: 10.1016/j.neuroscience.2007.06.040.

Naie, K. and Manahan-Vaughan, D. (2004) Regulation by metabotropic glutamate receptor 5 of LTP in the dentate gyrus of freely moving rats: relevance for learning and memory formation, *Cereb Cortex*, 14(2), pp. 189-198. doi: 10.1093/cercor/bhg118.

Neunuebel, J. P. and Knierim, J. J. (2012) Spatial firing correlates of physiologically distinct cell types of the rat dentate gyrus, *The Journal of neuroscience : the official journal of the Society for Neuroscience*, 32(11), pp. 3848-3858. doi: 10.1523/JNEUROSCI.6038-11.2012.

Nilssen, E. S. *et al.* (2019) Neurons and networks in the entorhinal cortex: A reappraisal of the lateral and medial entorhinal subdivisions mediating parallel cortical pathways, *Hippocampus*, 29(12), pp. 1238-1254. doi: 10.1002/hipo.23145.

Núñez-Ochoa, M. A. *et al.* (2021) Causal relationship of CA3 back-projection to the dentate gyrus and its role in CA1 fast ripple generation, *BMC Neurosci*, 22(1), pp. 37. doi: 10.1186/s12868-021-00641-4.

O'Keefe, J. and Dostrovsky, J. (1971) The hippocampus as a spatial map. Preliminary evidence from unit activity in the freely-moving rat, *Brain Res*, 34(1), pp. 171-175. doi: 10.1016/0006-8993(71)90358-1.

O'Keefe, J. and Nadel, L. (1978) *The hippocampus as a cognitive map*. Oxford university press.

Park, E., Dvorak, D. and Fenton, A. A. (2011) Ensemble place codes in hippocampus: CA1, CA3, and dentate gyrus place cells have multiple place fields in large environments, *PLoS One*, 6(7), pp. e22349-e22349. doi: 10.1371/journal.pone.0022349.

Park, S. A., Miller, D. S. and Boorman, E. D. (2021) Inferences on a multidimensional social hierarchy use a grid-like code, *Nat Neurosci*, 24(9), pp. 1292-1301. doi: 10.1038/s41593-021-00916-3.

Pastalkova, E. *et al.* (2006) Storage of spatial information by the maintenance mechanism of LTP, *Science*, 313(5790), pp. 1141-1144. doi: 10.1126/science.1128657.

Pedersen, T. L. (2022) *ggplot2*. Available at: https://www.rdocumentation.org/packages/ggplot2/versions/3.3.6.

Postans, M. *et al.* (2020) Uncovering a Role for the Dorsal Hippocampal Commissure in Recognition Memory, *Cerebral cortex*, 30(3), pp. 1001-1015. doi: 10.1093/cercor/bhz143.

Poulos, A. M., Christian, K. M. and Thompson, R. F. (2008) 3.19 - Procedural Learning: Classical Conditioning, in Byrne, J. H. (ed.) *Learning and Memory: A Comprehensive Reference.* Oxford: Academic Press, pp. 357-381.

Regnell, Christine E. *et al.* (2012) Hippocampal Adult Neurogenesis Is Maintained by Neil3-Dependent Repair of Oxidative DNA Lesions in Neural Progenitor Cells, *Cell Reports*, 2(3), pp. 503-510. doi: https://doi.org/10.1016/j.celrep.2012.08.008.

Reis, A. and Hermanson, O. (2012) The DNA glycosylases OGG1 and NEIL3 influence differentiation potential, proliferation, and senescence-associated signs in neural stem cells, *Biochem Biophys Res Commun*, 423(4), pp. 621-626. doi: 10.1016/j.bbrc.2012.04.125.

Rennó-Costa, C., Lisman, J. E. and Verschure, P. F. M. J. (2010) The mechanism of rate remapping in the dentate gyrus, *Neuron*, 68(6), pp. 1051-1058. doi: 10.1016/j.neuron.2010.11.024.

Rennó-Costa, C., Lisman, J. E. and Verschure, P. F. M. J. (2014) A Signature of Attractor Dynamics in the CA3 Region of the Hippocampus, *PLOS Computational Biology*, 10(5), pp. e1003641. doi: 10.1371/journal.pcbi.1003641.

Rennó-Costa, C. and Tort, A. B. L. (2017) Place and Grid Cells in a Loop: Implications for Memory Function and Spatial Coding, *J Neurosci*, 37(34), pp. 8062-8076. doi: 10.1523/jneurosci.3490-16.2017.

Rolseth, V. *et al.* (2008) Widespread distribution of DNA glycosylases removing oxidative DNA lesions in human and rodent brains, *DNA Repair (Amst)*, 7(9), pp. 1578-1588. doi: 10.1016/j.dnarep.2008.06.007.

Rolseth, V. *et al.* (2013) Loss of Neil3, the major DNA glycosylase activity for removal of hydantoins in single stranded DNA, reduces cellular proliferation and sensitizes cells to genotoxic stress, *Biochimica et Biophysica Acta (BBA) - Molecular Cell Research*, 1833(5), pp. 1157-1164. doi: https://doi.org/10.1016/j.bbamcr.2012.12.024.

Rolseth, V. *et al.* (2017) No cancer predisposition or increased spontaneous mutation frequencies in NEIL DNA glycosylases-deficient mice, *Sci Rep*, 7(1), pp. 4384. doi: 10.1038/s41598-017-04472-4.

Romano, C., Van den Pol, A. N. and O'Malley, K. L. (1996) Enhanced early developmental expression of the metabotropic glutamate receptor mGluR5 in rat brain: Protein, mRNA splice variants, and regional distribution, *Journal of Comparative Neurology*, 367(3), pp. 403-412. doi: https://doi.org/10.1002/(SICI)1096-9861(19960408)367:3<403::AID-CNE6>3.0.CO;2-9.

Rovira-Esteban, L. *et al.* (2020) Semilunar Granule Cells Are the Primary Source of the Perisomatic Excitatory Innervation onto Parvalbumin-Expressing Interneurons in the Dentate Gyrus, *eNeuro*, 7(4), pp. ENEURO.0323-0319.2020. doi: 10.1523/eneuro.0323-19.2020.

Rueckemann, J. W. *et al.* (2016) Transient optogenetic inactivation of the medial entorhinal cortex biases the active population of hippocampal neurons, *Hippocampus*, 26(2), pp. 246-260. doi: 10.1002/hipo.22519.

Russell, W. M. S. and Burch, R. L. (1959) *The principles of humane experimental technique*. Methuen.

Sanderson, D. J. *et al.* (2009) Enhanced long-term and impaired short-term spatial memory in GluA1 AMPA receptor subunit knockout mice: evidence for a dual-process memory model, *Learn Mem*, 16(6), pp. 379-386. doi: 10.1101/lm.1339109.

Scharfman, H. E. and Myers, C. E. (2016) Corruption of the dentate gyrus by "dominant" granule cells: Implications for dentate gyrus function in health and disease, *Neurobiol Learn Mem*, 129, pp. 69-82. doi: 10.1016/j.nlm.2015.09.005.

Scharfman, H. E. (2018) Advances in understanding hilar mossy cells of the dentate gyrus, *Cell Tissue Res*, 373(3), pp. 643-652. doi: 10.1007/s00441-017-2750-5.

Schiller, D. *et al.* (2015) Memory and space: towards an understanding of the cognitive map, *Journal of Neuroscience*, 35(41), pp. 13904-13911.

Schlesiger, M. I. *et al.* (2018) Hippocampal Global Remapping Can Occur without Input from the Medial Entorhinal Cortex, *Cell Rep*, 22(12), pp. 3152-3159. doi: 10.1016/j.celrep.2018.02.082.

Scoville, W. B. and Milner, B. (1957) Loss of recent memory after bilateral hippocampal lesions, *Journal of neurology, neurosurgery, and psychiatry*, 20(1), pp. 11.

Seibenhener, M. L. and Wooten, M. C. (2015) Use of the Open Field Maze to measure locomotor and anxiety-like behavior in mice, *J Vis Exp*, (96), pp. e52434. doi: 10.3791/52434.

Sejersted, Y. *et al.* (2011) Endonuclease VIII-like 3 (Neil3) DNA glycosylase promotes neurogenesis induced by hypoxia-ischemia, *Proc Natl Acad Sci U S A*, 108(46), pp. 18802-18807. doi: 10.1073/pnas.1106880108.

Senzai, Y. (2019) Function of local circuits in the hippocampal dentate gyrus-CA3 system, *Neurosci Res*, 140, pp. 43-52. doi: 10.1016/j.neures.2018.11.003.

Sestakova, N. *et al.* (2013) Determination of motor activity and anxiety-related behaviour in rodents: methodological aspects and role of nitric oxide, *Interdiscip Toxicol*, 6(3), pp. 126-135. doi: 10.2478/intox-2013-0020.

Sharif, F. *et al.* (2021) Subcircuits of Deep and Superficial CA1 Place Cells Support Efficient Spatial Coding across Heterogeneous Environments, *Neuron*, 109(2), pp. 363-376.e366. doi: https://doi.org/10.1016/j.neuron.2020.10.034.

Sheintuch, L. *et al.* (2020) Multiple Maps of the Same Spatial Context Can Stably Coexist in the Mouse Hippocampus, *Curr Biol*, 30(8), pp. 1467-1476.e1466. doi: 10.1016/j.cub.2020.02.018.

Sies, H. (2015) Oxidative stress: a concept in redox biology and medicine, *Redox Biol*, 4, pp. 180-183. doi: 10.1016/j.redox.2015.01.002.

Skaggs, W., McNaughton, B. and Gothard, K. (1992) An information-theoretic approach to deciphering the hippocampal code, *Advances in neural information processing systems*, 5.

Stefanini, F. *et al.* (2020) A Distributed Neural Code in the Dentate Gyrus and in CA1, *Neuron*, 107(4), pp. 703-716.e704. doi: 10.1016/j.neuron.2020.05.022.

Stensola, H. *et al.* (2012) The entorhinal grid map is discretized, *Nature*, 492(7427), pp. 72-78. doi: 10.1038/nature11649.

Stensola, T. and Moser, E. I. (2016) Grid Cells and Spatial Maps in Entorhinal Cortex and Hippocampus, in Buzsáki, G. and Christen, Y. (ed.) *Micro-, Meso- and Macro-Dynamics of the Brain.* Cham (CH): Springer

Copyright 2016, The Author(s). pp. 59-80.

Sun, Y. *et al.* (2017) Local and Long-Range Circuit Connections to Hilar Mossy Cells in the Dentate Gyrus, *eNeuro*, 4(2). doi: 10.1523/eneuro.0097-17.2017.

Taube, J. S., Muller, R. U. and Ranck, J. B., Jr. (1990) Head-direction cells recorded from the postsubiculum in freely moving rats. I. Description and quantitative analysis, *J Neurosci*, 10(2), pp. 420-435. doi: 10.1523/jneurosci.10-02-00420.1990.

Tavares, R. M. *et al.* (2015) A Map for Social Navigation in the Human Brain, *Neuron*, 87(1), pp. 231-243. doi: 10.1016/j.neuron.2015.06.011.

Thompson, L. T. and Best, P. J. (1990) Long-term stability of the place-field activity of single units recorded from the dorsal hippocampus of freely behaving rats, *Brain Res*, 509(2), pp. 299-308. doi: 10.1016/0006-8993(90)90555-p.

Tolman, E. C. (1948) Cognitive maps in rats and men, *Psychological review*, 55(4), pp. 189.

Tsao, A. *et al.* (2018) Integrating time from experience in the lateral entorhinal cortex, *Nature*, 561(7721), pp. 57-62. doi: 10.1038/s41586-018-0459-6.

Watts, M. E., Pocock, R. and Claudianos, C. (2018) Brain Energy and Oxygen Metabolism: Emerging Role in Normal Function and Disease, *Front Mol Neurosci*, 11, pp. 216. doi: 10.3389/fnmol.2018.00216.

Williams, P. A. *et al.* (2007) Semilunar Granule Cells: Glutamatergic Neurons in the Rat Dentate Gyrus with Axon Collaterals in the Inner Molecular Layer, *The Journal of Neuroscience*, 27(50), pp. 13756-13761. doi: 10.1523/jneurosci.4053-07.2007.

Wills, T. J. *et al.* (2005) Attractor Dynamics in the Hippocampal Representation of the Local Environment, *Science*, 308(5723), pp. 873-876. doi: doi:10.1126/science.1108905.

Wilson, D. M. (2017) *The base excision repair pathway : molecular mechanisms and role in disease development and therapeutic design*. New Jersey: World Scientific.

Winter, S. S. and Taube, J. S. (2014) Head Direction Cells: From Generation to Integration, in Derdikman, D. and Knierim, J. J. (ed.) *Space,Time and Memory in the Hippocampal Formation.* Vienna: Springer Vienna, pp. 83-106.

Witter, M. (2012) Chapter 5 - Hippocampus, in Watson, C., Paxinos, G. and Puelles, L. (ed.) *The Mouse Nervous System.* San Diego: Academic Press, pp. 112-139.

Witter, M. P. *et al.* (2000) Anatomical organization of the parahippocampal-hippocampal network, *Ann N Y Acad Sci*, 911, pp. 1-24. doi: 10.1111/j.1749-6632.2000.tb06716.x.

Witter, M. P. *et al.* (2017) Architecture of the Entorhinal Cortex A Review of Entorhinal Anatomy in Rodents with Some Comparative Notes, *Front Syst Neurosci*, 11, pp. 46. doi: 10.3389/fnsys.2017.00046.

Witter, M. P. (2018) Connectivity of the Hippocampus, in Cutsuridis, V.*, et al.* (ed.) *Hippocampal Microcircuits: A Computational Modeler's Resource Book.* Cham: Springer International Publishing, pp. 5-28.

Xu, W. and Wilson, D. A. (2012) Odor-evoked activity in the mouse lateral entorhinal cortex, *Neuroscience*, 223, pp. 12-20. doi: 10.1016/j.neuroscience.2012.07.067.

Xu, X. *et al.* (2012) The increased expression of metabotropic glutamate receptor 5 in subventricular zone neural progenitor cells and enhanced neurogenesis in a rat model of intracerebral hemorrhage, *Neuroscience*, 202, pp. 474-483. doi: https://doi.org/10.1016/j.neuroscience.2011.12.008.

Ye, J. *et al.* (2018) Entorhinal fast-spiking speed cells project to the hippocampus, *Proceedings of the National Academy of Sciences*, 115(7), pp. E1627-E1636. doi: doi:10.1073/pnas.1720855115.

Zemla, R. and Basu, J. (2017) Hippocampal function in rodents, *Current Opinion in Neurobiology*, 43, pp. 187-197. doi: 10.1016/j.conb.2017.04.005.

Zhang, X., Schlögl, A. and Jonas, P. (2020) Selective Routing of Spatial Information Flow from Input to Output in Hippocampal Granule Cells, *Neuron*, 107(6), pp. 1212-1225.e1217. doi: 10.1016/j.neuron.2020.07.006.

7 Appendices

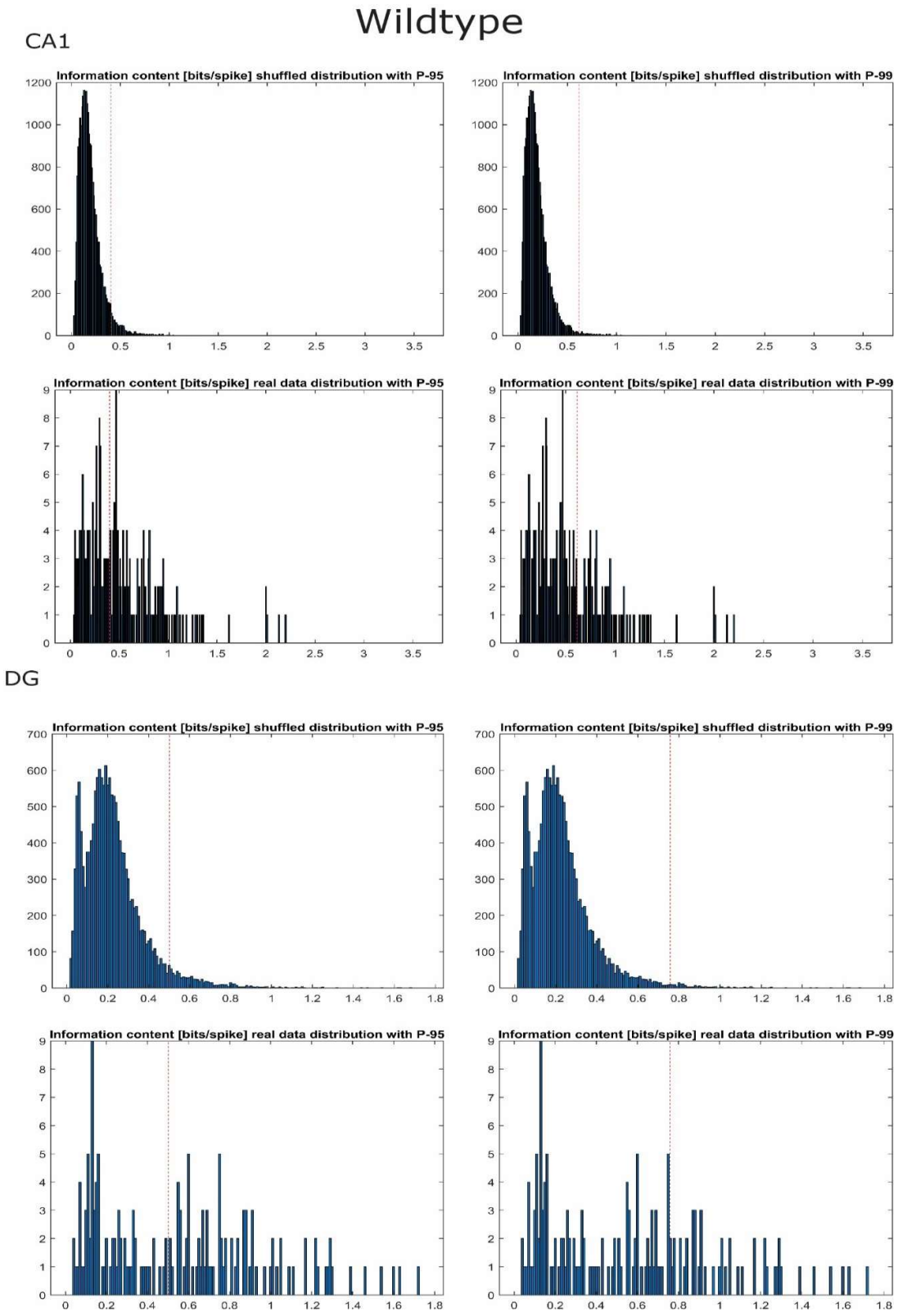

Figure 18. Shuffled and observed distributions for information content.
Data for the wildtype mouse in both CA1 and DG.

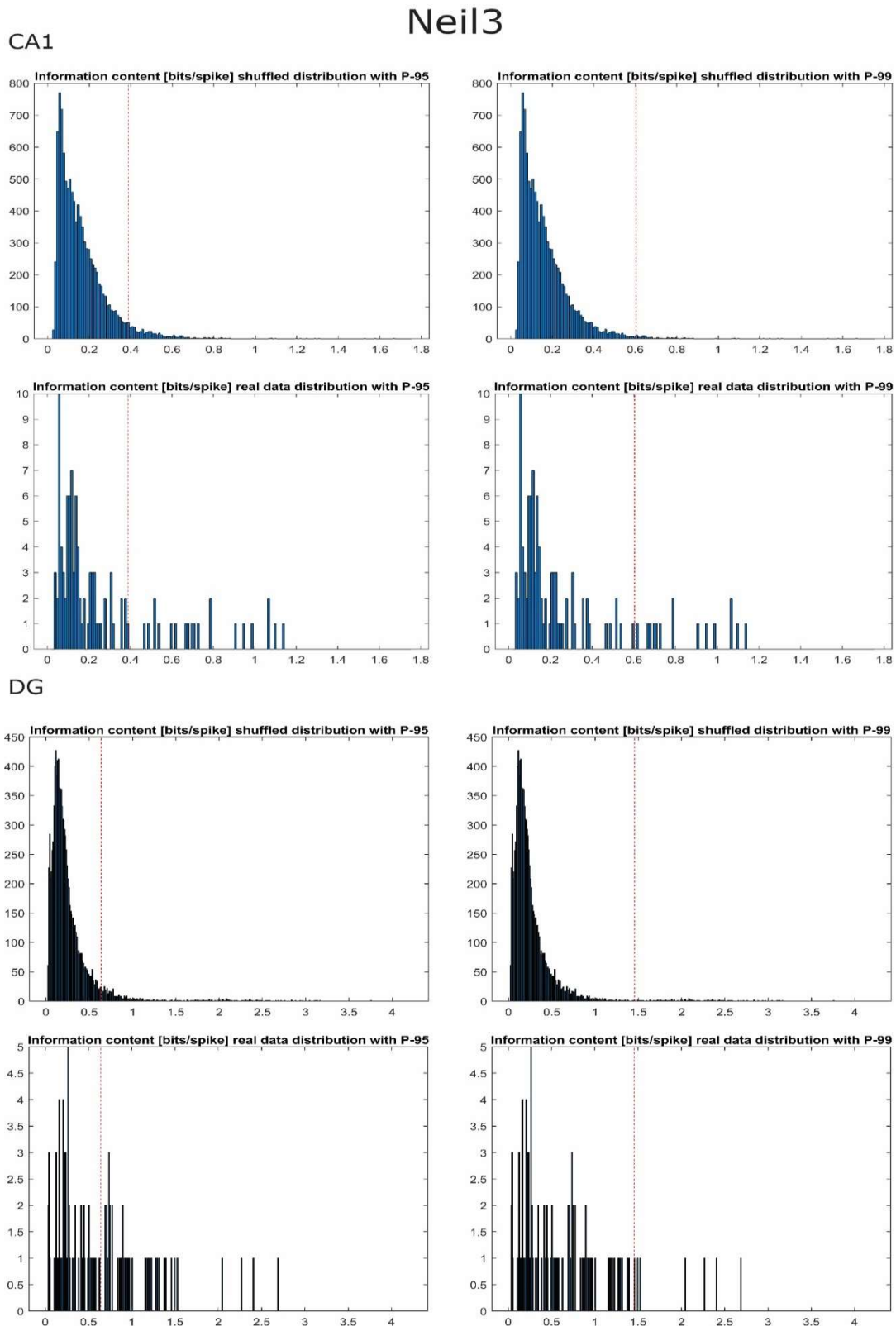

Figure 19. Shuffled and observed distributions for information content.
Data for the *Neil3*$^{-/-}$ mouse fin both CA1 and DG.

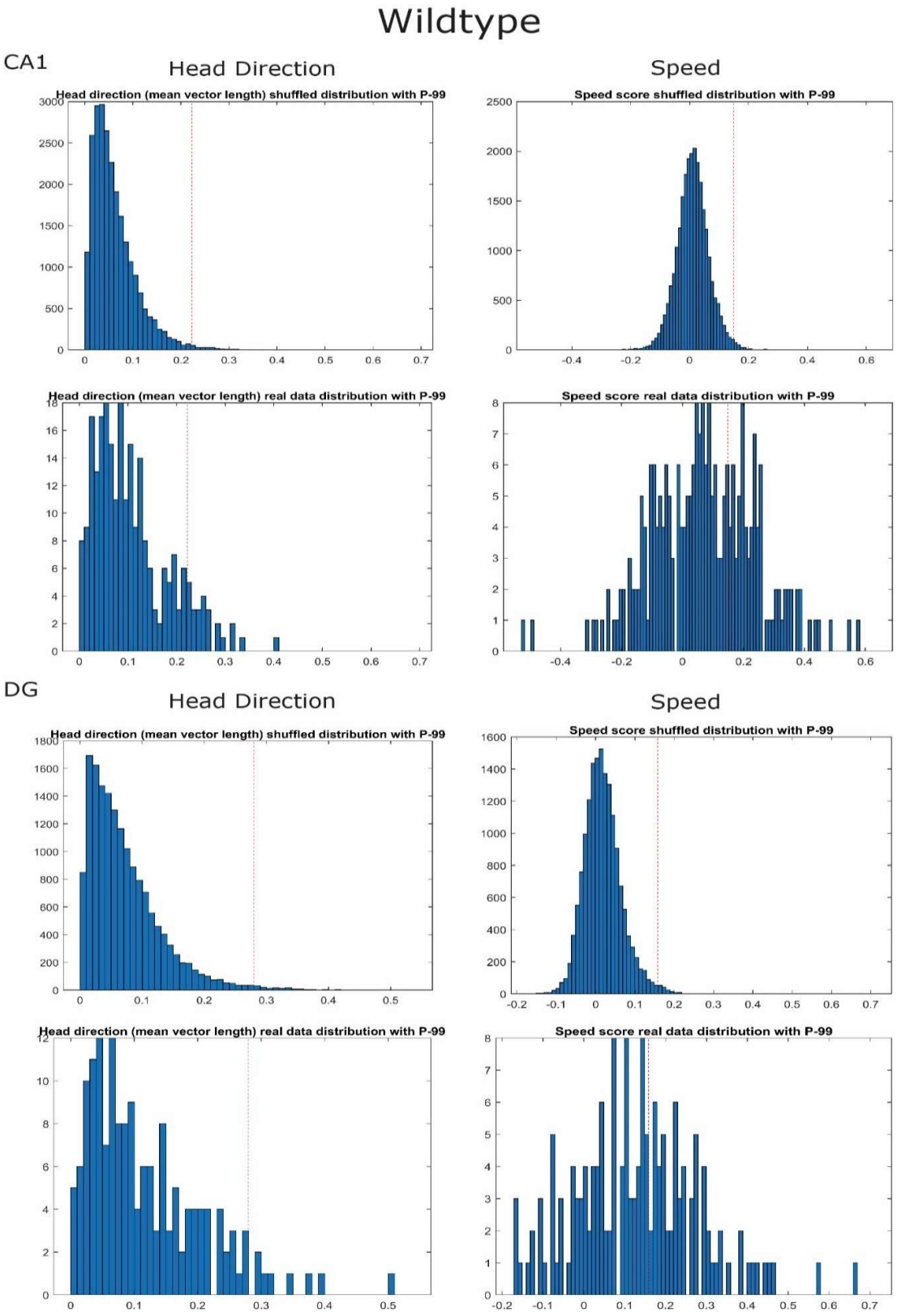

Figure 20. Shuffled and observed distributions for HD score and speed score.
Data for the wildtype mouse in both CA1 and DG.

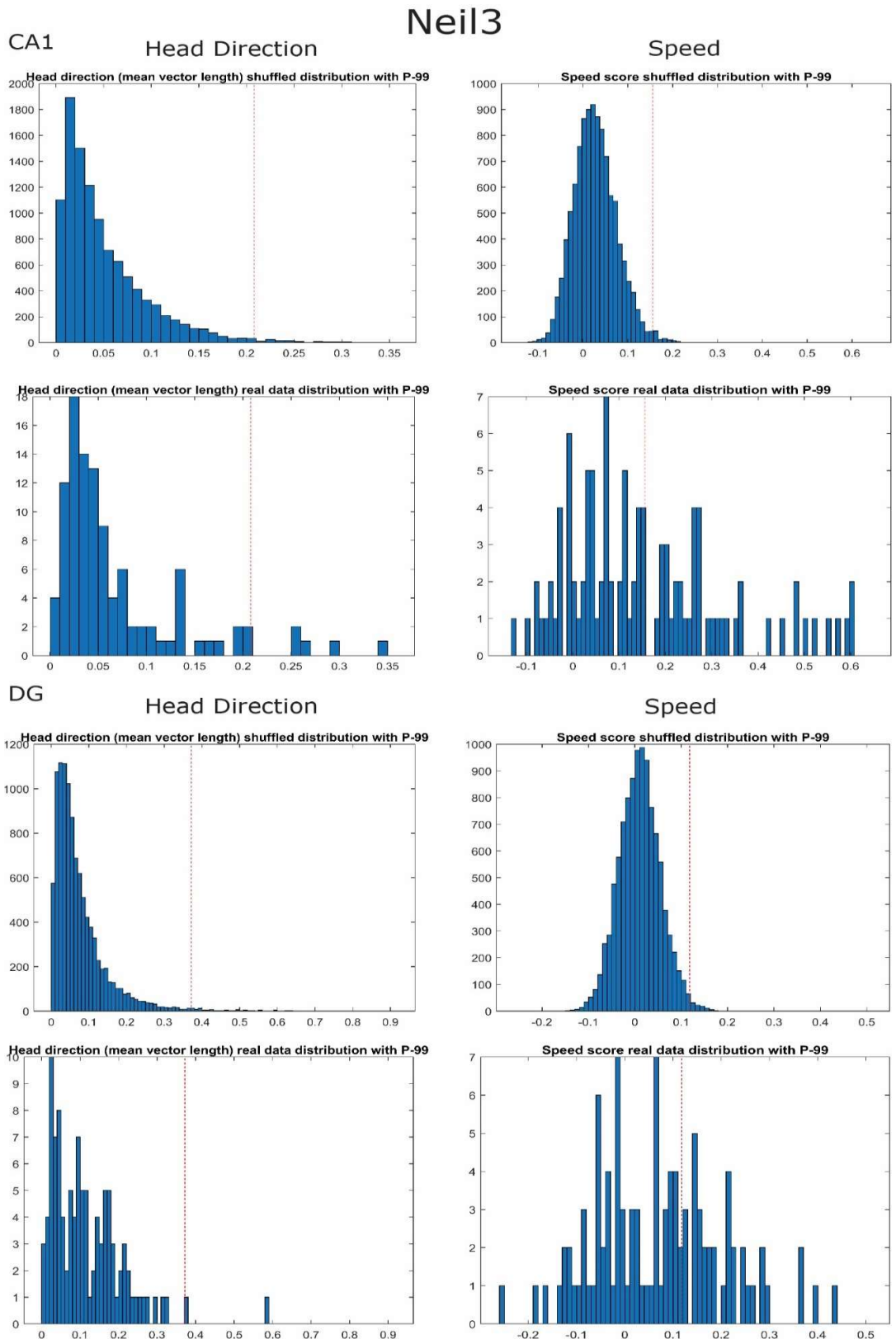

Figure 21. Shuffled and observed distributions for HD score and speed score. Data for the *Neil3*$^{-/-}$ mouse in both CA1 and DG.

Appendix E

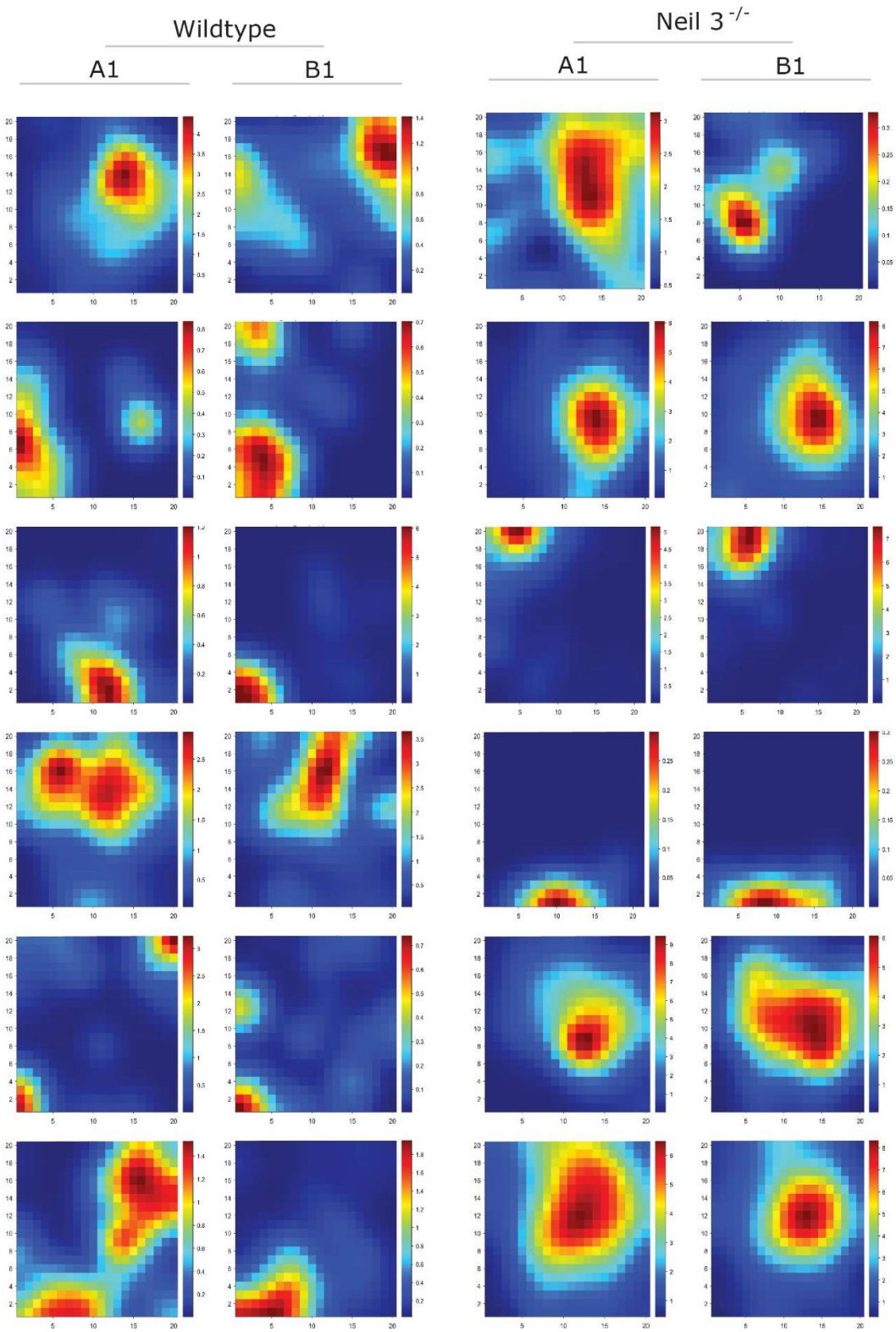

Figure 22. Rate maps for the A1-B1 global remapping condition.
Data from six selected place cells in each genotype

Appendix F

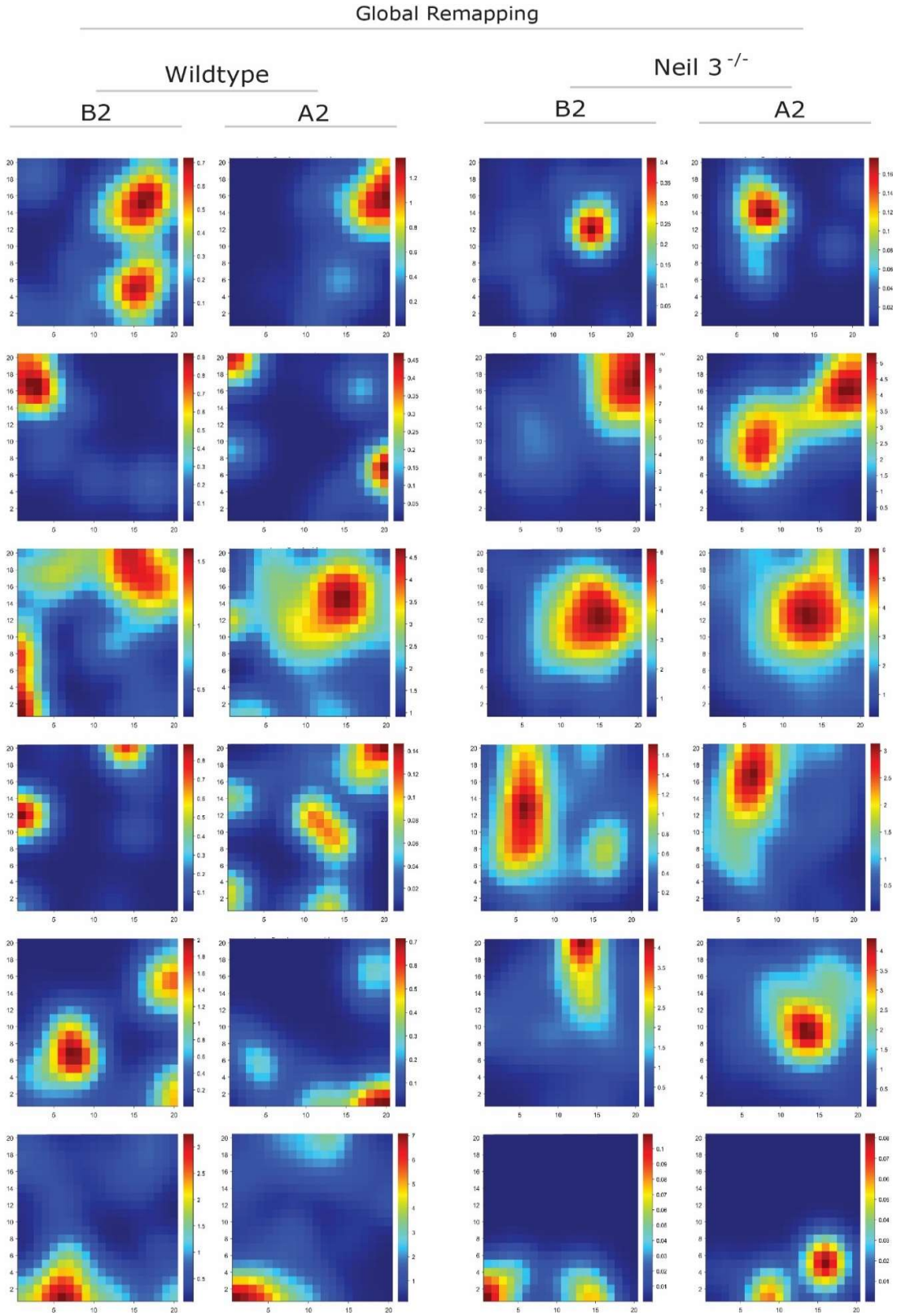

Figure 23. Rate maps for the B2-A2 global remapping condition.
Data from six selected place cells in each genotype

Appendix G

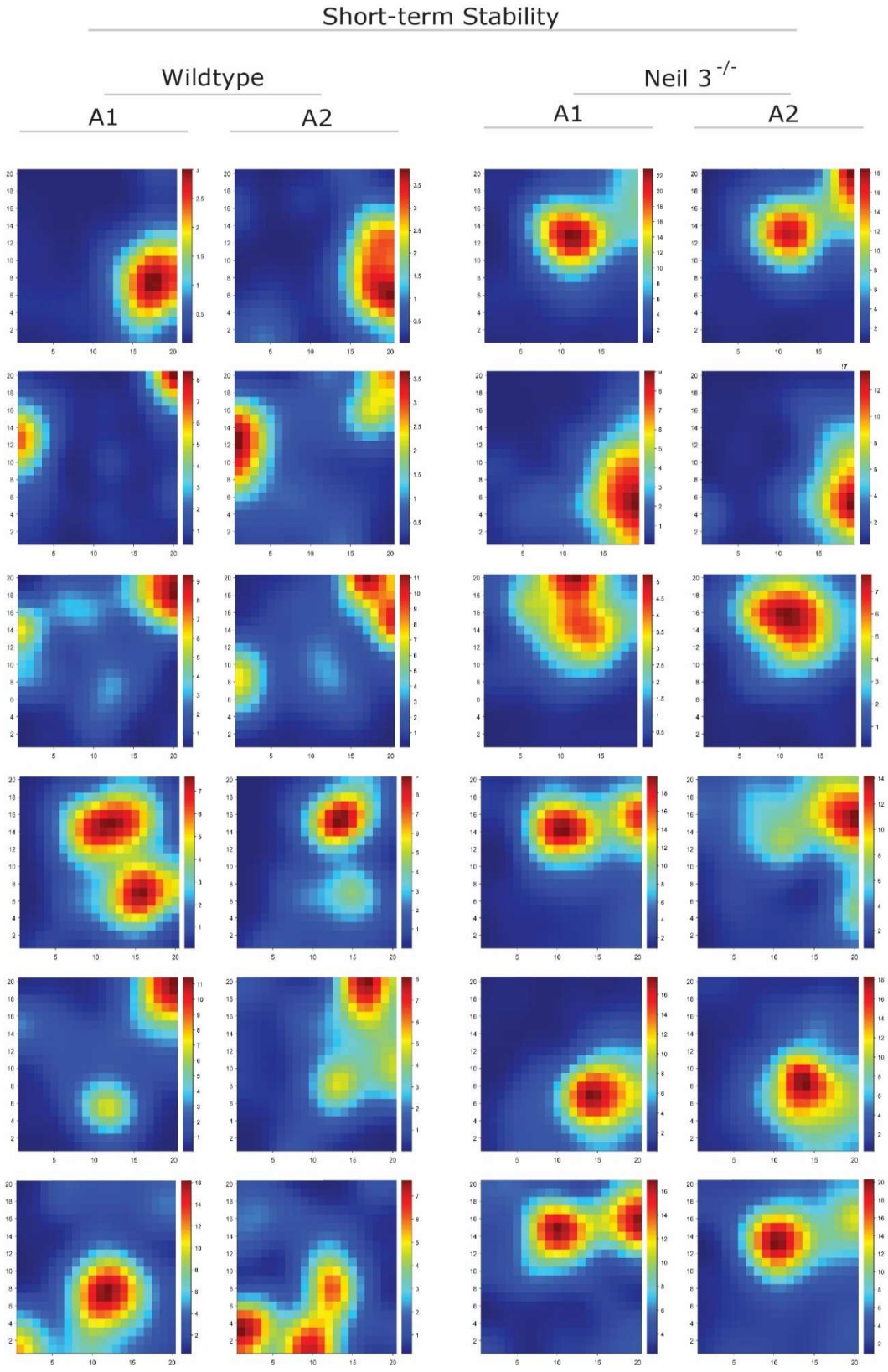

Figure 24. Rate maps for the A1-A2 short-term stability condition.
Data from six selected place cells in each genotype

Appendix H

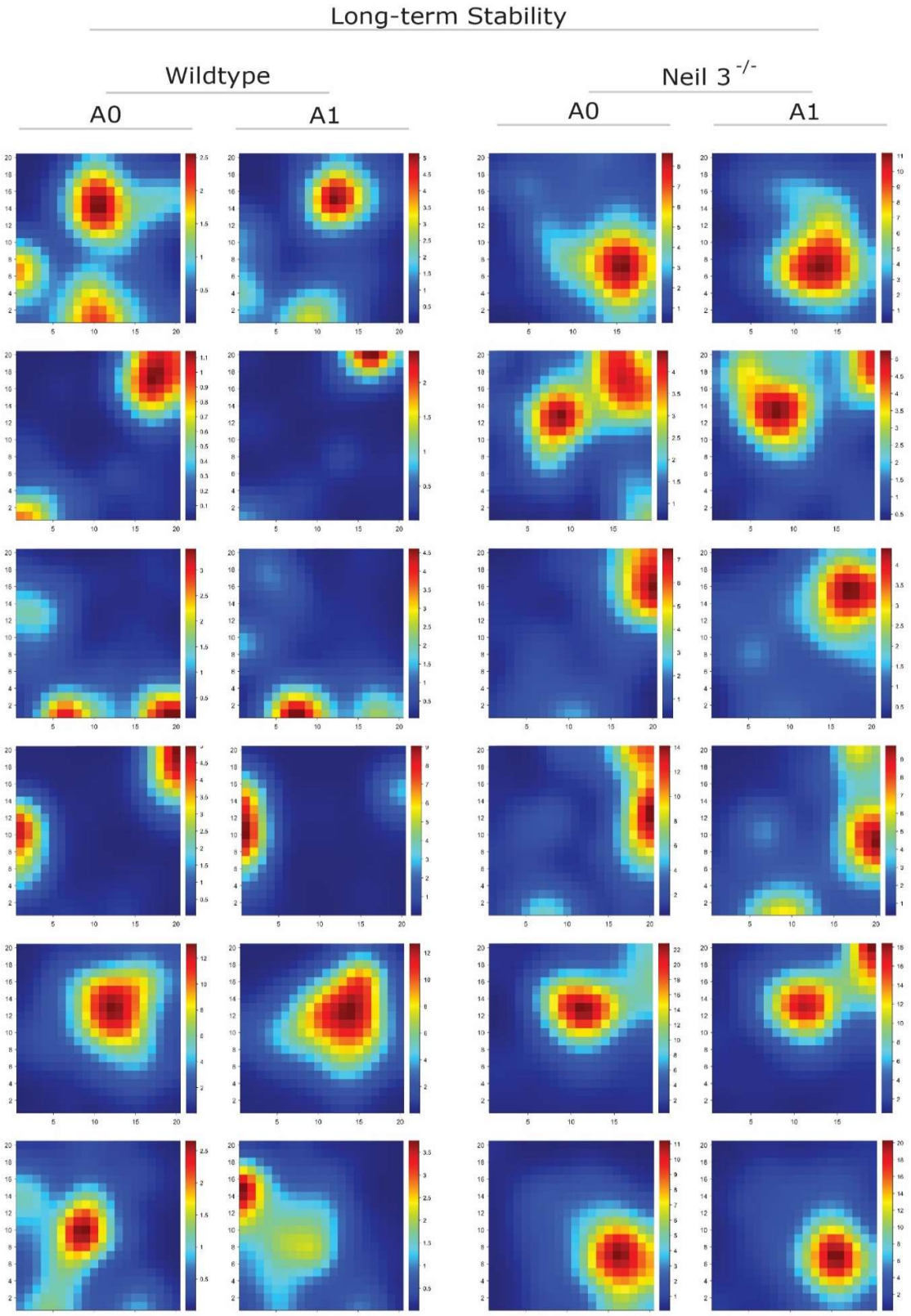

Figure 25. Rate maps for the A0-A1 long-term stability condition.
Data from six selected place cells in each genotype

Vidar Langseth Saasen

NEIL3 Impacts Hippocampal Spatial Representations

NTNU
Norwegian University of
Science and Technology